Topological invariants and adiabatic principle in correlated systems

Koji Kudo

February 2021

Topological invariants and adiabatic principle in correlated systems

Koji Kudo
Doctoral Program in Physics

Submitted to the Graduate School of
Pure and Applied Sciences
in Partial Fulfillment of the Requirements
for the Degree of Doctor of Philosophy in
Science

at
University of Tsukuba

Contents

Introduction

One of the most important challenges in condensed matter physics is to develop unified and simple picture for understanding phases of matter. The so-called symmetry breaking is one of the most fundamental concepts to classify material phases, which has been quite successful to describe a wide variety of phase transitions. While the Landau's symmetry breaking theory have been becoming important cornerstone for modern physics, recent intensive studies have revealed that there are other types of materials in which phases are not identified by their symmetry breaking patterns. This new class is called topological phases, which are characterized by topological invariants instead of the conventional order parameters. The topological invariants may emerge as physical observables, but most of them cannot be measured directly from the bulk. Instead, these appear at edges as low energy boundary states, which are characteristic properties of topological phases. For theoretical discoveries of topological phase transitions and topological phases of matter, D. J. Thouless, F. D. M. Haldane, and J. M. Kosterlitz were awarded the 2016 Nobel Prize in physics. Recent years have seen a massive growth of interests in topological phases. Although the topological phases were historically discovered through efforts to understand the underlying physics behind a quantum phenomenon, its concept have been nowadays extended to various systems and have provided a new versatile platform in modern condensed matter physics. Because of its universality and diversity, theoretical and experimental research of topological phases is extremely essential for building a broad foundation of material science.

Historically, the discovery of the integer QH (IQH) effect in 1980 [1] opened the door to the era of topological phases in condensed matter physics. The IQH systems exhibit quantum phenomena associated with phase transitions, which are identified by not conventional order parameters but the topological index known as the Chern number [2–6]. It is closely related to the emergence of gapless edge modes around boundaries, which is called the bulk-edge correspondence [7, 8]. The Haldane phases of integer Heisenberg spin chains [9, 10] are also the typical example of topological phases without symmetry breaking. The electron-electron interactions in the QH phases give birth to even more topologically nontrivial material phases. The fractional QH (FQH) effect [11, 12] is known today as one of topologically ordered phases [13, 14], which is an incompressible quantum liquid with fractionalized excitations. The quasiparticles describing the excitations carry the fractional charges and the fractional statistics [12, 15–19]. These fractionalizations are closely related to the topological degeneracy [20–24]. The non-Abelian FQH effect [25–28], some quantum spin liquids [29–34], etc., are also known as the topologically ordered phase with long-range entanglement [35–37]. Some of topologically ordered states exhibits excitations with non-Abelian anyons, which can be used for the so-called topological quantum computation. [33, 38, 39].

In recent years, the topological insulators/superconductors [40–43] have been studied intensively. The topological insulators are interpreted as a kind of QH phases with time reversal symmetry, where the spin-orbit interactions play an important role. Recent intensive studies have revealed that internal symmetry brings further diversity into topological phases if the idea of topology is augmented by symmetry. Indeed, many kinds of topological phases of

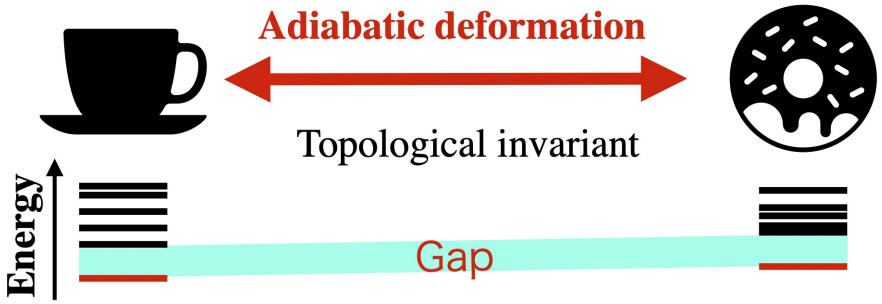

Figure 1: Adiabatic deformation

noninteracting fermions are classified systematically [44–47]. These systematic classifications plays an important role for exploring hitherto unknown various topological phases. The electron-electron interactions in these topological materials engender new physics that does not arise in the noninteracting problem. Recently, a wide variety of correlated topological phases have been clarified, some of which include the fractional Chern insulators [48–50], the fractional topological insulators [51, 52], etc. Furthermore, the concepts of the Mott transition and the Kondo effect, which are the typical example of strongly correlate materials, have been applied to physics of topological phases, which have given novel phases of matter such as the topological Mott insulators [53–57] and the topological Kondo insulators [58–61]. Also, the electron correlations have an even more significant effects on the topological classification [62–75]. Because of this diversity of correlation effects in topological phases, theoretical study on correlated topological materials has become increasingly important for developing the modern theory of the topological phases.

The purpose of this thesis is to establish fundamental concepts and to develop novel materials of topological phases in correlated systems. This thesis consists of two parts, Part I "topological invariants" and Part II "adiabatic principle". Part I gives arguments on topological invariants for characterizing correlated topological systems. In Chapter 1, we first give a generic setup for the Chern number and the Berry phase and discuss their gauge structures. After the general arguments, the Z_Q Berry phases that are quantized due to symmetry of the system are introduced. We also review the TKNN formula and the Niu-Thouless-Wu formula to describe the relation of physical observables and topological invariants. In Chapter 2, it is numerically demonstrated that the integration in evaluating the many-body Chern number for correlated systems can be actually skipped if the system size is sufficiently large. Analyzing the Hofstadter model with or without electron correlations, we show the exponential accuracy of the single-plaquette approximation with respect to the system size. We also discuss the usefulness of the one-plaquette Chern number in systems in which topological phase transitions occur.

Part II gives arguments on the adiabatic principle for characterizing correlated topological systems, which consists of three sections. The adiabatic deformation is a fundamental concept in the theory of topological phases (see in Fig. 1). In Chapter 3, we first revisit a simple problem to demonstrate that the (non-Abelian) Berry phases characterize the geometrical structures of wave functions involved in the adiabatic development. The concept of the adiabatic deformation gives a sophisticated view for characterizing phases of matter. From this perspective, in Chapter 4, we propose a new topological state "higher-order topological Mott insulator" that exhibits a generalized bulk-edge correspondence. It is numerically demonstrated that this correlated topological states are realized in the Hubbard model on a kagome lattice. Their topological nature are simply understood from adiabatically deformed

systems, whose information is encoded in the quantized Berry phase. In Chapter 4, we move onto the problem of the adiabatic deformations for the QH effects. According to the adiabatic heuristic arguments, the FQH and IQH states are adiabatically connected with each other by flux-attachment. In this chapter, we numerically demonstrate that the energy gap of the QH states on a torus are indeed smooth and finite even though the topological degeneracy changes wildly. We also analytically derive the relation between the many-body Chern number and the wild change of the topological degeneracy. This is a generalization of the Streda formula of the Hofstadter butterfly in the single-particle problem. This formula we discover implies what is fundamental in topological invariants is the continuity of the energy gap, rather than the continuity of states.

Part I

Topological invariants

Chapter 1

Berry phase and Chern number

Over the past few decades, topology has been developing a guiding principles in modern condensed matter physics. Topological numbers such as the Berry phase and the Chern number serve as a kind of order parameters beyond Landau's symmetry breaking theory. In this chapter, we first give a generic setup for the Berry phases and the Chern number in relation to their gauge structures. While the Chern number is always quantized, the Berry phases generally have any real numbers. However, specific systems bring the quantization of the Berry phases due to their symmetry. As an example of this quantized Berry phase, the Z_Q Berry phases defined in the system on hyper-Pyrochlore lattices are considered. Lastly, we review the TKNN formula and Niu-Thouless-Wu formula to discuss the relation between the Chern number and the quantized Hall conductance.

1.1 General setup

1.1.1 Berry phase

The Berry phase characterizes the geometrical structures of wave functions defined in the adiabatic development, which was historically discovered in the study of the adiabatic theorem in the quantum mechanics [4, 5, 76]. This encodes the geometrical structures of the subspace given by the ground states evolved adiabatically. Its concept is useful for characterizing topological phases. In this subsection, let us here begin by giving general arguments on the (non-Abelian) Berry phases in relation to the gauge structures [4, 5, 76–80]. The arguments associated with the adiabatic theorem is given in Chapter 3.

Let us now consider an Hermitian operator $H(\boldsymbol{x})$, where $\boldsymbol{x} = (x_1, \ldots, x_d)$ is a vector in a d-dimensional parameter space. It gives the following eigenvalue equation as

$$H(\boldsymbol{x})\psi_i(\boldsymbol{x}) = \epsilon_i(\boldsymbol{x})\psi_i(\boldsymbol{x}). \tag{1.1}$$

Using the eigenvectors ψ_i's $(i = 1, \cdots, M)$, we define the M-dimensional multiplet as

$$\Psi = (\psi_1, \cdots, \psi_M)\,. \tag{1.2}$$

We here assume that Ψ includes all of degenerated eigenstates, i.e., when Ψ includes ψ_i, Ψ should include ψ_j if $\epsilon_j = \epsilon_i$. Due to this assumption, it seems that the multiplet Ψ is specified uniquely by a set of eigenvalues $(\epsilon_1, \cdots, \epsilon_M)$ determined by $\boldsymbol{x}$. However, this naive argument is not correct since one has the freedom to change the basis; taking a different basis, we have another representation of the multiplet as $\Psi'(\boldsymbol{x}) = \Psi(\boldsymbol{x})\omega(\boldsymbol{x})$, where $\omega(\boldsymbol{x})$ is an M-dimensional unitary matrix. Generally, ω is not diagonal if Ψ includes sets of

degenerated eigenstates. Using the multiplet defined above, let us define the non-Abelian Berry connection as

$$\boldsymbol{A} = \Psi^\dagger d\Psi, \tag{1.3}$$

where $d = \sum_i \frac{\partial}{\partial x_i} dx_i$. We have the relations $\boldsymbol{A}^\dagger = -\boldsymbol{A}$ because of $\boldsymbol{A}^\dagger = (d\Psi^\dagger)\Psi = -\Psi^\dagger d\Psi = -\boldsymbol{A}$, where $\Psi^\dagger\Psi = 1$ has been used. The Berry connection is not gauge invariant as follows:

$$\boldsymbol{A}' = \Psi'^\dagger d\Psi' = \omega^\dagger \boldsymbol{A}\omega + \omega^\dagger d\omega. \tag{1.4}$$

Integrating $\boldsymbol{A}$ along a closed loop C defined in the parameter space, we have the non-Abelian Berry phases as [76]

$$U(C) = P\exp\left\{\int_C \boldsymbol{A}\right\}, \tag{1.5}$$

where P is the path ordering symbol. By the gauge transformation $\boldsymbol{A'} = \omega^\dagger \boldsymbol{A}\omega + \omega^\dagger d\omega$, it is transformed to [1]

$$U'(C) = \omega(\boldsymbol{x}_0)^\dagger U'(C)\omega(\boldsymbol{x}_0), \tag{1.6}$$

where we assume that the starting point and the terminal point of the closed path C is given by $\boldsymbol{x}_0$. This relation implies that the eigenvalues of $U_q[C]$, $\det U_q[C]$ and $\mathrm{tr}\, U_q[C]$ are gauge invariants.

Let us here mention properties of the Abelian Berry phase. We denote the Abelian Berry connection by $A = \boldsymbol{A}$ and assume that the gauge transformation is given by $\omega(\boldsymbol{x}) = e^{i\chi(\boldsymbol{x})}$. The definition of the Berry phase $e^{i\gamma(C)} = U(C)$ implies that we have [4]

$$\gamma(C) = \frac{1}{i}\oint_C A \mod 2\pi. \tag{1.7}$$

To ensure its gauge invariance, "mod 2π" is important: the naive integration of A is not gauge invariant as

$$\oint_C A' = \oint_C A + \oint_C \omega^* d\omega = \oint_C A + i\oint_C d\chi = \oint_C A + i2n\pi$$

where n is an integer.

1.1.2 Chern number

Let us now move onto the discussions on the Chern number. We first define the non-Abelian Berry connection as follows:

$$\boldsymbol{F} = d\boldsymbol{A} + \boldsymbol{A}^2. \tag{1.8}$$

[1] Rewriting the Berry connection as $\boldsymbol{A} = \mathcal{A}\cdot d\boldsymbol{x}$ with $\mathcal{A} = \Psi^\dagger \boldsymbol{\nabla}_{\boldsymbol{x}}\Psi$ and $\boldsymbol{\nabla}_{\boldsymbol{x}} = (\partial_{x_i}, \cdots, \partial_{x_d})$, we have [80]

$$\begin{aligned}
e^{\boldsymbol{A}'(\boldsymbol{x})\cdot d\boldsymbol{x}} &= 1 + \boldsymbol{A}'(\boldsymbol{x})\cdot d\boldsymbol{x} + O(d\boldsymbol{x}^2) \\
&= 1 + \omega^\dagger(\boldsymbol{x})\boldsymbol{A}(\boldsymbol{x})\omega(\boldsymbol{x})\cdot d\boldsymbol{x} + \omega(\boldsymbol{x})^\dagger\boldsymbol{\nabla}\omega(\boldsymbol{x})\cdot d\boldsymbol{x} + O(d\boldsymbol{x}^2) \\
&= \omega^\dagger(\boldsymbol{x})\left(1 + \boldsymbol{A}(\boldsymbol{x})\cdot d\boldsymbol{x}\right)\omega(\boldsymbol{x}) + \omega^\dagger(\boldsymbol{x})\boldsymbol{\nabla}\omega(\boldsymbol{x})\cdot d\boldsymbol{x} + O(d\boldsymbol{x}^2) \\
&= \omega^\dagger(\boldsymbol{x})\left(1 + \boldsymbol{A}(\boldsymbol{x})\cdot d\boldsymbol{x}\right)\left(\omega(\boldsymbol{x}) + \boldsymbol{\nabla}\omega(\boldsymbol{x})\cdot d\boldsymbol{x}\right) + O(d\boldsymbol{x}^2) \\
&= \omega^\dagger(\boldsymbol{x})e^{\boldsymbol{A}(\boldsymbol{x})\cdot d\boldsymbol{x}}\omega(\boldsymbol{x} + d\boldsymbol{x}) + O(d\boldsymbol{x}^2).
\end{aligned}$$

By the gauge transformation, it is deformed to [2]

$$\boldsymbol{F}' = \omega^\dagger d\boldsymbol{A}\omega + \omega^\dagger \boldsymbol{A} \wedge \boldsymbol{A}\omega = \omega^\dagger \boldsymbol{F}\omega. \tag{1.9}$$

Although the Berry curvature $\boldsymbol{F}$ itself depends on the gauge, $\mathrm{Tr}\boldsymbol{F}$ is a gauge invariant. Then integrating $\mathrm{Tr}\boldsymbol{F}$ on an orientable compact surface S in the parameter space, we define the Chern number as [77, 81]

$$C = \frac{1}{2\pi i}\int_S \mathrm{Tr}\,\boldsymbol{F}, \tag{1.10}$$

Since the integrand is a gauge invariant, the Chern number C is also gauge invariant. We here note that because of $\mathrm{Tr}\,\boldsymbol{A}\wedge\boldsymbol{A} = 0$, [3] the Chern number is written in terms of the Berry connections as follows:

$$C = \frac{1}{2\pi i}\int_S \mathrm{Tr}\, d\boldsymbol{A}. \tag{1.11}$$

From the relation $\mathrm{Tr}\,\boldsymbol{F} = \mathrm{Tr}\, d\boldsymbol{A}$, it seems that the term $\boldsymbol{A}\wedge\boldsymbol{A}$ in the definition of the non-Abelian Berry curvature is unnecessary. However, this argument is not correct since $\mathrm{Tr}\boldsymbol{F}$ would not become a gauge invariant if that term is absence.

Now, let us demonstrate the quantization of the Chern number analytically. Since there is no boundaries on S, one naturally expects that the Chern number would vanish according to Stokes theorem. This simple discussion, however, is not valid if the Berry connection is not defined well on S globally. To apply the Stokes theorem properly, let us divide the ill-defined region into patches S_i $(i = 0, 1, \cdots)$ and locally assign a well-defined Berry connection $\boldsymbol{A}_i = \Psi_i^\dagger d\Psi_i$ there, see Fig. 1.1. The wave functions defined in the patches are related to the original one, which we denote by Ψ_0, by the gauge transformation, i.e., $\Psi_i = \Psi_0\omega_i$. It implies that their local Berry connections are given by

$$\boldsymbol{A}_i = \omega_i^\dagger \boldsymbol{A}_0\omega_i + \omega_i^\dagger d\omega_i. \tag{1.12}$$

By using it and applying the Stokes theorem, the Chern number is expressed as [6, 77]

$$C = \sum_{i=0}\frac{1}{2\pi i}\int_{S_i}\mathrm{Tr}\, d\boldsymbol{A_i} \tag{1.13}$$

$$= \sum_{i=1}\frac{1}{2\pi i}\int_{\partial S_i}\mathrm{Tr}\,\omega_i^\dagger d\omega_i. \tag{1.14}$$

[2] We have

$$\begin{aligned} d\boldsymbol{A}' &= d\left(\omega^\dagger\boldsymbol{A}\omega + \omega^\dagger d\omega\right) \\ &= d\omega^\dagger\wedge\boldsymbol{A}\omega + \omega^\dagger d\boldsymbol{A}\omega - \omega^\dagger\boldsymbol{A}\wedge d\omega + d\omega^\dagger\wedge d\omega \\ \boldsymbol{A}'\wedge\boldsymbol{A}' &= \left(\omega^\dagger\boldsymbol{A}\omega + \omega^\dagger d\omega\right)\wedge\left(\omega^\dagger\boldsymbol{A}\omega + \omega^\dagger d\omega\right) \\ &= \omega^\dagger\boldsymbol{A}\wedge\boldsymbol{A}\omega + \omega^\dagger\boldsymbol{A}\wedge d\omega - d\omega^\dagger\wedge\boldsymbol{A}\omega - d\omega^\dagger\wedge d\omega, \end{aligned}$$

where $\omega^\dagger\omega = 1 \Rightarrow d\omega^\dagger\omega = -\omega^\dagger d\omega$ has been used.

[3] We have

$$\begin{aligned} \mathrm{Tr}\,\boldsymbol{A}\wedge\boldsymbol{A} &= \mathrm{Tr}\left[\Phi^\dagger d\Phi\wedge\Phi^\dagger d\Phi\right] \\ &= \sum_{\alpha,\beta=x,y}\mathrm{Tr}\left[\Phi^\dagger\left(\partial_\alpha\Phi\right)\Phi^\dagger\left(\partial_\beta\Phi\right)\right]d\theta_\alpha\wedge d\theta_\beta \\ &= -\sum_{\alpha,\beta=x,y}\mathrm{Tr}\left[\Phi^\dagger\left(\partial_\beta\Phi\right)\Phi^\dagger\left(\partial_\alpha\Phi\right)\right]d\theta_\beta\wedge d\theta_\alpha \\ &= -\mathrm{Tr}\,\boldsymbol{A}\wedge\boldsymbol{A}. \end{aligned}$$

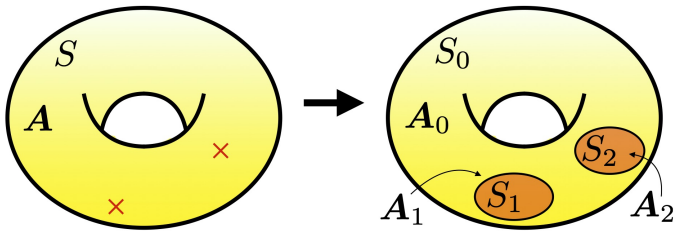

Figure 1.1: Berry connections $\boldsymbol{A}$, $\boldsymbol{A}_0$, $\boldsymbol{A}_1$, and $\boldsymbol{A}_2$.

Because of $\mathrm{Tr}\,\omega_i^\dagger d\omega_i = \mathrm{Tr}\, d\log\omega_i = d\,\mathrm{Tr}\,\log\omega_i = d\,\log\det\omega_i$, the Chern number reduces to the winding number defined along the closed circle ∂S_i as follows:

$$C = \sum_{i=1} \frac{1}{2\pi} \int_{\partial S_i} d\chi_i, \tag{1.15}$$

where $e^{i\chi_i} = \det\omega_i$. The presence of the winding number demonstrates the quantization of the Chern number.

1.2 Quantized Berry phase

Although the Beery phases generally take an arbitrary real value unlike the Chern number, it is quantized in some cases due to symmetry of systems [79, 82–86]. It implies that the quantized Berry phase is an adiabatic invariant under deformations that preserve the symmetry. In this section, let us review the Z_Q-quantized Berry phases for polyacetylene, kagome, and pyrochlore lattices [83] and discuss the mechanism of the quantizations. As mentioned in Chapter 4, this Z_Q-quantized Berry phases work well as an order parameter of topological phases such as higher-order topological Mott insulators.

Let us consider a system of spinless electrons on a hyper-Pyrochlore lattice in d-dimensions. This series includes a kagome lattice ($d = 2$), a pyrochlore lattice ($d = 3$), etc. We assume that the Hamiltonian is given by $H = H_\triangle + H_\triangledown$ with

$$H_\gamma = t_\gamma \sum_{ij\in\gamma} c_i^\dagger c_j + \mathrm{h.c.} \tag{1.16}$$

where $n_i = c_i^\dagger c_i$, $c_i^\dagger$ is the creation operator on site i, $\gamma = \triangle$ or $\triangledown$, and $i, j \in \triangle(\triangledown)$ indicates the summation over the nearest-neighbor pairs $i < j$ belonging to upward (downward) triangles [kagome] or tetrahedron [pyrochlore], etc. For defining the Berry phase, let now us pick up a certain downward triangle or tetrahedron [see Fig. 1.2 (a)] in the considered system. Then, labeling the site indices as $1, \cdots, Q \equiv d+1$, let us define a unitary operator as

$$U(\vec{\theta}) = \exp\left\{ i \sum_i^Q n_i \phi_i \right\}, \tag{1.17}$$

where ϕ_i is a function of $\vec{\theta}$ as

$$\phi_i = \sum_{j=1}^{i} \theta_j, \tag{1.18}$$

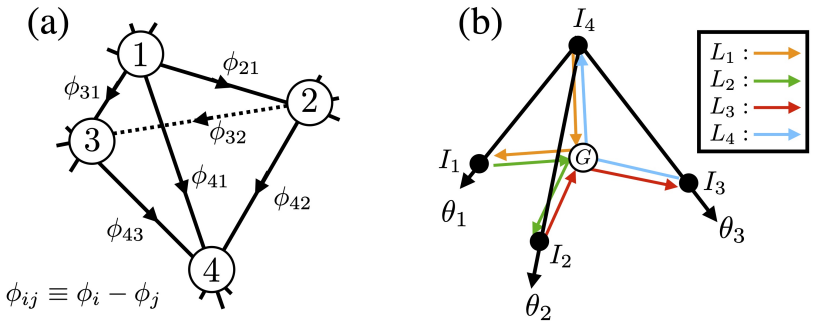

Figure 1.2: (a) Peierls phase induced by $U(\vec{\theta})$ for the Pyrochlore lattice. (b) Integration paths L_i's for the Pyrochlore lattice.

and Q-dimensional vector $\vec{\theta} = (\theta_1, \cdots, \theta_Q)$ is a parameter defined in mod 2π. Let us now write the Hamiltonian as

$$H(\vec{\theta}) = H_\triangle + U(\vec{\theta}) H_\triangledown U^\dagger(\vec{\theta}) \tag{1.19}$$

This modification introduces the Peierls phases to some bonds as shown in Fig. 1.2(a). Because of the local twist, this procedure is not a unitary operation with respect to the Hamiltonian. Then defining the ground state of the Hamiltonian $H(\vec{\theta})$ as $\left|G(\vec{\theta})\right\rangle$, the Berry phase is given by

$$\gamma_i = \frac{1}{i} \oint_{L_i} d\vec{\theta} \cdot A(\vec{\theta}), \;\; A(\vec{\theta}) = \left\langle G(\vec{\theta}) \right| \boldsymbol{\nabla}_{\vec{\theta}} \left| G(\vec{\theta}) \right\rangle . \tag{1.20}$$

The integration paths L_i's ($i = 1, \cdots, Q$) are given as follows. We first define Q points $I_1, \cdots, I_Q$ in the parameter space as

$$\begin{aligned} I_1 &= (2\pi, 0, \cdots, 0) \\ I_2 &= (0, 2\pi, 0, \cdots, 0) \\ &\vdots \\ I_Q &= (0, \cdots, 0, 2\pi). \end{aligned}$$

and the center of gravity as $G = (2\pi/Q, \cdots, 2\pi/Q)$. Setting $\phi_Q = 0$, i.e.,

$$\theta_Q = -(\theta_1 + \cdots + \theta_{Q-1}), \tag{1.21}$$

we define a line connecting I_i with G as shown in Fig. 1.2(b) (the case of pyrochlore lattices). They are described by the following vector as

$$\vec{f}_i(t) = \frac{2\pi}{Q}(\overset{1}{t}, \cdots, \overset{i-1}{t}, -(Q\overset{i}{-}1)t, \overset{i+1}{t}, \cdots, \overset{Q}{t},) \text{ for } 0 \le t \le 1,$$

where the $i-1$th element with $i = 1$ is defined as the Qth element. Along these lines, we define the path integral $L_i : I_{i-1} \to G \to I_i$ for $i = 1, \cdots, Q$, where $I_0 = I_Q$.

Let us give a proof of the quantization of γ_i. Now, we assume that the system has a symmetry with respect to a cyclic permutation of the site indices as $(1, 2, \cdots, Q) \to (Q, 1, 2, \cdots, Q-1)$. For example, this unitary operation for the pyrochlore lattices is associated with C_3 symmetry and mirror symmetry as shown in Fig. 1.3. Denoting this unitary operator by U, we have

$$UH(\vec{\theta})U^\dagger = H(g\vec{\theta}), \tag{1.22}$$

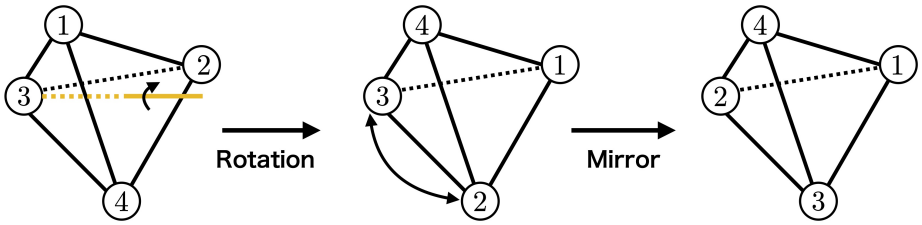

Figure 1.3: Unitary operation for a pyrochlore lattice.

where g is a $Q \times Q$ unitary matrix satisfying $g\vec{\theta} = (\theta_Q, \theta_1, \theta_2, \cdots, \theta_{Q-1})$. Noting that

$$g\vec{f}_i(t) = \vec{f}_{i+1}(t), \tag{1.23}$$

for $i = 1, \cdots, Q$, where $\vec{f}_{Q+1} = \vec{f}_1$, the equivalence between γ_i and γ_{i-1} is given. [4] Namely, we have

$$\gamma_1 = \gamma_2 = \cdots = \gamma_Q \mod 2\pi. \tag{1.24}$$

Because the sum of the loops L_i's is equal to zero, the sum of the Berry phases γ_i's is vanishing, i.e., $\sum_i \gamma_i = 0 \mod 2\pi$. They imply

$$\gamma_1 = \gamma_2 = \cdots = \gamma_Q = \frac{2\pi}{Q} n \mod 2\pi, \tag{1.25}$$

where $n = 1, 2, \cdots, Q$.

In some cases, the quantized Berry phase can be computed analytically. Let us first calculate γ_i of systems that are adiabatically connected into the system with the Hamiltonian $H = H_\bigtriangledown$. Due to the quantization of the Berry phase, it reduces to the problem of calculating γ_i in that deformed system. Since we have

$$H(\vec{\theta}) = U(\vec{\theta}) H U^\dagger(\vec{\theta}), \tag{1.26}$$

[4] The proof is given as follows:

$$\begin{aligned}
\gamma_i &= \sum_j \frac{1}{i} \int_{L_i} d\theta_j \left\langle G(\vec{\theta}) \right| \frac{\partial}{\partial \theta_j} \left| G(\vec{\theta}) \right\rangle \\
&= \sum_j \frac{1}{i} \int_{L_{i-1}} d\left(\sum_k g_{jk} \theta'_k \right) \left\langle G(g\vec{\theta}') \right| \sum_l \frac{\partial \theta'_l}{\partial \theta_j} \frac{\partial}{\partial \theta'_l} \left| G(g\vec{\theta}') \right\rangle, \ \vec{\theta} = g\vec{\theta}' \\
&= \sum_j \frac{1}{i} \int_{L_{i-1}} d\left(\sum_k g_{jk} \theta'_k \right) \left\langle G(g\vec{\theta}') \right| \sum_l (g^{-1})_{lj} \frac{\partial}{\partial \theta'_l} \left| G(g\vec{\theta}') \right\rangle \\
&= \sum_{jkl} g_{jk} (g^{-1})_{lj} \frac{1}{i} \int_{L_{i-1}} d\theta'_k \left\langle G(g\vec{\theta}') \right| \frac{\partial}{\partial \theta'_l} \left| G(g\vec{\theta}') \right\rangle \\
&= \sum_{kl} \delta_{kl} \frac{1}{i} \int_{L_{i-1}} d\theta'_k \left\langle G(g\vec{\theta}') \right| \frac{\partial}{\partial \theta'_l} \left| G(g\vec{\theta}') \right\rangle \\
&= \frac{1}{i} \int_{L_{i-1}} d\vec{\theta}' \cdot \left\langle G(g\vec{\theta}') \right| \nabla_{\vec{\theta}'} \left| G(g\vec{\theta}') \right\rangle \\
&= \frac{1}{i} \int_{L_{i-1}} d\vec{\theta}' \cdot \left\langle G(\vec{\theta}') \right| U^\dagger \nabla_{\vec{\theta}'} U \left| G(\vec{\theta}') \right\rangle \\
&= \frac{1}{i} \int_{L_{i-1}} d\vec{\theta}' \cdot \left\langle G(\vec{\theta}') \right| \nabla_{\vec{\theta}'} \left| G(\vec{\theta}') \right\rangle \\
&= \gamma_{i-1}.
\end{aligned}$$

the Berry connection is given by

$$A_i(\vec{\theta}) = \langle G| U^\dagger(\vec{\theta}) \frac{\partial}{\partial \theta_i} U(\vec{\theta}) |G\rangle = i \sum_{k=i}^{Q} \langle G| n_k |G\rangle \tag{1.27}$$

where $|G\rangle$ is the ground state of H and $\frac{\partial}{\partial\theta_i}U = \sum_{k=1}^{Q} \frac{\partial\phi_k}{\partial\theta_i}\frac{\partial}{\partial\phi_k}U = \sum_{k=i}^{Q}\frac{\partial}{\partial\phi_k}U = i\sum_{k=i}^{Q} n_k U$ has been used. Then, the Berry phase specified by L_1 is given by

$$\gamma_1 = \frac{1}{i}\oint_{L_1} d\vec{\theta}\cdot A(\vec{\theta}) = 2\pi \langle G| n_1 |G\rangle . \tag{1.28}$$

Let us next consider systems that are adiabatically connected into the system whose Hamiltonian is given by $H = H_\triangle$. This insensitivity of the local twists implies that the Berry connection is given by $A(\vec{\theta}) = 0$, i.e.,

$$\gamma_i = 0. \tag{1.29}$$

This quantized Berry phases is useful to characterize topological phases and describe phase transitions. In the next part discussing adiabatic principle, we introduce its spin counterpart to detect the higher-order topological Mott insulating states.

1.3 Quantized Hall conductance and Chern number

The QH effect is a typical example of topological phases in condensed matter physics. It demonstrates how topology enriches phases of matter beyond Landau's symmetry breaking theory. In this section, we first review the Laughlin's argument to demonstrate the quantization of the Hall conductance in the IQH effect. In this argument, the quantized Hall conductance is shown in term of the gauge invariance. According to the TKNN formula, the quantized Hall conductance is essentially described by the Chern number. After discussing this formula, we also review the Niu-Thouless-Wu formula to demonstrate the fractional quantization in the FQH effect, which is a generalization of the TKNN formula.

Before entering on discussions of the QH effect, we shortly discuss the Hall effect of classical systems based on the Drude theory [87–89]. Let us now consider a two dimensional system of electrons under the uniform magnetic field. According to the Drude theory, the single-particle momentum $\boldsymbol{p}$ are given by

$$\frac{d\boldsymbol{p}}{dt} = e\left(\boldsymbol{E} + \frac{\boldsymbol{p}}{m}\times\boldsymbol{B}\right) - \frac{\boldsymbol{p}}{\tau}, \tag{1.30}$$

where $\boldsymbol{E}$ is the electric field, $e<0$ is the elementary charge, m is the electron mass, $\boldsymbol{B}$ is the magnetic field, and τ is the mean free path. Assuming $d\boldsymbol{p}/dt = 0$ and $\boldsymbol{B} = B\boldsymbol{e}_z$, we have $e\boldsymbol{E} = -\boldsymbol{p}/m\times\boldsymbol{B} + \boldsymbol{p}/\tau$, i.e.,

$$\begin{bmatrix} E_x \\ E_y \end{bmatrix} = \begin{bmatrix} -\omega_c p_y/e + p_x/(e\tau) \\ \omega_c p_x/e + p_y/(e\tau) \end{bmatrix} = \begin{bmatrix} 1/(e\tau) & -\omega_c/e \\ \omega_c/e & 1/(e\tau) \end{bmatrix} \begin{bmatrix} p_x \\ p_y \end{bmatrix}, \tag{1.31}$$

where $\omega_c = eB/m$ is the cyclotron frequency. Defining the resistivity tensor $\boldsymbol{\rho}$ as

$$\boldsymbol{E} = \boldsymbol{\rho}\boldsymbol{i},\ \boldsymbol{\rho} = \begin{bmatrix} \rho_{xx} & \rho_{xy} \\ \rho_{yx} & \rho_{yy} \end{bmatrix}, \tag{1.32}$$

where $\boldsymbol{i} = (i_x, i_y)$ is the current density and assuming $\boldsymbol{i} = ne\boldsymbol{p}/m$ with n being the electrons number per unit volume, we have

$$\boldsymbol{\rho} = \begin{bmatrix} m/(ne^2\tau) & -m\omega_c/(ne^2) \\ m\omega_c/(ne^2) & m/(ne^2\tau) \end{bmatrix}. \tag{1.33}$$

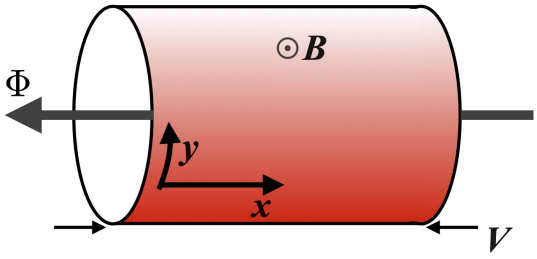

Figure 1.4: Two-dimensional system on a cylinder.

The important point here is that the Hall resistivity ρ_{xy} in the Drude theory is proportional to the magnetic field B. However, systems subjected to low temperatures with the strong magnetic field give the quantization of the Hall conductance: The IQH effect [1] gives the vanishing longitudinal conductance and the quantized Hall conductance as follows:

$$\sigma_{xx} = 0, \ \sigma_{xy} = s\frac{e^2}{\hbar}, \tag{1.34}$$

where $\boldsymbol{\sigma} = \boldsymbol{\rho}^{-1}$ is the conductivity tensor and s is an integer. In the next subsection, we show the quantization of the Hall conductance based on the Laughlin's argument [2].

1.3.1 Laughlin's argument

Let us consider a system with non-interacting electrons under the magnetic field. The periodic boundary condition is imposed only in the y direction, i.e., $\psi(x, y + L) = \psi(x, y)$ with L being the circumference of the loop. Let us now consider a gauge transformation given by the magnetic flux Φ that is threaded through the loop, see Fig. 1.4. It is described by the vector potential $\mathcal{A} = \nabla\chi(\boldsymbol{r})$ with

$$\chi(\boldsymbol{r}) = \frac{\Phi}{L}y. \tag{1.35}$$

The wave function $\psi(\boldsymbol{r})$ is deformed into $\psi(\boldsymbol{r})e^{ie\chi(\boldsymbol{r})/\hbar}$. Assuming that the states are extended along the y direction, the periodic boundary condition $\psi(x, y + L)e^{ie\chi(x,y+L)/\hbar} = \psi(x, y)e^{ie\chi(x,y)/\hbar}$ reduces to $e^{i2\pi\Phi e/\hbar} = 1$. Namely, the allowed flux for a gauge transformation is an integral multiple of the quantum flux $\phi_0 = h/e$.

Because of the gauge invariance, threading ϕ_0 maps the system back into itself. This procedure allows the transfer of electrons from one edge to the other. With the potential drop V, the energy change is given as

$$\Delta E = neV, \tag{1.36}$$

where n is the number of the transferred electrons. According to the Byers-Yang formula [90], the current in the y direction is given as

$$i_y = \frac{1}{L}\frac{\Delta E}{\Delta\Phi} = \frac{1}{L}\frac{neV}{\phi_0} = \frac{ne^2V}{hL} = \frac{ne^2}{h}E_x. \tag{1.37}$$

where $E_x = LV$. This result clearly demonstrates the quantization of the Hall conductance in the unit of e^2/h.

1.3.2 TKNN formula

Let us now discuss the quantization of the Hall conductance in terms of the Chern number [3, 6]. We consider a system of non-interacting electrons under the magnetic field. The Bloch Hamiltonian and its Bloch state are denoted by $H_{\boldsymbol{k}}$ and $|u^\alpha_{\boldsymbol{k}}\rangle$, where $\boldsymbol{k}$ is the single-particle momentum and α is the band index. According to the Kubo formula, the Hall conductance is given by

$$\sigma_{xy} = i\frac{e^2}{\hbar}\sum_{\epsilon_\alpha<\epsilon_F<\epsilon_\beta}\int_{\mathrm{BZ}}\frac{dk^2}{(2\pi)^2}\frac{\langle u^\alpha_{\boldsymbol{k}}|\partial_{k_y}H_{\boldsymbol{k}}|u^\beta_{\boldsymbol{k}}\rangle\langle u^\beta_{\boldsymbol{k}}|\partial_{k_x}H_{\boldsymbol{k}}|u^\alpha_{\boldsymbol{k}}\rangle - (x\leftrightarrow y)}{(\epsilon^\beta_{\boldsymbol{k}}-\epsilon^\alpha_{\boldsymbol{k}})^2}, \tag{1.38}$$

where ϵ_α is the eigenenergy of $H_{\boldsymbol{k}}$ and ϵ_F is the Fermi energy. Then, it reduces to the following expression:

$$\sigma_{xy} = \frac{e^2}{\hbar}\sum_{\epsilon_\alpha<\epsilon_F} C_\alpha, \tag{1.39}$$

This is the TKNN formula [3, 6]. The band Chern number C_α is defined as

$$\begin{aligned} C_\alpha &= \frac{1}{2\pi i}\int_{\mathrm{BZ}} dk^2\, F_\alpha(\boldsymbol{k}),\\ F_\alpha(\boldsymbol{k}) &= [\nabla_{\boldsymbol{k}}\times A_\alpha(\boldsymbol{k})]_z\,,\\ A_\alpha(\boldsymbol{k}) &= \langle u^\alpha_{\boldsymbol{k}}|\nabla_{\boldsymbol{k}}u^\alpha_{\boldsymbol{k}}\rangle\,. \end{aligned} \tag{1.40}$$

This expression is rewritten in terms of the non-Abelian Berry connection as follows:

$$\begin{aligned} C &= \frac{1}{2\pi i}\int_{\mathrm{BZ}} dk^2 \mathrm{Tr}\,[\nabla_{\boldsymbol{k}}\times \boldsymbol{A}(\boldsymbol{k})]_z\,,\\ \boldsymbol{A}(\boldsymbol{k}) &= \boldsymbol{u}^\dagger_{\boldsymbol{k}}\nabla_{\boldsymbol{k}}\boldsymbol{u}_{\boldsymbol{k}},\\ \boldsymbol{u}_{\boldsymbol{k}} &= (|u^1_{\boldsymbol{k}}\rangle,\cdots,|u^{N_\mathrm{b}}_{\boldsymbol{k}}\rangle), \end{aligned} \tag{1.41}$$

where N_b is the number of the bands under the Fermi energy. Clearly, we have $C=\sum_\alpha C_\alpha$. The existence of the Chern number demonstrates the quantization of the Hall conductance.

1.3.3 Niu-Thouless-Wu formula

Let us here move onto the discussions of the Chern number in the FQH effect. The FQH effect [11] is a typical example of a quantum liquid state with the topological order [13, 20, 91] such as fractionalized excitations [12, 15–19] and the topological degeneracy [20, 91–93]. In this subsection, we focus on discussions mainly on the Niu-Thouless-Wu formula [94] that describes the fractional quantization of the Hall conductance in the FQH effect. This is a generalization of the TKNN formula.

Let us consider a two-dimensional system of electrons in which the twisted boundary conditions are imposed. The twisted angles are denoted by $\vec{\theta}=(\theta_x,\theta_y)$. Defining the m-fold ground state multiplet as $\Phi=(|G_1\rangle,\cdots,|G_m\rangle)$, the Hall conductance specified by the twisted angle $\vec{\theta}$ is given by [94]

$$\sigma_{xy}(\vec{\theta}) = \frac{1}{m}\frac{e^2}{\hbar}C(\vec{\theta}), \tag{1.42}$$

where $C(\vec{\theta})=-2\pi i\mathrm{Tr}\boldsymbol{F}(\vec{\theta})$ and $\boldsymbol{F}(\vec{\theta})$ is the Berry curvature defined as

$$\boldsymbol{F} = [\boldsymbol{\nabla}_{\vec{\boldsymbol{\theta}}}\times\boldsymbol{A}+\boldsymbol{A}\times\boldsymbol{A}]_z, \tag{1.43}$$

$$\boldsymbol{A} = \Phi^\dagger\boldsymbol{\nabla}_{\vec{\theta}}\Phi. \tag{1.44}$$

Assuming that the physical observable $\sigma_{xy}(\vec{\theta})$ is not strongly sensitive to the boundary condition, we take the average over all possible values of the twisted angles:

$$\sigma_{xy} = \frac{1}{(2\pi)^2}\int_{T^2} d^2\theta \sigma_{xy}(\vec{\theta}) = \frac{1}{m}\frac{e^2}{\hbar}C, \tag{1.45}$$

where C is the Chern number. This is the so-called Niu-Thouless-Wu formula [94]. The appearance of the Chern number demonstrates the quantization of the Hall conductance.

The Niu-Thouless-Wu formula is a many-body counterpart of the TKNN formula. To see it, let us now demonstrate that the Niu-Thouless-Wu formula reduces to the TKNN formula when particles are noninteracting. Let us consider the system on a square lattice with $N_{\rm site} = N \times N$ sites, whose Hamiltonian is $H = \boldsymbol{c}^\dagger \boldsymbol{h} \boldsymbol{c}$. Here, $\boldsymbol{c}^\dagger = (c_1^\dagger, \cdots, c_{N_{\rm site}}^\dagger)$, $c_i^\dagger$ is a creation operator on the site i and $\boldsymbol{h}$ is an $N_{\rm site} \times N_{\rm site}$ matrix. We here impose the twisted boundary conditions. Assuming that the Fermi energy lies in a band gap and choosing the magnetic unit cell of the size $n_x \times n_y$, the ground state is constructed from a set of single-particle states as

$$|G(\theta_x, \theta_y)\rangle = \prod_{\alpha=1}^{N_{\rm b}} \prod_{i_x=1}^{N/n_x} \prod_{i_y=1}^{N/n_y} \left(\boldsymbol{c}^\dagger \boldsymbol{\varphi}_\alpha(\boldsymbol{k}_{(i_x,i_y)})\right)|0\rangle, \tag{1.46}$$

$$\boldsymbol{k}_{(i_x,i_y)}(\vec{\theta}) = \left(\frac{2\pi i_x + \theta_x}{N}, \frac{2\pi i_y + \theta_y}{N}\right) \tag{1.47}$$

where $\boldsymbol{\varphi}_\alpha(\boldsymbol{k}_{(i_x,i_y)})$ is the eigenvector of $\boldsymbol{h}$ associated with the band index α and the momentum $\boldsymbol{k}_{(i_x,i_y)}$, $|0\rangle$ is a vacuum, and $N_{\rm b}$ is the number of bands under the Fermi energy. The Berry connection is given by

$$A(\vec{\theta}) = \left\langle G(\vec{\theta}) \middle| \nabla_{\vec{\theta}} \middle| G(\vec{\theta}) \right\rangle = \mathrm{tr}\, \boldsymbol{a}(\vec{\theta}), \tag{1.48}$$

where $\boldsymbol{a}$ is the non-Abelian Berry connection [77–79] defined as

$$\begin{aligned}
&\boldsymbol{a}(\vec{\theta}) = \boldsymbol{\varphi}(\vec{\theta})^\dagger \nabla_{\vec{\theta}} \boldsymbol{\varphi}(\vec{\theta}), \\
&\boldsymbol{\varphi}(\vec{\theta}) = (\boldsymbol{\varphi}_1(\boldsymbol{k}_{(1,1)}), \boldsymbol{\varphi}_1(\boldsymbol{k}_{(1,2)}), \cdots, \boldsymbol{\varphi}_{N_{\rm b}}(\boldsymbol{k}_{(n_x/N, n_y/N)})),
\end{aligned}$$

where $\boldsymbol{\varphi}$ is the multiplet describing the ground state. Noting that the trace of the non-Abelian Berry curvature is given by $\mathrm{tr}\, \boldsymbol{f} = \mathrm{tr}\, (\nabla_{\vec{\theta}} \times \boldsymbol{a})_z$, we have

$$F = [\nabla_{\vec{\theta}} \times A]_z = [\nabla_{\vec{\theta}} \times (\mathrm{tr}\, \boldsymbol{a})]_z = \mathrm{tr}\, (\nabla_{\vec{\theta}} \times \boldsymbol{a})_z = \mathrm{tr}\, \boldsymbol{f}. \tag{1.49}$$

Then, let us now define the single-particle Abelian Berry connection and curvature with respect to the momentum $\boldsymbol{k}$ as

$$a'_\alpha(\boldsymbol{k}) = \varphi_\alpha(\boldsymbol{k})^\dagger \boldsymbol{\nabla}_{\boldsymbol{k}} \varphi_\alpha(\boldsymbol{k}) \tag{1.50}$$

$$f'_\alpha(\boldsymbol{k}) = [\nabla_{\boldsymbol{k}} \times a_\alpha(\boldsymbol{k})]_z. \tag{1.51}$$

Because of $\mathrm{tr}\, \boldsymbol{f} = (1/N^2)\sum_{\alpha=1}^{N_{\rm b}} \sum_{i_x=1}^{N/n_x} \sum_{i_y=1}^{N/n_y} f'_\alpha(\boldsymbol{k}_{(i_x,i_y)})$, [5] the many-body Chern number of the Niu-Thouless-Wu formula C is given by the sum of the band Chern number integrating

[5] We have

$$\begin{aligned}
\mathrm{tr}\, \boldsymbol{f} &= \mathrm{tr}\, (\nabla_{\vec{\theta}} \times \boldsymbol{a})_z \\
&= \mathrm{tr}\, (\nabla_{\vec{\theta}} \times (\boldsymbol{\varphi}^\dagger \nabla_{\vec{\theta}} \boldsymbol{\varphi}))_z \\
&= \frac{1}{N^2} \mathrm{tr}\, (\nabla_{\boldsymbol{k}} \times (\boldsymbol{\varphi}^\dagger \nabla_{\boldsymbol{k}} \boldsymbol{\varphi}))_z \\
&= \frac{1}{N^2} \sum_{\alpha=1}^{N_{\rm b}} \sum_{i_x=1}^{N/n_x} \sum_{i_y=1}^{N/n_y} f'_\alpha(\boldsymbol{k}_{(i_x,i_y)}).
\end{aligned}$$

on the magnetic Brillouin zone C_α as follows: [6]

$$C = \sum_{\alpha=1}^{N_\mathrm{b}} C_\alpha. \tag{1.52}$$

[6] We have

$$\begin{aligned}
C &= \frac{1}{2\pi i}\int_{T^2} d\theta^2 F \\
&= \frac{1}{2\pi i}\int_{T^2} d\theta^2 \,\mathrm{tr}\, \boldsymbol{f} \\
&= \frac{1}{2\pi i}\int_{T^2} \frac{d\theta^2}{N^2} \sum_{\alpha=1}^{N_\mathrm{b}} \sum_{i_x=1}^{N/n_x} \sum_{i_y=1}^{N/n_y} f'_\alpha(\boldsymbol{k}_{(i_x,i_y)}) \\
&= \frac{1}{2\pi i}\int_{T^2} \frac{d\theta^2}{N^2} \sum_{\alpha=1}^{N_\mathrm{b}} \sum_{i_x=1}^{N/n_x} \sum_{i_y=1}^{N/n_y} f'_\alpha\left(\frac{2\pi i_x+\theta_x}{N}, \frac{2\pi i_y+\theta_y}{N}\right) \\
&= \sum_{\alpha=1}^{N_\mathrm{b}} \frac{1}{2\pi i}\int_0^{2\pi/n_x}\int_0^{2\pi/n_y} dk_x dk_y f'_\alpha\left(k_x,k_y\right).
\end{aligned}$$

Chapter 2

One-plaquette Chern number

The many-body Chern number in the Niu-Thouless-Wu formula significantly works as a kind of order parameter in many-body problems. Its evaluation is significantly important in the study of correlated topological phases, where numerical approaches are often necessary but highly demanding. In this chapter, considering the Hofstadter problems with or without electron correlations, we numerically demonstrates that the integration in the many-body Chern number can be skipped if system sizes are sufficiently large. The lack of integration is practically important since it significantly reduces the computational cost. We also discuss its quantization in the vicinity of quantum phase transitions such as plateau transitions in the IQH effect.

2.1 Topological invariant without integration

The many-body Chern number in the Niu-Thouless-Wu formula is a generalization of the Chern number in the TKNN formula for many-body problems. Recently, a wide variety of topological phases in correlated systems has been identified by using the many-body Chern number [95–106]. As shown in the previous chapter, even though their expressions are almost same, the integration in the Niu-Thouless-Wu formula has different origin from that of the TKNN formula. The integration over the twisted angles of the boundary conditions is an average operation based on the assumption that the integrand, namely the Berry curvature, is insensitive to the boundary condition. Recent mathematical works [107–110] have revealed that the integration is indeed unnecessary since the Berry curvature at a fixed twisted angle is itself effectively quantized in thermodynamically large systems.

In this chapter, we investigate the validity of using the topological number without integration in practical problems numerically [111]. To demonstrate it, we introduce the "one-plaquette Chern number" as follows. In numerical calculations of the Chern number, one usually discretize the twisted angles $\vec{\theta} = (\theta_x, \theta_y)$ as

$$\theta_\mu = \frac{2\pi}{N_\theta} n_\mu \tag{2.1}$$

with $n_\mu = 1, 2, \cdots, N_\theta$. According to the Fukui-Hatsugai-Suzuki formula [112], the Chern number is exactly quantized even though the integration is replaced by a summation [see Fig. 2.1(a)]:

$$\mathcal{C} = \frac{1}{2\pi i} \sum_{\vec{\theta}} \mathcal{F}(\vec{\theta}), \tag{2.2}$$

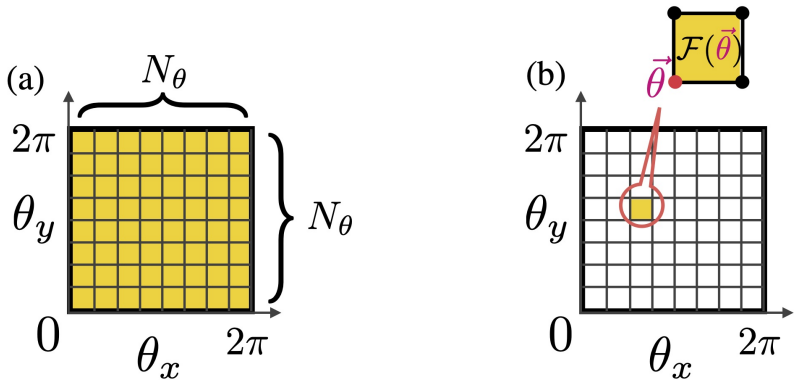

Figure 2.1: (a) Chern number and (b) one-plaquette Chern number.

where $\mathcal{F}(\vec{\theta})$ is the discretized Berry curvature as

$$\mathcal{F}(\vec{\theta}) = \log[U_x(\vec{\theta})U_y(\vec{\theta}+\delta_x)U_x(\vec{\theta}+\delta_y)^{-1}U_y(\vec{\theta})^{-1}],$$
$$U_\mu(\vec{\theta}) = \det\left[\Phi^\dagger(\vec{\theta})\Phi(\vec{\theta}+\delta_\mu)\right] / \left|\det\left[\Phi^\dagger(\vec{\theta})\Phi(\vec{\theta}+\delta_\mu)\right]\right|,$$

and Φ is the ground state multiplet. Here, $\delta_x = (\frac{2\pi}{N_\theta}, 0)$ and $\delta_y = (0, \frac{2\pi}{N_\theta})$. Note that the discretized Berry curvature $\mathcal{F}(\vec{\theta})$ is a gauge-invariant even if one does not fix the phases of $\Phi(\vec{\theta})$. By using it, we define the one-plaquette Chern number [see Fig. 2.1(b)] as

$$\mathcal{C}(\vec{\theta}) = \frac{1}{2\pi i} N_\theta^2 \mathcal{F}(\vec{\theta}). \tag{2.3}$$

Due to the absence of the summation, $\mathcal{C}$ can be any real number. In the next sections, we numerically show that $\mathcal{C}$ of the IQH and FQH systems on lattices is almost quantized and it gives exponential accuracy with respect to the system size.

2.2 Exponential accuracy of the one-plaquette Chern number

2.2.1 Noninteracting case

Model

We first consider the one-plaquette Chern number in the IQH systems. This discussion is important for the successive discussion of FQH systems. In the following, we set $N_\theta = 20$ unless otherwise stated. Let us consider the system of spin-polarized electrons on a square lattice under a uniform magnetic field. The system size is set as $N \times N$ sites. The Hamiltonian is given by

$$H = -t \sum_{\langle ij \rangle} e^{i\phi_{ij}} c_i^\dagger c_j, \tag{2.4}$$

where $t > 0$ is a hopping parameter, $c_i^\dagger$ (c_i) is the creation (annihilation) operator on site i, ϕ_{ij} is the Peierls phase that describes the magnetic field. Here, the twisted boundary conditions are imposed, i.e.,

$$c^\dagger_{n_x+N,n_y} = e^{i\theta_x} c_{n_x,n_y}$$
$$c^\dagger_{n_x,n_y+N} = e^{i\theta_y} c_{n_x,n_y}.$$

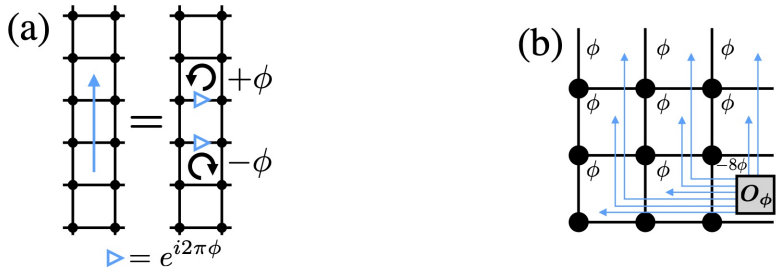

Figure 2.2: (a) String with the flux ϕ. (b) Sketches of 3×3 square lattice with the string gauge ϕ_{ij}.

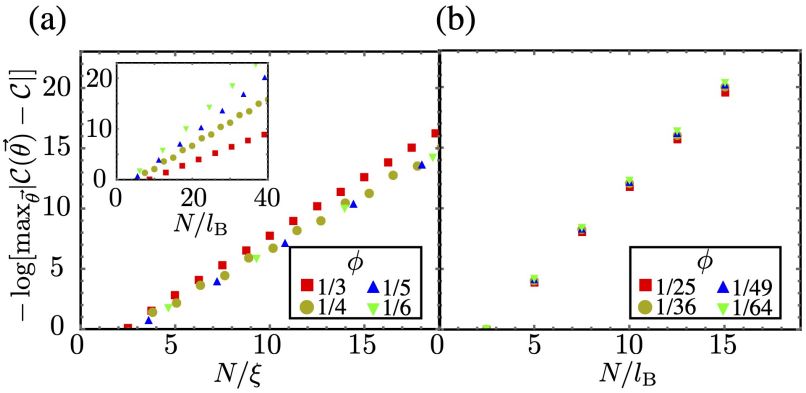

Figure 2.3: The difference of $\mathcal{C}$ and $\mathcal{C}(\vec{\theta})$ is shown as a function of the system size (a) N/ξ and (b) $N/l_{\rm B}$. The inset in (a) shows $N/l_{\rm B}$-dependence of $\mathcal{C}(\vec{\theta})$ in a strong magnetic field for comparison.

As for the Peierls phase ϕ_{ij}, the string gauge [113] is employed. Let us here explain it shortly. Let us consider a string as shown in Fig. 2.2(a) on sites and assign the phases $e^{i2\pi\phi}$. They give the magnetic fluxes $+\phi$ and $-\phi$ at the plaquette with the initial and terminal points of the string. Therefore, the gauge described by the strings shown in Fig. 2.2(b) gives the flux $\phi \times (1 - N^2)$ into the plaquette that has the origin O_ϕ while ϕ to the other plaquettes. The condition for the uniform magnetic field is given by $e^{i2\pi\phi(1-N^2)} = e^{i2\pi\phi}$, i.e.,

$$\phi = \frac{N_\phi}{N^2}, \ N_\phi = 1, 2, \cdots, N^2, \tag{2.5}$$

where N_ϕ corresponds to the total magnetic flux. When the number of fluxes per plaquette is set as $\phi = p/q$ with p and q being coprime, the system provides q single-particle bands. Since the p low-energy bands, where each band has N^2/q one-body states, gives the lowest Landau level in the continuum limit, the lowest Landau band is defined as a group of these $(N^2/q)p = N_\phi$ states. Thus, we define the filling factor for the Landau band as

$$\nu = N_{\rm e}/N_\phi, \tag{2.6}$$

where $N_{\rm e}$ is the number of electrons.

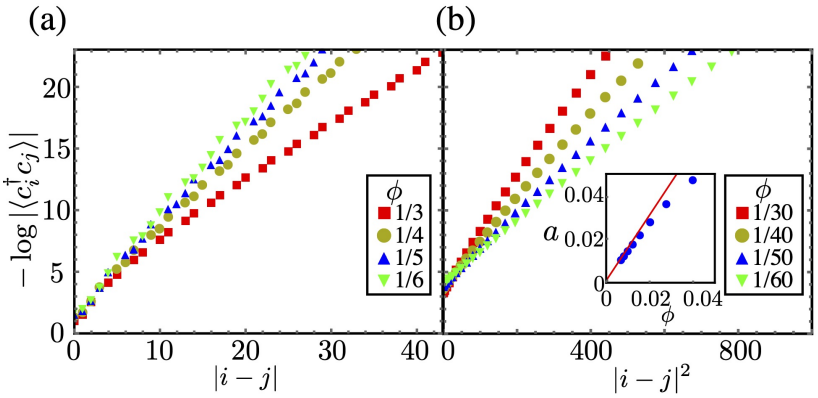

Figure 2.4: The correlation functions $|\langle c_i^\dagger c_j\rangle|$ are shown as functions of the distance $|i-j|$ in (a) a strong magnetic field and (b) a weak magnetic field. For $\phi = 1/q$, the system size is set as (a) $N = 30q$ and (b) $N = 3q$. The inset in (b) shows the exponent $a(\phi)$ with weak magnetic fields. The red line shows $1/(4l_{\rm B}^2) = \pi\phi/2$.

One-plaquette Chern number

Here, we consider the system at $\nu = 1$. The ground state is given by occupying the lowest Landau band completely:

$$\Phi(\vec{\theta}) = \prod_{k=1}^{N_\phi} d_k^\dagger(\vec{\theta})\,|0\rangle\,, \tag{2.7}$$

where $d_k^\dagger(\vec{\theta}) = \boldsymbol{c}^\dagger\psi_k(\vec{\theta})$ is the creation operator of the corresponding state k belonging to the lowest Landau band, $\boldsymbol{c}^\dagger = (c_1^\dagger, \cdots, c_{N^2}^\dagger)$, and ψ_k is the eigenvector of the Hamiltonian H. In Fig. 2.3, $\max_{\vec{\theta}}|\mathcal{C}(\vec{\theta}) - \mathcal{C}|$ is shown as a function of the system size under (a) a strong magnetic field $\phi \approx 1$ and (b) a weak magnetic field $\phi \ll 1$. Here, $\max_{\vec{\theta}}$ indicates the maximum value over all $N_\theta^2 = 400$ plaquettes. This result implies the exponential accuracy of the one-plaquette Chern number as follows:

$$|\mathcal{C}(\vec{\theta}) - \mathcal{C}| < Ae^{-cN} \tag{2.8}$$

where A and c are some coefficients. It means that for sufficient large systems, the one-plaquette Chern number works well as the quantized topological number. Here, the coefficient c is proportional to $1/\xi$ or $1/l_{\rm B}$. Since the correlation length ξ and the magnetic length $l_{\rm B}$ generally become smaller if the energy gap increases, the quantization of the one-plaquette Chern number is closely related to the energy gap.

In Fig. 2.3(a), the system size N is rescaled by the correlation length ξ in a strong magnetic field and the magnetic length $l_{\rm B} = \sqrt{1/(2\pi\phi)}$ in a weak magnetic field. The correlation length ξ is extracted from the correlation function $\langle c_i^\dagger c_j\rangle$. In Fig. 2.4(a), we plot $|\langle c_i^\dagger c_j\rangle|$ in a strong magnetic field $\phi = 1/q$ ($q = 3, 4, 5.6$). It implies that they obey

$$|\langle c_i^\dagger c_j\rangle| \propto e^{-\frac{|i-j|}{\xi(N)}}. \tag{2.9}$$

Using these data, we determine $\xi(N)$ for each ϕ by extrapolation. Here, some singular points appears at $|i-j| = q, 2, \cdots$, which we do not use to obtain $\xi(N)$. Then, we repeat this process for several system sizes $100 \le N \le 200$ and calculate ξ in the thermodynamic

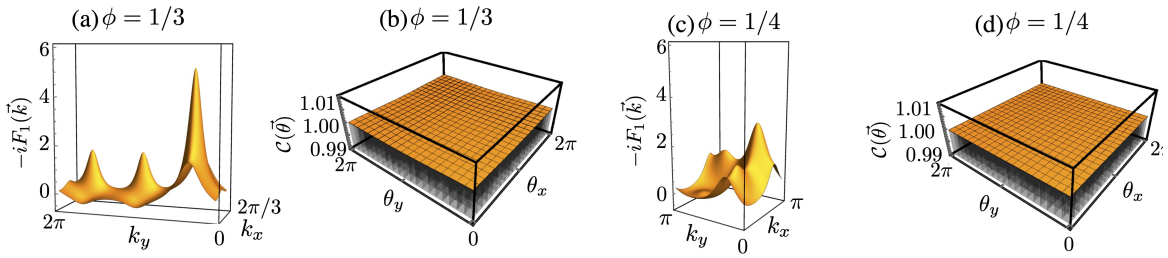

Figure 2.5: (a)(c)Single-particle Berry curvature and (b)(d)one-plaquette Chern number.

limit. In Fig. 2.3(a), we use the obtained thermodynamic value to rescale the system size. In the inset of Fig. 2.3(a), the results with respect to the system size scaled by $l_{\rm B}$ are shown. Clearly, the property that all data collapse nicely as shown in Fig. 2.3(a) is lost. In a weak magnetic field, on the other hand, the behavior of the correlation function $|\langle c_i^\dagger c_j\rangle|$ is different from that in a strong one, which we can see in Fig. 2.4(b). For each value of ϕ, they obey

$$|\langle c_i^\dagger c_j\rangle| \propto e^{-a(N)|i-j|^2}. \tag{2.10}$$

By the extrapolation as we did in a strong magnetic field, we calculate the coefficient $a(N)$ and evaluate the thermodynamic value as $a = \lim_{N\to\infty} a(N)$. In the inset of Fig. 2.4(b), we show it as a function of ϕ. The red line in the figure indicates $1/(4l_{\rm B}^2) = \pi\phi/2$, which corresponds to the behavior in the continuum limit as [114]

$$|\langle c^\dagger(z)c(z')| = (\nu/(2\pi l_{\rm B}^2))e^{-\frac{1}{4}|z-z'|^2}, \tag{2.11}$$

where $z = (x - iy)/l_{\rm B}$. In the weak magnetic field limit, our numerical values of a in the inset approaches to it, which justifies the use of $l_{\rm B}$ to rescale the system size in Fig. 2.3(b).

Before moving to the interacting problems, let us here discuss the exponential behavior in terms of the Euler-Maclaurin formula. In Fig. 2.5(a) and (c), we plot the single-particle Berry curvature $F_1(\vec{k})$ for $\phi = 1/3$ and $\phi = 1/4$, where the magnetic unit cell is given by 3×1 and 2×2, respectively. Even though the single-particle Berry curvature exhibits a strong dependence on the momentum $\vec{k}$, the one-plaquette Chern number is insensitive to the value of $\vec{\theta}$ as shown in Fig. 2.5(b) and (d), where we set the system size as $N = 24$. This insensitivity can be explained from the Euler-Maclaurin formula [115]. [1] Choosing the magnetic unit cell with the size $n_x \times n_y$, the Chern number and the one-plaquette Chern

[1] According to the Euler-Maclaurin formula [115], the difference between an integral of a function $F(x)$ and a related sum is given by

$$\begin{aligned}&\left[\sum_{k=0}^{m} F(a+kh) - \frac{1}{2}\left(F(b)+F(a)\right)\right] - \frac{1}{h}\int_a^b F(t)dt \\ &= \sum_{k=1}^{n-1} \frac{h^{2k-1}}{(2k)!} B_{2k}\left\{F^{(2k-1)}(b) - F^{(2k-1)}(a)\right\} + \frac{h^{2n}}{(2n)!} B_{2n} \sum_{k=0}^{m-1} F^{(2n)}(a+kh+\theta h),\end{aligned} \tag{2.12}$$

where the interval $[a, b]$ is divided into m equal parts, $h = (b-a)/m$, θ is a real with $0 \le \theta \le 1$, and B_n is the nth Bernoulli number.

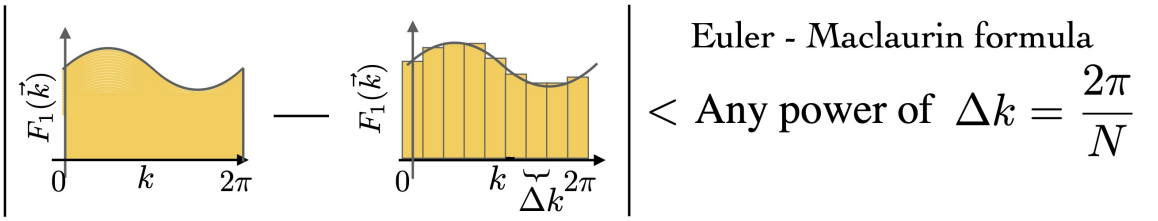

Figure 2.6: Conceptual diagram of the difference between the Chern number $\mathcal{C}$ and the one-plaquette Chern number $\mathcal{C}$.

number are expressed as

$$\mathcal{C} = C = \frac{1}{2\pi i}\int_0^{2\pi/n_x} dk_x \int_0^{2\pi/n_y} dk_y F_1(\boldsymbol{k}) \tag{2.13}$$

$$\mathcal{C}(\vec{\theta}) \approx \frac{2\pi}{iN^2}\sum_{i_x=1}^{N/n_x}\sum_{i_y=1}^{N/n_y} F_1(\frac{2\pi i_x+\theta_x}{N}, \frac{2\pi i_y+\theta_y}{N}). \tag{2.14}$$

It implies that the one-plaquette Chern number approximates the quantized Chern number by replacing the integral over the Brillouin zone with the Riemann sum, see Fig. 2.6. Here, the representative points in the Brillouin zone are specified by the twisted angles $\vec{\theta}$. Since the Brillouin zone is a torus, the boundary contribution of the Euler-Maclaurin formula is vanishing if assuming $F_1(\vec{k})$ is a smooth function. It suggests that the error due to the discretization is smaller than any powers of the system size [116], which implies the exponential accuracy of $\mathcal{C}(\vec{\theta})$.

2.2.2 Interacting case

Let us now move onto the discussions on the validity of the one-plaquette Chern number in the FQH effect. In the following, we first describe our model and how to construct the pseudopotentials for effectively investigating the correlation effects. After giving arguments about the lattice analogue of Laughlin state accompanied by the topological degeneracy, we discuss the exponential accuracy of the one-plaquette Chern number.

Model

Let us here consider the Hamiltonian $H = H_{\text{kin}} + H_{\text{int}}$ with

$$H_{\text{kin}} = -t\sum_{\langle ij\rangle} e^{i\phi_{ij}} c_i^\dagger c_j \tag{2.15}$$

$$H_{\text{int}} = V\sum_{\langle ij\rangle} n_i n_j. \tag{2.16}$$

In order to reduce the computational costs inherent to the many-body problems, we construct the pseudopotentials [16, 117–119] that enable us to treat the electron-electron interactions within the lowest Landau level. Constructing the projection matrix $P(\vec{\theta})$ into the lowest Landau band by using the lowest eigenvectors belonging to that band as

$$P(\vec{\theta}) = \psi(\vec{\theta})\psi^\dagger(\vec{\theta}), \tag{2.17}$$

where $\psi = (\psi_1, \cdots, \psi_{N_\phi})$, we define the projected creation operators:

$$\tilde{\boldsymbol{c}}^\dagger(\vec{\theta}) = (\tilde{c}_1(\vec{\theta}), \cdots, \tilde{c}_{N^2}(\vec{\theta})) = \boldsymbol{c}^\dagger P(\vec{\theta}). \tag{2.18}$$

Note that the canonical anticommutations for these projected operators are no longer satisfied. Replacing $c_i^\dagger$, c_j with $\tilde{c}_i^\dagger$, $\tilde{c}_j$, one get the pseudopotentials projected into the lowest Landau band as

$$\begin{aligned}\tilde{H}_{\text{int}}(\vec{\theta}) &= V \sum_{\langle ij \rangle} \tilde{c}_i^\dagger(\vec{\theta}) \tilde{c}_j^\dagger(\vec{\theta}) \tilde{c}_j(\vec{\theta}) \tilde{c}_i(\vec{\theta}) \\ &= \sum_{klmn} V_{klmn}(\vec{\theta}) d_k^\dagger(\vec{\theta}) d_l^\dagger(\vec{\theta}) d_m(\vec{\theta}) d_n(\vec{\theta}),\end{aligned} \tag{2.19}$$

where $V_{klmn} = V \sum_{\langle ij \rangle} (\psi_k)_i^* (\psi_l)_j^* (\psi_m)_j (\psi_n)_i$, and the summation is restricted to the states of the lowest Landau band. Choosing the strength of the interaction V in such a way that the typical energy scale of the electron-electron interactions is much larger than the energy width of the lowest Landau band but still sufficiently smaller than the band gap of the Landau bands, the ground state of the Hamiltonian is approximately given by diagonalizing the pseudopotential $\tilde{H}_{\text{int}}$. When taking the following orthonormal basis for diagonalizing the pseudopotential $\tilde{H}_{\text{int}}$ as

$$\Psi(\vec{\theta}) = (\left|\Psi_1(\vec{\theta})\right\rangle, \left|\Psi_2(\vec{\theta})\right\rangle, \cdots, \left|\Psi_{N_{\text{dim}}}(\vec{\theta})\right\rangle), \tag{2.20}$$

$$\left|\Psi_i(\vec{\theta})\right\rangle = \prod_{k=1}^{N_{\text{e}}} d_{i_k}^\dagger(\vec{\theta}) \left|0\right\rangle, \tag{2.21}$$

where $N_{\text{dim}} =_{N_\phi} C_{N_{\text{e}}}$, we have the eigenvalue equation

$$\tilde{h}_{\text{int}}(\vec{\theta}) \boldsymbol{u}_i(\vec{\theta}) = \tilde{E}_i(\vec{\theta}) \boldsymbol{u}_i(\vec{\theta}). \tag{2.22}$$

Here, $\tilde{h}_{\text{int}}(\vec{\theta}) = \Psi^\dagger(\vec{\theta}) \tilde{H}_{\text{int}} \Psi(\vec{\theta})$ is a $N_{\text{dim}} \times N_{\text{dim}}$ matrix. Then, the ground state is given by

$$\left|G_k(\vec{\theta})\right\rangle = \Psi(\vec{\theta}) \boldsymbol{u}_k(\vec{\theta}). \tag{2.23}$$

The overlap between the ground states specified by different twisted angles, $\vec{\theta}$ and $\vec{\theta}'$, is given by

$$\left\langle G_k(\vec{\theta}) \middle| G_l(\vec{\theta}') \right\rangle = \boldsymbol{u}_k^\dagger(\vec{\theta}) O(\vec{\theta}, \vec{\theta}') \boldsymbol{u}_k(\vec{\theta}'), \tag{2.24}$$

where $O(\vec{\theta}, \vec{\theta}') = \Psi^\dagger(\vec{\theta}) \Psi(\vec{\theta}')$ is a matrix for correction and its element is given by

$$O_{ij}(\vec{\theta}, \vec{\theta}') = \det\left[\tilde{\psi}_i^\dagger(\vec{\theta}) \tilde{\psi}_j(\vec{\theta}')\right], \tag{2.25}$$

where $\tilde{\psi}_i = (\psi_{i_1}, \cdots, \psi_{i_{N_{\text{e}}}})$ is the multiplet composed of the single-particle wave functions of the lowest Landau band chosen by the many-body basis $\left|\Psi_i(\vec{\theta})\right\rangle$. By evaluating the link variable U_μ in this way [103, 112], we compute the one-plaquette Chern number.

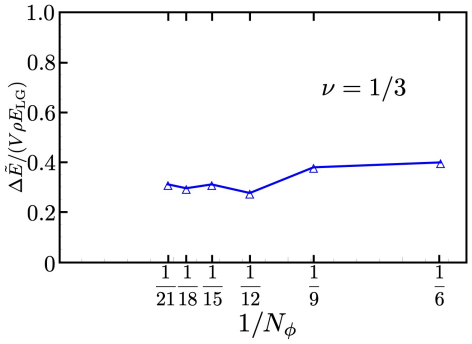

Figure 2.7: The energy gap at $\nu = 1/3$ are shown as functions of the total number of fluxes N_ϕ. The ground states are always three-fold quasidegenerated.

Lattice analogue of the Laughlin state

Within the above framework, we plot in Fig. 2.7 the energy gap at $\nu = 1/3$ as a function of the total number of fluxes N_ϕ. Here, we set $N = 3N_{\rm e}$ and $\phi = 1/N$ with $N_{\rm e} = 2, 3, \cdots, 7$. The energy gap is scaled by $V\rho E_{\rm LG}$, where $\rho = N_{\rm e}/N^2$ and $E_{\rm LG}$ is the Landau gap of the non-interacting case [103]. Since the ground states always give the three-fold topological degeneracy, we plot the excitation gap defined by the fourth excited states. The figure indicates that the energy gap is finite for the large N_ϕ limit. Furthermore, the Chern number of the three-fold degenerated ground sates is one, which is consistent with the lattice analogue of the Laughlin state [12].

Before moving to the arguments about the one-plaquette Chern number, let us show that the degeneracy is derived from the translational invariance of the lattice model [120]. We first rewrite the kinetic term of the Hamiltonian as

$$H_{\rm kin} = -t\sum_{n=1}^{N_x}\sum_{m=1}^{N_y}\left(e^{i\phi^x_{n,m}}c^\dagger_{n+1,m}c_{n,m} + te^{i\phi^y_{n,m}}c^\dagger_{n,m+1}c_{n,m}\right). \tag{2.26}$$

Let us assume that the Landau gauge is employed for the Peierls phase $\phi^\alpha_{n,m}$ ($\alpha = x, y$), i.e.,

$$\phi^x_{n,m} = 0,\ \phi^y_{n,m} = 2\pi\phi n. \tag{2.27}$$

It implies that the magnetic flux is given by $\phi = n/N_x$ with n being an integer. In Fig. 2.8(a), the sketch of the Landau gauge is given.

Let us now define a translations operator $T(a, b)$ as

$$T(a,b)c^\dagger_{n,m}T(a,b)^\dagger = c^\dagger_{n+a,m+b}. \tag{2.28}$$

Using it, we define a new Hamiltonian as $H'_{\rm kin} = T(1,0)H_{\rm kin}T(1,0)^\dagger$. This transformation is expressed as

$$\begin{aligned}
H'_{\rm kin} &= \sum_{n=1}^{N_x}\sum_{m=1}^{N_y}\left(te^{i\phi^x_{n,m}}c^\dagger_{n+2,m}c_{n+1,m} + te^{i\phi^y_{n,m}}c^\dagger_{n+1,m+1}c_{n+1,m}\right)\\
&= \sum_{n=2}^{N_x+1}\sum_{m=1}^{N_y}\left(te^{i\phi^x_{n-1,m}}c^\dagger_{n+1,m}c_{n,m} + te^{i\phi^y_{n-1,m}}c^\dagger_{n,m+1}c_{n,m}\right)\\
&= \sum_{n=1}^{N_x}\sum_{m=1}^{N_y}\left(te^{i\phi^x_{n-1,m}}c^\dagger_{n+1,m}c_{n,m} + te^{i\phi^y_{n-1,m}}c^\dagger_{n,m+1}c_{n,m}\right),
\end{aligned} \tag{2.29}$$

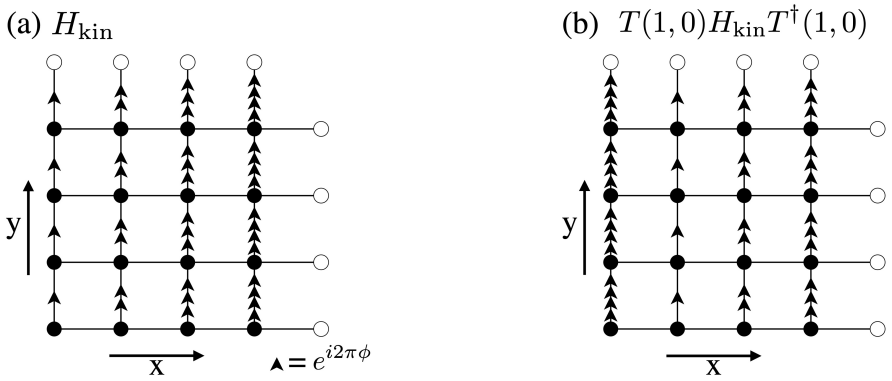

Figure 2.8: Sketches of 4×4 square lattices with the Landau gauge.

where we have used the relation $e^{\phi^x_{N_x,m}} = e^{\phi^x_{0,m}}$ at the last part. From Fig. 2.8, one can confirm that $H'_{\rm kin}$ is not identical to $H_{\rm kin}$ but related to $H_{\rm kin}$ by a gauge transformation. Indeed, defining a local gauge transformation U_G as

$$U_G c^\dagger_{n,m} U_G^\dagger = e^{-i2\pi\phi m} c^\dagger_{n,m}, \tag{2.30}$$

we have

$$\begin{aligned} U_G H_{\rm kin} U_G^\dagger &= \sum_{n=1}^{N_x}\sum_{m=1}^{N_y} U_G \left(t e^{i\phi^x_{n,m}} c^\dagger_{n+1,m} c_{n,m} + t e^{i\phi^y_{n,m}} c^\dagger_{n,m+1} c_{n,m} \right) U_G^\dagger \\ &= \sum_{n=1}^{N_x}\sum_{m=1}^{N_y} \left(t e^{i\phi^x_{n,m}} c^\dagger_{n+1,m} c_{n,m} + t e^{i\phi^y_{n,m}} e^{-i2\pi\phi} c^\dagger_{n,m+1} c_{n,m} \right) \\ &= H'_{\rm kin}, \end{aligned} \tag{2.31}$$

where $\phi^x_{n,m} = \phi^x_{n-1,m} = 0$ and $\phi^y_{n,m} - 2\pi\phi = \phi^y_{n-1,m}$ have been used. These relations imply $U_G H_{\rm kin} U_G^\dagger = T(1,0) H_{\rm kin} T^\dagger(1,0)$, i.e.,

$$[H_{\rm kin}, T^\dagger(1,0) U_G]. \tag{2.32}$$

On the other hand, the Hamiltonian $H_{\rm kin}$ also commutes $T(0,1)$. Thus, the eigenvectors of $H_{\rm kin}$ is specified by $T(0,1)$ as follows:

$$H_{\rm kin}|k_y\rangle_l = E_l(k_y)|k_y\rangle_l \tag{2.33}$$

$$T(0,1)|k_y\rangle_l = e^{ik_y}|k_y\rangle_l, \tag{2.34}$$

where $k_y = 2\pi n_y/N_y$ ($n_y = 1, \cdots, N_y$) is the Bloch wave number and l is the index of bands. Let us then expand the single-particle state $|k_y\rangle_l$ as

$$|k_y\rangle_l = \sum_{n=1}^{N_x}\sum_{m=1}^{N_y} \psi^l_{n,m} c^\dagger_{n,m}|0\rangle, \tag{2.35}$$

where $\psi^l_{n+N_x,m} = \psi^l_{n,y+N_y} = \psi^l_{n,m}$. Equation (2.34) reduces to

$$T(0,1)|k_y\rangle_l = \sum_{n=1}^{N_x}\sum_{m=1}^{N_y} \psi^l_{n,m} c^\dagger_{n,m+1}|0\rangle = \sum_{n=1}^{N_x}\sum_{m=1}^{N_y} \psi^l_{n,m-1} c^\dagger_{n,m}|0\rangle. \tag{2.36}$$

It implies $\psi^l_{n,m-1} = e^{ik_y}\psi^l_{n,m}$. By using these relations, let us now consider the state $T^\dagger(1,0)U_G\,|k_y\rangle_l$. We have

$$\begin{aligned}
T(0,1)T^\dagger(1,0)U_G|k_y\rangle_l &= T(0,1)T^\dagger(1,0)\sum_{n=1}^{N_x}\sum_{m=1}^{N_y} e^{-i2\pi\phi m}\psi^l_{n,m}c^\dagger_{n,m}|0\rangle \\
&= \sum_{n=1}^{N_x}\sum_{m=1}^{N_y} e^{-i2\pi\phi m}\psi^l_{n,m}c^\dagger_{n-1,m+1}|0\rangle \\
&= \sum_{n=1}^{N_x}\sum_{m=2}^{N_y+1} e^{-i2\pi\phi(m-1)}\psi^l_{n,m-1}c^\dagger_{n-1,m}|0\rangle \\
&= \sum_{n=1}^{N_x}\sum_{m=1}^{N_y} e^{-i2\pi\phi(m-1)}\psi^l_{n,m-1}c^\dagger_{n-1,m}|0\rangle + |R\rangle, \\
&= e^{i2\pi\phi}e^{ik_y}\sum_{n=1}^{N_x}\sum_{m=1}^{N_y} e^{-i2\pi\phi m}\psi^l_{n,m}c^\dagger_{n-1,m}|0\rangle + |R\rangle \\
&= e^{i2\pi\phi+ik_y}T^\dagger(1,0)U_G|k_y\rangle_l + |R\rangle, \qquad (2.37)
\end{aligned}$$

where the ket $|R\rangle$ is written as

$$\begin{aligned}
|R\rangle &= \sum_{n=1}^{N_x} e^{-i2\pi\phi N_y}\psi^l_{n,N_y}c^\dagger_{n-1,N_y+1}|0\rangle - \sum_{n=1}^{N_x}\psi^l_{n,0}c^\dagger_{n-1,1}|0\rangle \\
&= \sum_{n=1}^{N_x}\psi^l_{n,N_y}\left(e^{-i2\pi\phi N_y}-1\right)c^\dagger_{n-1,1}|0\rangle. \qquad (2.38)
\end{aligned}$$

It means that if $e^{-i2\pi\phi N_y}=1$, the state $T^\dagger(1,0)U_G\,|k_y\rangle_l$ is an eigenvector of $T(0,1)$, i.e.,

$$T^\dagger(1,0)U_G\,|k_y\rangle_l = |k_y+\Delta k_y\rangle\,, \qquad (2.39)$$

where $\Delta k_y = 2\pi\phi$. For example, the system satisfying $N_x = N_y$ gives $\phi N_y = 1$, which meets the above condition.

Equation (2.39) provides a proof of existence of topological degeneracy exhibited by many-electron systems. Let us assume that the magnetic flux $\phi = N_\phi/(N_xN_y)$ is written as $\phi = n/N_x$ and $\phi = n'/N_y$ with n and n' being integers, i.e., the number of the total flux satisfies $N_\phi = nN_y = n'N_x$. Setting the filling factor as $\nu < 1$, let us take the basis that spans the subspace projected into the lowest Landau band by $\left|k_y^1,\cdots,k_y^{N_\mathrm{e}}\right\rangle$. Because of $[H_\mathrm{int}, T(0,1)] = 0$, the Hamiltonian H_int is block-diagonalized with respect to the total wave number defined as $K_y = \sum_{i=1}^{N_e} k_y^i$. Noting that $[H_\mathrm{int}, T^\dagger(1,0)U_G] = 0$, we have

$$\begin{aligned}
&\langle k_y'^1,\cdots,k_y'^{N_e}|H_\mathrm{int}|k_y^1,\cdots,k_y^{N_e}\rangle \\
=&\langle k_y'^1,\cdots,k_y'^{N_e}|U_G^\dagger T(1,0)H_\mathrm{int}T^\dagger(1,0)U_G|k_y^1,\cdots,k_y^{N_e}\rangle \\
=&\langle k_y'^1+\Delta k_y,\cdots,k_y'^{N_e}+\Delta k_y|H_\mathrm{int}|k_y^1+\Delta k_y,\cdots,k_y^{N_e}+\Delta k_y\rangle, \qquad (2.40)
\end{aligned}$$

This implies that the block Hamiltonian of H_int specified by the total wave number K_y is essentially equivalent to that by $K_y + \Delta K_y$, where

$$\Delta K_y = \Delta k_y \times N_\mathrm{e} = 2\pi\phi N_\mathrm{e} = 2\pi\frac{N_\phi N_\mathrm{e}}{N_xN_y} = 2\pi nn'\frac{N_\mathrm{e}}{N_\phi} = 2\pi nn'\nu. \qquad (2.41)$$

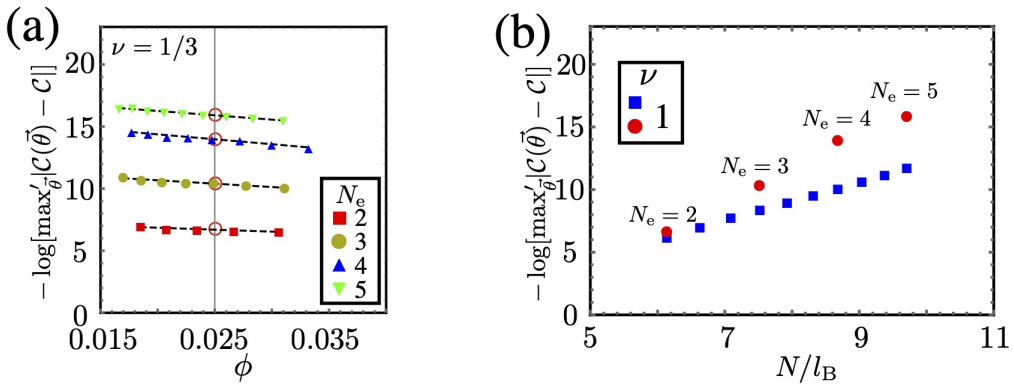

Figure 2.9: (a) Difference between the one-plaquette Chern number and the quantized Chern number at $\nu = 1/3$. The dashed lines are given by the linear approximation. The red circles indicates the values at $\phi = 0.025$. In panel (b), the values obtained in (a) at $\phi = 0.025$ are shown as functions of the scaled system size N/l_B.

When setting the parameters as $N_x = N_y = N_\phi$ and $\phi = 1/N_\phi$, we have $\Delta K_y = 2\pi\nu$. It means that the many-body state at $\nu = p/q$ (p, q:coprimes) exhibits at least q-fold degeneracy. This discussion can be applied to the problem of the pseudopotential $\tilde{H}_{\rm int}$ since we have

$$\left\langle k_y^1, \cdots, k_y^{N_e} \right| H_{\rm int} \left| k_y^1, \cdots, k_y^{N_e} \right\rangle = \left\langle k_y^1, \cdots, k_y^{N_e} \right| \tilde{H}_{\rm int} \left| k_y^1, \cdots, k_y^{N_e} \right\rangle . \tag{2.42}$$

One-plaquette Chern number

Let us investigate the accuracy of the one-plaquette Chern number of the FQH states. Here, the three-fold degenerated ground state multiplets at $\nu = 1/3$ are considered. An ideal way to investigate the system size dependence of the one-plaquette Chern number is that we compute $\mathcal{C}(\vec{\theta})$ as a function of N with fixing the magnetic flux ϕ to a certain value as we did in the subsection of the noninteracting case. However, this way requires huge computational resources and it is indeed difficult to do it in our numerical calculation. To overcome this difficulty, we use the scaling lows observed in the previous subsection. In Fig. 2.9(a), we plot $\max'_{\vec{\theta}}|\mathcal{C}(\vec{\theta}) - \mathcal{C}|$ at $\nu = 1/3$ as function of ϕ, where $\max'_{\vec{\theta}}$ indicates the maximum value over randomly chosen 20 plaquettes in $N_\theta^2 = 400$ ones. In this calculation to generate this figure, we change the system size N with fixing the particle number N_e and the total flux number N_ϕ, which brings the modification of the flux per plaquette $\phi = N_\phi/N^2$. Deducing the values of the one-plaquette Chern number at $\phi = 0.025$ from this figure based on the linear extrapolation, we generate Fig. 2.9(b) in which the accuracy are shown as functions of the scaled system size $N/l_B = \sqrt{2\pi N_\phi}$. Since the considered systems are in a weak magnetic field, the system size is rescaled by the magnetic length. The numerical result implies that the one-plaquette Chern number given by the FQH states is also quantized for a sufficiently large system size. In Fig. 2.9(b), the same calculation of the IQH state is repeated as a sanity check of our calculation process, which is consistent with the results given in the previous subsection.

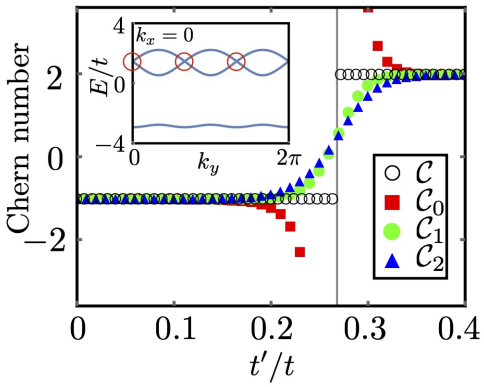

Figure 2.10: Chern number and one-plaquette Chern numbers as functions of the ratio t'/t. The inset shows the band structure at $t'/t = 2-\sqrt{3}$. Red circles indicates the band touching points.

2.3 Quantum phase transitions and the one-plaquette Chern number

2.3.1 NNN model

Let us here investigate the validity of using the one-plaquette Chern number for systems in which the excitation gap closes. To demonstrate it, we consider two systems: NNN model and disordered system. In this subsection, we focus on the problem of the NNN model.

We consider the Hamiltonian with the nearest-neighbor and next nearest-neighbor hoppings as follows:

$$H = -t\sum_{\langle ij\rangle} e^{i\phi_{ij}} c_i^\dagger c_j - t'\sum_{\langle\langle ij\rangle\rangle} e^{i\phi'_{ij}} c_i^\dagger c_j. \tag{2.43}$$

For $\phi = 1/3$ and $\nu = 2$, we have the phase transition at $t'/t = 2-\sqrt{3} \approx 0.268$, where the Chern number jumps from -1 to 2 [121].

As shown in the inset of Fig. 2.10, the band gap for $t'/t = 2-\sqrt{3}$ closes at $\vec{k} = (0,0), (0,2\pi/3), (0,4\pi/3)$. Correspondingly, the Berry curvature exhibits sharp peaks at those points. As discussed above, the one-plaquette Chern numbers in noninteracting problem are given by the sum of the single-particle Berry curvature over the discretized Brillouin zone, where the choice of the representative points are decided to the system size N and the twisted angles $\vec{\theta}$. This fact implies that the one-plaquette Chern number in this problem strongly depends on $\vec{\theta}$, i.e., the choice of the plaquette. In Fig. 2.10, we plot the three types of the one-plaquette Chern number, $\mathcal{C}_0 = \mathcal{C}(0,0)$, $\mathcal{C}_1 = \mathcal{C}(\pi,0)$, and $\mathcal{C}_2 = \mathcal{C}(\pi,\pi)$, as functions of the ratio t'/t. Here, we set $N = 30$. Only the one-plaquette Chern number $\mathcal{C}_0$ diverges near $t'/t = 2-\sqrt{3}$ while $\mathcal{C}_1$ and $\mathcal{C}_2$ do not, which is consistent with that the sum only in $\mathcal{C}_0$ includes the points of the Berry curvature peaks. On the other hand, $\mathcal{C}_1$ and $\mathcal{C}_2$ also do not work well as the topological invariant around $t'/t = 2-\sqrt{3}$ compared to the quantized Chern number $\mathcal{C}$. Generally, the energy gap becomes small near the phase transition point and it induces the increase of the correlation length. This means that the scaled system size becomes smaller even if the system size is fixed itself, which breaks the quantization of the one-plaquette Chern number.

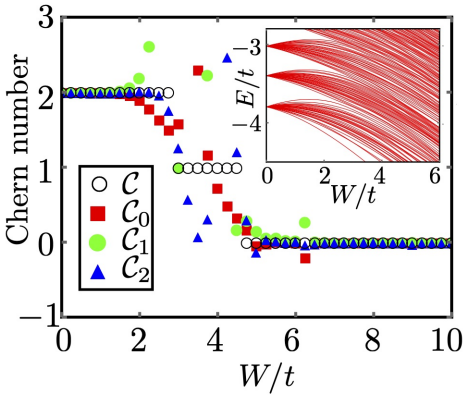

Figure 2.11: Chern number and one-plaquette Chern numbers as functions of the ratio W/t. The inset shows the randomness strength dependence of the single-particle energy.

2.3.2 Disordered system

Let us next consider the system in which a strong disorder is presence. The Hamiltonian that we consider is

$$H = -t \sum_{\langle ij \rangle} e^{i\phi_{ij}} c_i^\dagger c_j + \sum_i w_i n_i, \tag{2.44}$$

where w_i is the on-site potential at site i. It represents uniform random numbers between $[-W/2, W/2]$, where W is the strength of the randomness. Generally, due to the random potentials, most of single-particle states are localized. As its strength increases, extended states, which carry the nonzero Chern number, float up in spectra and the ground state becomes the Anderson insulator when the all extended states go across the Fermi level [113, 122–126]. This phase transition is confirmed in Fig. 2.11, where the QH state with the quantized Chern number $\mathcal{C} = 2$ becomes the Anderson insulator with $\mathcal{C} = 0$ as the value of W increases. In Fig. 2.11, we also plot the one-plaquette Chern numbers. It indicates that they work well in the two situations: the quantum Hall states in a small W and Anderson insulating states in a large W. However, they do not quantized near the phase transition points. As in the case of the NNN model, for the quantization, we need to set system size that is sufficiently large than the correlation length.

2.4 Conclusion

In this chapter, we have demonstrated that one can skip the integration procedure in the Niu-Thouless-Wu formula for calculating the topological invariant if the system is sufficiently large. We have shown that the one-plaquette Chern numbers defined in the Hofstadter problem with or without the electron-electron interactions give the exponential accuracy with respect to the system size. Since the numerical integration in many-body problems generally requires significant computational costs, its lack is helpful to numerically characterize correlated topological phases. In fact, our methodology has been discussed in recent works [127–129]. We also have investigated the validity of using the one-plaquette Chern number for detecting topological phase transitions.

Before closing the conclusion, we mention the shapes of the "plaquette" of the one-plaquette Chern number. In the above arguments, the shape is fixed to a square. However,

the one-plaquette Chern number is well-defined for any shape. We expect that the one-triangle-plaquette Chern number, which requires eigenvectors only at three points, also gives the quantization for a sufficiently large system.

Part II

Adiabatic principle

Chapter 3

Adiabatic theorem in topological phenomena

The adiabatic theorem is one of the most fundamental concept in the quantum mechanics. In this chapter, we first consider a simple problem of quantum mechanics to show that the Berry phase characterizes the geometrical structures of wave functions involved in the adiabatic development. The concept of the adiabatic deformation also gives a concise way to characterize topological materials. This perspective is essential in the following discussions on the higher-order topological Mott insulators and the adiabatic heuristic principle for the quantum Hall states.

3.1 Adiabatic problem and Berry phase

Let us here derive the non-Abelian Berry phases in a general way based on the adiabatic theorem [4,5,76,80]. We consider a system whose Hamiltonian $H(\boldsymbol{R})$ depends on parameters $\boldsymbol{R} = (R_1, R_2, \cdots)$. Let us assume that $\boldsymbol{R}(t)$ is the time-varying parameter and $\boldsymbol{R}(T) = \boldsymbol{R}(0)$. This implies that the change of the Hamiltonian in $0 \leq t \leq T$ is given by a transport along a closed path C in the parameter space. We also assume that the ground state exhibits q-fold degeneracy at any point on C. Denoting the ground state multiplet at time t by $\Psi(t) = (|\psi_1(t)\rangle, \cdots, |\psi_q(t)\rangle)$, we have the Schroedinger equation as

$$i\hbar \frac{\partial}{\partial t} \Psi(t) = H(t)\Psi(t) \tag{3.1}$$

At any instant, the basis is constructed from the eigenstates of the snapshot Hamiltonian $H(\boldsymbol{R}(t))$:

$$H(\boldsymbol{R}(t))\Phi(\boldsymbol{R}(t)) = E_g(\boldsymbol{R}(t))\Phi(\boldsymbol{R}(t)), \tag{3.2}$$

where $\Phi(\boldsymbol{R}) = (|\phi_1(\boldsymbol{R})\rangle, \cdots, |\phi_q(\boldsymbol{R})\rangle$ and $E_g(\boldsymbol{R})$ is the ground state energy. When assuming the adiabatic development, i.e., $\boldsymbol{R}(t)$ is slowly varied (T is sufficiently large) and the energy gap does not close, the system remains in its instantaneous ground state. Then, we write the solution of Eq. (3.1) with the initial condition $\Psi(0) = \Phi(\boldsymbol{R}(0))$ as

$$\Psi(t) = \exp\left\{-\frac{i}{\hbar}\int_0^T E(t')dt'\right\}\Phi(\boldsymbol{R}(t))U_q(t), \tag{3.3}$$

where $U_q(t)$ is a q-dimensional unitary matrix. To determine the explicit form of $U_q(t)$, we substitute it into Eq. (3.1):

$$\begin{aligned}\left(i\hbar\frac{\partial}{\partial t}-H(t)\right)\Psi(t)=&\left(i\hbar\frac{\partial}{\partial t}-H(t)\right)\exp\left\{-\frac{i}{\hbar}\int_0^t E(t')dt'\right\}\Phi(\boldsymbol{R}(t))U_q(t)\\ =&i\hbar\left(\frac{\partial\Phi(\boldsymbol{R}(t))}{\partial t}U_q(t)+\Phi(\boldsymbol{R}(t))\frac{\partial U_q(t)}{\partial t}\right).\end{aligned}\tag{3.4}$$

Using $\Psi^\dagger(\boldsymbol{R}(t))\Psi(\boldsymbol{R}(t))=1$, we have

$$\begin{aligned}\frac{\partial U_q(t)}{\partial t}=&-\Phi^\dagger(\boldsymbol{R}(t))\frac{\partial\Phi(\boldsymbol{R}(t))}{\partial t}U_q(t)\\ =&-\Phi^\dagger(\boldsymbol{R}(t))\boldsymbol{\nabla}_{\boldsymbol{R}}\Phi(\boldsymbol{R}(t))U_q(t)\cdot\frac{d\boldsymbol{R}(t)}{dt}\\ =&-\boldsymbol{A}(\boldsymbol{R}(t))U_q(t)\cdot\frac{d\boldsymbol{R}(t)}{dt},\end{aligned}\tag{3.5}$$

where $\boldsymbol{A}(\boldsymbol{R})=\Phi^\dagger(\boldsymbol{R})\frac{\partial}{\partial\boldsymbol{R}}\Phi(\boldsymbol{R})$ is the non-Abelian Berry connection. Then, we have [1]

$$U_q(t+dt)=e^{-\boldsymbol{A}(\boldsymbol{R}(t))\cdot d\boldsymbol{R}(t)}U_q(t)+O(dt^2).\tag{3.7}$$

It implies that $U_q(t)$ is given in terms of path-ordered integrals by

$$\begin{aligned}U_q(t)=&e^{-\boldsymbol{A}(\boldsymbol{R}(t))\cdot d\boldsymbol{R}(t)}\cdots\cdots\cdots e^{-\boldsymbol{A}(\boldsymbol{R}(0))\cdot d\boldsymbol{R}(0)}U_q(0)+O(dt^2)\\ =&Pe^{-\int_{\boldsymbol{R}(0)}^{\boldsymbol{R}(t)}\boldsymbol{A}(\boldsymbol{R})\cdot d\boldsymbol{R}},\end{aligned}\tag{3.8}$$

where $U_q(0)=1$ has been used. Consequently, the non-Abelian Berry phase are given by

$$U_q[C]=Pe^{-\oint_C\boldsymbol{A}(\boldsymbol{R})\cdot d\boldsymbol{R}}.\tag{3.9}$$

This geometrical phases arising in the adiabatic development are derived from the fact that the wave functions are constrained to a subspace of the Hilbert space during the evolution. The Aharonov-Bohm effect in the quantum mechanics is the typical example of the Berry phase, where the vector potential describing the magnetic field results in the nontrivial connection defined by the wave functions [4]. Before closing this section, we would like to mention the argument about the fractional statistics in the FQH effect as an historical example of significant applications of the Berry phase [15, 18, 19] (Detailed discussions on fractional statistics are given in Chapter 5.) The emergence of the fractionalized excitations is one of the defining features of the FQH effect. For example, the excitations of the Laughlin wave function at $\nu=1/m$ is described by quasiholes that carry the fractional charges e/m and the fractional statistics $2\pi/m$ [12, 15–17]. Let us now rederive it in terms of the Berry phases defined by adiabatic moves of quasiholes. The Laughlin wave function [12] at $\nu=1/m$ with m being odd is given by

$$\Psi_{1/m}=\prod_{i<j}(z_i-z_j)^m e^{-\sum_k|z_k|^2/4},\tag{3.10}$$

[1]

$$\begin{aligned}U_q(t+dt)=&U_q(t)+\frac{\partial U_q(t)}{\partial t}dt+O(dt^2)\\ =&U_q(t)-\boldsymbol{A}(\boldsymbol{R}(t))U_q(t)\cdot\frac{d\boldsymbol{R}(t)}{dt}dt+O(dt^2)\\ =&\left(1-\boldsymbol{A}(\boldsymbol{R}(t))\cdot d\boldsymbol{R}(t)\right)U_q(t)+O(dt^2)\\ =&e^{-\boldsymbol{A}(\boldsymbol{R}(t))\cdot d\boldsymbol{R}(t)}U_q(t)+O(dt^2)\end{aligned}\tag{3.6}$$

where $z = x_i + iy_i$. By piercing the Laughlin state at $\eta_1, \eta_2, \cdots$ with infinitely thin solenoids and adiabatically passing the flux quantums through them, an excited state with quasiholes is given by

$$\tilde{\Psi}^{+\eta}_{1/m} = \prod_k \prod_i (z_i - \eta_k)\Psi_m. \tag{3.11}$$

Since this wave function is not normalized, let us denote the normalized one by

$$\Psi^{+\eta}_{1/m} = \frac{1}{\sqrt{\mathcal{Z}}}\tilde{\Psi}^{+\eta}_{1/m} \text{ with } \mathcal{Z} = \left\langle \tilde{\Psi}^{+\eta}_{1/m} \middle| \tilde{\Psi}^{+\eta}_{1/m} \right\rangle. \tag{3.12}$$

Applying the differential form expression, let us now calculate its Berry connection. Defining $d = \frac{\partial}{\partial \eta_i} d\eta_i + \frac{\partial}{\partial \bar{\eta}_i} d\bar{\eta}_i$ and noting that that $\tilde{\Psi}^{+\eta}_{1/m}$ is holomorphic, i.e., not dependent on $\bar{\eta}_i$, we have

$$\begin{aligned}
\left| d\Psi^{+\eta}_{1/m} \right\rangle &= -\frac{1}{2}\frac{1}{\mathcal{Z}\sqrt{\mathcal{Z}}} d\mathcal{Z} \left| \tilde{\Psi}^{+\eta}_{1/m} \right\rangle + \frac{1}{\sqrt{\mathcal{Z}}} \left| d\tilde{\Psi}^{+\eta}_{1/m} \right\rangle \\
&= -\frac{1}{2}\frac{1}{\mathcal{Z}\sqrt{\mathcal{Z}}} \left(\frac{\partial \mathcal{Z}}{\partial \eta_i} d\eta_i + \frac{\partial \mathcal{Z}}{\partial \bar{\eta}_i} d\bar{\eta}_i \right) \left| \tilde{\Psi}^{+\eta}_{1/m} \right\rangle + \frac{1}{\sqrt{\mathcal{Z}}} \left| \frac{\partial}{\partial \eta_i} \tilde{\Psi}^{+\eta}_{1/m} \right\rangle d\eta_i
\end{aligned}$$

By using it, the Berry connection $A = \left\langle \Psi^{+\eta}_{1/m} \middle| d\Psi^{+\eta}_{1/m} \right\rangle$ is given by

$$\begin{aligned}
A &= -\frac{1}{2}\frac{1}{\mathcal{Z}} \left(\frac{\partial \mathcal{Z}}{\partial \eta_i} d\eta_i + \frac{\partial \mathcal{Z}}{\partial \bar{\eta}_i} d\bar{\eta}_i \right) + \frac{1}{\mathcal{Z}} \frac{\partial \mathcal{Z}}{\partial \eta_i} d\eta_i \\
&= \frac{1}{2} \left(\frac{\partial \log \mathcal{Z}}{\partial \eta_i} d\eta_i - \frac{\partial \log \mathcal{Z}}{\partial \bar{\eta}_i} d\bar{\eta}_i \right)
\end{aligned}$$

where $\frac{\partial}{\partial \eta_i} \left\langle \tilde{\Psi}^{+\eta}_{1/m} \right| = 0$ has been used. To compute the Berry connection, it is necessary to calculate the normalization factor. According to the discussions in relation to a two-dimensional one-component plasma with some extra charges [18, 19], one can evaluate the normalization factor with good accuracy as

$$\begin{aligned}
\mathcal{Z} &= \int \prod_i d^2 z_i \exp\left\{ \sum_{i,j} \log |z_i - \eta_j|^2 + m \sum_{k<l} \log |z_k - z_l|^2 - \frac{1}{2} \sum_i |z_i|^2 \right\} \\
&\to \exp\left\{ -\frac{1}{m} \sum_{i<j} \log |\eta_i - \eta_j|^2 + \frac{1}{2m} \sum_i |\eta_i|^2 \right\}.
\end{aligned}$$

From it, we get the Berry connection as

$$A = \left(-\frac{1}{2m} \sum_{j \neq i} \frac{1}{\eta_i - \eta_j} + \frac{1}{4m} \bar{\eta}_i \right) d\eta_i + \left(\frac{1}{2m} \sum_{j \neq i} \frac{1}{\bar{\eta}_i - \bar{\eta}_j} - \frac{1}{4m} \eta_i \right) d\bar{\eta}_i. \tag{3.13}$$

In order to demonstrate the fractional charge in the Laughlin state, let us calculate the Berry phase defined by dragging a quasihole at η_i round a closed path that does not enclose any of other quasiholes, see Fig. 3.1(a). The Berry phase is given by

$$\gamma = \frac{1}{i} \int_C A = \frac{1}{i} \frac{1}{4m} \int_C (\bar{\eta}_i d\eta_i - \bar{\eta}_i d\eta_i) = \frac{S}{m}, \tag{3.14}$$

where we have used $\int_C \bar{\eta}_i d\eta_i = i2S$ with S being the area surrounded by C. Since we here use magnetic length $l_{\mathrm{B}} = \sqrt{\hbar/eB}$ as a unit of length, the given AB phases is expressed by

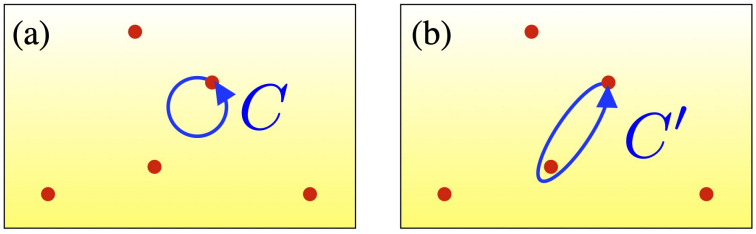

Figure 3.1: The paths to compute (a) the fractional charge and (b) the fractional statistics.

$\exp\{iS/(ml_{\rm B}^2)\} = \exp\{i2\pi e\Phi/(mh)\}$ with $\Phi = BS$. One can interpret this result as the AB phase given by particles with fractional charges as

$$e^* = e/m. \tag{3.15}$$

Let us next demonstrate the fractional statistics in the same manner as the case of the fractional charges. The Berry phase defined by dragging a quasihole at η_i round another at η_j [see Fig. 3.1(b)] is given by

$$\begin{aligned}\gamma' = \frac{1}{i}\int_{C'} A &= \frac{1}{i}\frac{1}{4m}\int_{C'}(\bar{\eta}_i d\eta_i - \bar{\eta}_i d\eta_i) - \frac{1}{i}\frac{1}{2m}\int_{C'}\left(\frac{d\eta_i}{\eta_i-\eta_j} - \frac{d\bar{\eta}_i}{\bar{\eta}_i-\bar{\eta}_j}\right) \\ &= \frac{S'}{m} - \frac{2\pi}{m}.\end{aligned} \tag{3.16}$$

The first term is the AB phase discussed above. The second term is interpreted as the statistical phase associated with two exchanges of particles. It clearly demonstrates the appearance of anyons in the excitations of the Laughlin state.

3.2 Adiabatic deformation of topological systems

The origin of the Berry phases is found in the adiabatic theorem as shown above. Generally, topological invariants associated with the Berry connection (see Chapter 1) encode the geometrical structures of the subspace given by the ground states evolved adiabatically, which has been quite successful to describe various topological phenomena. The concept of the adiabatic deformation also give a concise way to characterize topological phases in concrete problems. Let us assume that a given system has complex structures to analyze its topological nature. By adiabatically deforming it into simple systems, the original topological characters are easily investigated by simple calculations. As an example, let us here consider the system of spinful interacting electrons on a kagome lattice shown in Fig. 3.2(a). In a certain situation, this system exhibits a nontrivial topological phenomenon closely related with their C_3 symmetry (the details are given in the next chapter). While its characterization is a highly nontrivial problem, one can simplify this system based on the adiabatic deformation. What is important here is that this adiabatic development should preserve their symmetry that characterize the topological phenomena [79, 84, 130–133] (C_3 in this case). In the case of the higher-order topological Mott insulators, the system is adiabatically connected into the decoupled system shown in Fig. 3.2(b). Namely, the topological nature of the original complex system is diagnosed by the study of the three-site problem. This implies that the Z_3 quantized Berry phase, whose quantization is protected by the C_3 symmetry, works as a kind of the order parameter [83].

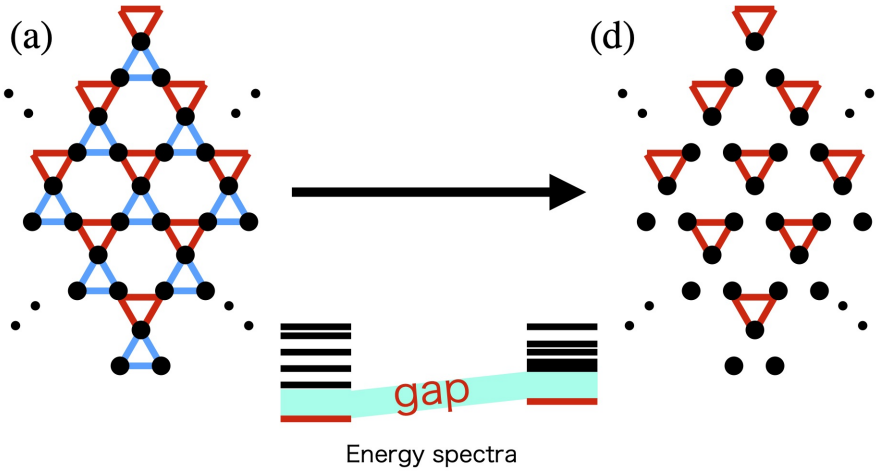

Figure 3.2: Adiabatic deformation of the system on a kagome lattice.

Before closing this chapter, we refer to the origin of topological and adiabatic invariants. The topological invariant associated with the Berry connection is defined by using the eigenstates. Therefore, one naturally expects that states should be continuously changed during adiabatic developments. In the last chapter of this part, however, we find a new formula that implies what is deformed continuously is not states but an energy gap.

Chapter 4

Higher-order topological Mott insulator

The bulk-edge correspondence is a fundamental feature of the topological phases. Generalizing this concept in terms of the high-order physics and the Mott physics, we propose a new topological states "higher-order topological Mott insulator" (HOTMI). We also demonstrate that the HOTMI states emerge in the Hubbard model on a kagome lattice. Its topological nature are easily understood from the three-site problem by adiabatically deforming the systems, whose information is encoded in the spin Z_3-Berry phase. Clarifying the relation between the corner-Mott states and the topological invariant, we show the bulk-edge correspondence of the HOTMI in the Hubbard model.

4.1 Bulk-edge correspondence and its generalization

The bulk-edge correspondence [7, 8] is a remarkable phenomenon of the topological phase such as the quantum Hall effect and topological insulators/superconductors [3, 40–43]. The bulk topological index in d-dimensional systems predicts the emergence of gapless edge states around $d-1$-dimensional boundaries. Recently, a new class of topological states "higher-order topological insulators/superconductors" are proposed [85, 134–144], where the conventional bulk-edge correspondence does not apply; the bulk topological invariants in d-dimensional systems give gapless charge excitations around not $d-1$-dimensional boundaries but $d-2$ or $d-3$-dimensional boundaries as shown in Fig. 4.1. Recent intensive studies have revealed that this higher-order physics is ubiquitous and indeed observed in a wide variety of materials [145–148].

The effects of the electron-electron interactions enrich material phases dramatically. Intensive studies in decades have elucidated a wide variety of correlated topological phenomena [149–155]. For example, the topological classification for noninteracting particles [44–47] are essentially modified by the electron correlation effects [62–75]. Also, impacts of the correlation effects have been addressed in terms of the Mott physics [53–57], which have found the topological Mott insulating states as a new correlated topological state. These recent progresses gives a simple question "How do electron-electron interactions enrich higher-order bulk-boundary correspondence?".

The correlation effects in the higher-order topological insulators are recently discussed in terms of a field theory [156]. In this chapter, we address this problem by analyzing a practical model. Then we find a new correlated topological state which is called "higher-order topological Mott insulator" (HOTMI) [157], which exhibits a generalized bulk-edge correspondence. The HOTMI exhibits a generalized bulk-edge correspondence in which the bulk topology in d dimensions results only in gapless spin excitations at $d-n$-dimensional

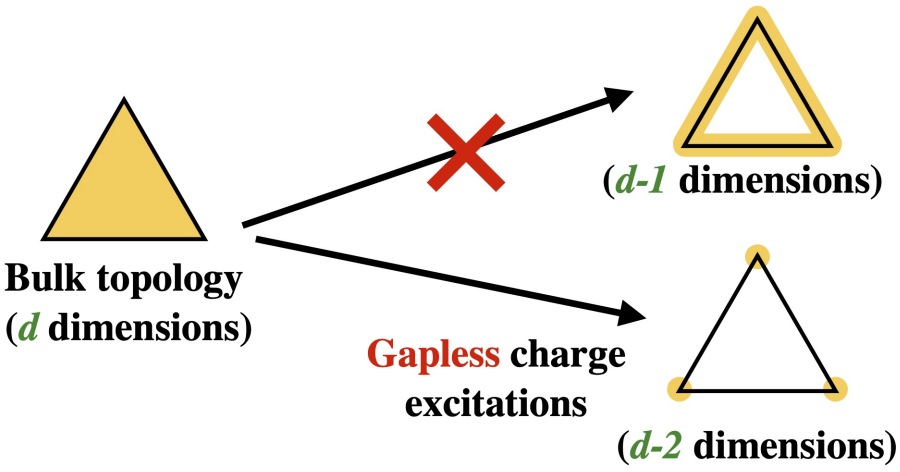

Figure 4.1: The higher-order topological insulator in two dimensions.

$(2 \leq n)$ boundaries. Due to the correlation effects, these boundary states are gapped as for charge excitations. The remainder of this part, we numerically demonstrate that a Hubbard model on a kagome lattice exhibits the HOTMI phases. The topological nature of the HOTMI states on a kagome lattice is simply understood from a decoupled system that is adiabatically connected to the original system. The information of this adiabatic continuity is obtained by calculating the quantized spin-Berry phase. The following numerical calculations are based on the exact diagonalization approach using the Lanczos algorithm. The mechanism of this method is described in the Sec. 4.4 of this part as an supplemental. We also describe the computational costs required for diagonalizing the Hamiltonian.

4.2 HOTMI on a kagome lattice

Let us start with describing our model and topological invariants that is used to characterize the HOTMI. The system of spinful electrons on a kagome lattice is considered. The Hamiltonian is expressed as

$$H = H_{\rm kin}^{\triangle} + H_{\rm kin}^{\triangledown} + H_{\rm int}, \tag{4.1}$$

where each term is defined by

$$H_{\rm kin}^{\gamma} = t_{\gamma} \sum_{i,j\in\gamma} \sum_{\alpha,\beta=\uparrow,\downarrow} c_{i\alpha}^{\dagger} \sigma_{\alpha\beta}^{z} c_{j\beta} + \text{h.c.}, \tag{4.2}$$

$$H_{\rm int} = U \sum_{i} \left(n_{i\uparrow} - \frac{1}{2} \right) \left(n_{i\downarrow} - \frac{1}{2} \right). \tag{4.3}$$

Here, $\gamma = \triangle$ or $\triangledown$ indicates the type of the triangles in the kagome lattice as shown in Fig. 4.2, $c_{i\alpha}^{\dagger}$ is the creation operator on site i with spin $\alpha =\uparrow,\downarrow$, $n_{i\alpha} = c_{i\alpha}^{\dagger} c_{i\alpha}$, and $\sum_{i,j\in\gamma}$ indicates the summation over the nearest neighbor pairs of the sites that belong to the triangle γ. For simplicity, we introduce the parameters t and ϕ defined by

$$t_{\triangle} = t \sin\phi, \; t_{\triangledown} = t \cos\phi \tag{4.4}$$

as shown in Fig. 4.2. In the following, we consider the half-filled system and set the parameters as $U \leq 0$, $t < 0$, and $0 \leq \phi \leq \pi/2$ unless otherwise stated. Due to the spin-dependence

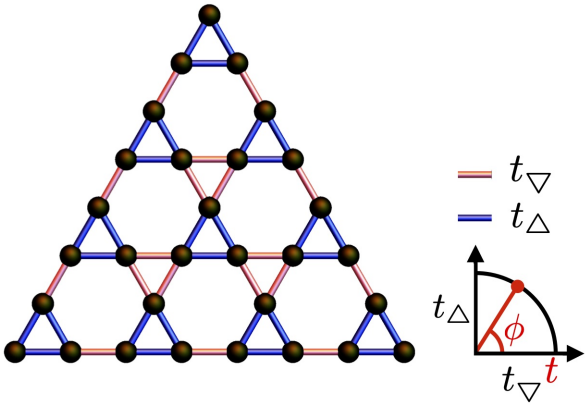

Figure 4.2: Sketch of the kagome lattice under the open boundary condition.

of the hopping seen in $H_{\rm kin}$, this system breaks time-reversal symmetry but preserves $U(1)$ symmetry with respect to the spin-rotation.

In order to diagnose the topological origin of the bulk systems, we calculate the spin-counterpart of the quantized $\mathcal{Z}_3$-Berry phase [83,158] discussed in the first chapter. Namely, using the unitary operator as

$$U_-(\vec{\theta}) = e^{in_1^-\theta_1}e^{-in_2^-\theta_2}, \tag{4.5}$$

where $n_i^- = n_{i\uparrow} - n_{i\downarrow}$ and the site indices 1 and 2 are chosen in a specific downward triangle, we replace the term $H_{\rm kin}^{\bigtriangledown}$ with $U_-(\vec{\theta})H_{\rm kin}^{\bigtriangledown}U_-^\dagger(\vec{\theta})$. Then, by defining the spin-Berry connection as $A_-(\vec{\theta})$, the $\mathcal{Z}_3$ spin-Berry phase is given by

$$\gamma_- = \frac{1}{i}\int_C A_-, \tag{4.6}$$

where C indicates the integral path: $\vec{\theta} = \vec{f}(t)$ $(0 \le t \le 1)$ defined by $\vec{f}(t) = 2\pi(t,t)$ for $0 \le t < 1/3$ and $\vec{f}(t) = 2\pi(t, 1/2 - t/2)$ for $1/3 \le t < 1$. Since the considered system has C_3 symmetry, the Berry phase always quantized as $\gamma_- = 2\pi n/3$ with $n = 0, 1, 2$. As discussed in the first chapter, we can compute γ_- analytically in some cases. For $t_\bigtriangleup = 0$ shown in Fig. 4.3(a), the Hamiltonian is expressed as $H(\vec{\theta}) = U_-(\vec{\theta})HU_-^\dagger(\vec{\theta})$, which implies that the Berry phase is given by $\gamma_- = 2\pi \langle G| n_1^- |G\rangle$. In Fig. 4.3(b), we plot energy as functions of U/t by solving the three-site problem, where the states with $S^z_{\rm tot} = 1/2$ give the lowest energy. It implies that the Berry phase for finite U/t is given by

$$\gamma_- = \frac{2\pi}{3}. \tag{4.7}$$

On the other hand, the system with $t_\bigtriangledown = 0$ gives

$$\gamma_- = 0. \tag{4.8}$$

These results suggest that the spin-Berry phase characterizes the topological origin that the two decoupled limit systems have. By using it, we discuss the topological character of the HOTMI below.

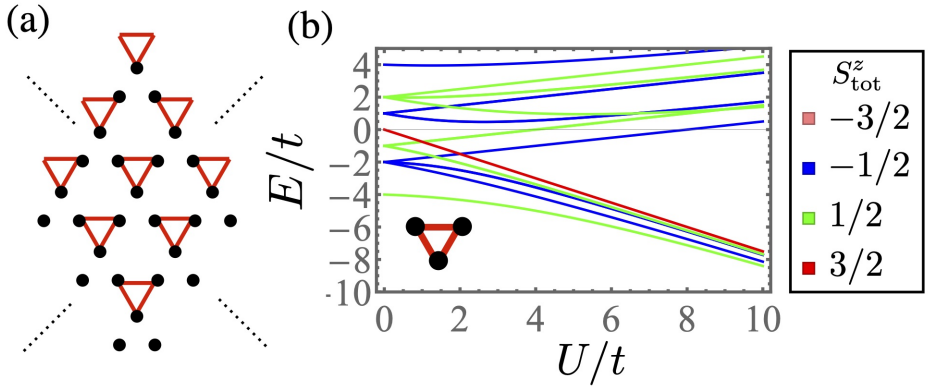

Figure 4.3: (a) Sketch of the kagome lattice with $t_\triangle = 0$. (b) Energy E/t as functions of U/t in the three-site problem. The total S^z are expressed by the color of plots. The energies with $S^z_{\rm tot} = \pm 3/2$ are degenerated at any U/t.

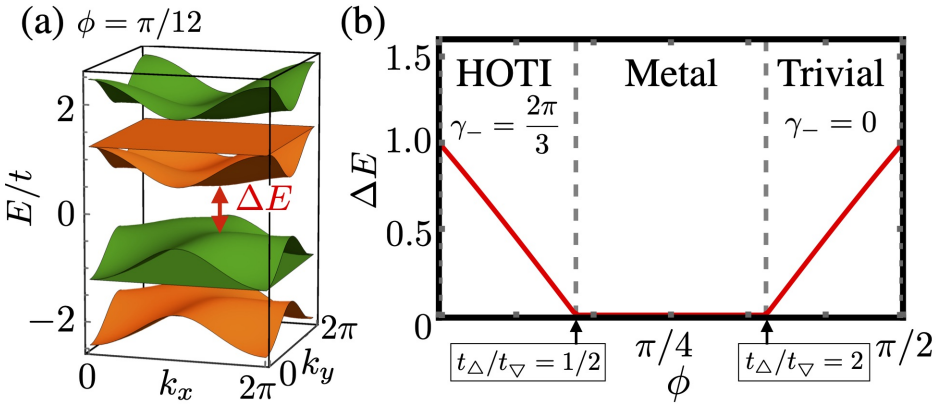

Figure 4.4: (a) Energy bands at $\phi = \pi/12$. The spin S_z of the single particle is expressed by the color. (Green:$S_z = 1/2$, Orange:$S_z = -1/2$) (b) Energy gap as a function of the angle ϕ.

4.2.1 Band structure

Before moving onto the interacting problems, we review the behaviors of the noninteracting higher-order topological insulators on a kagome lattice [83,86]. Figure 4.4(a) shows the band structure of our model with $U/t = 0$. Because of the U(1) spin rotational symmetry, each band is identified by S_z. The energy bands with $S_z = \pm 1/2$ are symmetric with respect to $E/t = 0$. In Fig. 4.4(b), the energy gap ΔE is shown as a function of ϕ. Although the systems are gapless in the region of $1/2 \leq t_\triangle/t_\triangledown \leq 2$, the gaped ground states are obtained in the other regions: the higher-order topological insulators in $t_\triangle/t_\triangledown < 1/2$ and the trivial insulators in $2 < t_\triangle/t_\triangledown$ as formulated in Ref. 86. These features are derived from the patterns of the bonds, which are characterized by the $\mathcal{Z}_3$ Berry phase [83] as summarized in Fig. 4.4(b). In the following, we focus on the discussions on the correlation effects in the higher-order topological insulators on the kagome lattice.

4.2.2 Strong correlation limit

Let us first consider the Hubbard model on the kagome lattice in the strong correlation limit $1 \ll U/t$ to investigate the correlation effects effectively. Based on the degenerate perturbation theory, we construct the effective Hamiltonian. Since each electrons is completely localized into each site in this limit, the effective Hamiltonian is described by a spin model. Its Hamiltonian is given by

$$\begin{aligned} H_{\rm eff} &= H^{(2)}_{\triangle} + H^{(2)}_{\triangledown} + H^{(3)}_{\triangle} + H^{(3)}_{\triangledown}, \\ H^{(2)}_{\gamma} &= J^{(2)}_{\gamma} \sum_{i,j,k\in\gamma} \left(-\frac{1}{2}\boldsymbol{S}^2_{ijk} + {S^z_{ijk}}^2 + \frac{3}{8} \right), \\ H^{(3)}_{\gamma} &= J^{(3)}_{\gamma} \sum_{i,j,k\in\gamma} S^z_{ijk} \left(-3\boldsymbol{S}^2_{ijk} + 4{S^z_{ijk}}^2 + \frac{9}{4} \right), \end{aligned} \tag{4.9}$$

where $H^{(2)}_{\gamma}$ and $H^{(3)}_{\gamma}$ are the second-order and the third-order effective Hamiltonians, respectively. (In the last of this section, we describe the derivation of the effective model in details.) Here, $J_{\triangle} = J^{(n)} \sin^n \phi$, $J_{\triangledown} = J^{(n)} \cos^n \phi$, $J^{(n)} = 4t^n/U^{n-1}$, $\boldsymbol{S}_{ijk} = \boldsymbol{S}_i + \boldsymbol{S}_j + \boldsymbol{S}_k$, and $\sum_{i,j,k\in\gamma}$ indicates the summation over the nearest neighbor three sites that belong to the triangle γ. If the effective Hamiltonian includes only the second-order, the system reduces to the XXZ model with the time-reversal symmetry while the original Hubbard Hamiltonian does not have time-reversal invariance. To remove the symmetry that is artificially produced, we add the third-order perturbation. In the following, we set the system size as $N_{\rm UC} = 9$ in the periodic boundary condition and $N_{\rm UC} = 10$ in the open boundary condition shown in Fig. 4.2, where $N_{\rm UC}$ is the number of the unit cell.

Bulk properties

In Fig. 4.5(a), we plot the magnetization $S^z_{\rm tot}$ of the ground state as a function of ϕ and $J^{(3)}/J^{(2)} = t/U$ under the periodic boundary condition. Let us first discuss the system with $\phi = 0$ and $\pi/2$, which reduces to the three-site problem. If the Hamiltonian includes only the second-order term $H^{(2)}$, the many-body state $|S_{123} = 3/2, S^z_{123} = \pm 1/2\rangle$ with the Kramers pair becomes the ground state. This degeneracy is broken by the third-order term $H^{(3)}$ and $|S_{123} = 3/2, S^z_{123} = 1/2\rangle$ [see, Fig. 4.5(b)] becomes the unique ground state. It implies that the systems at $\phi = 0$ and $\pi/2$ are gapped and their gaps are characterized by $J^{(3)}$. These ground states should survive when we make a sufficiently small change of ϕ compared with that gap. This naive expectation is consistent with Fig. 4.5(a) in which the ground state with $S^z_{\rm tot} = N_{\rm UC}/2 = 4.5$ is obtained in a finite region of ϕ. In Fig. 4.5(c), we plot the spin-Berry phase γ_- for $J^{(3)}/J^{(2)} = 0.1$ only in the region of ϕ in which the magnetization of the ground state is given by $S^z_{\rm tot} = N_{\rm UC}/2 = 4.5$. The result indicates that two regions around $\phi = 0$ and $\phi = \pi/2$ are characterized by $\gamma_- = 2\pi/3$ and 0, respectively. Here, we construct the spin-Berry phase of the spin model by replacing the operator n_i^- in the unitary operator $U_-(\vec{\theta})$ with $2S^z_i$. As shown below, the ground states with $\gamma_- = 2\pi/3$ and $\gamma_- = 0$ are the HOTMI and the trivial insulator, respectively .

Corner-Mott states

In order to verify the bulk-edge correspondence of the HOTMI, let us now consider the system imposed on the open boundary condition as shown in Fig. 4.2. In Fig. 4.6(a), we plot the many-body energy as function of ϕ, where we set $J^{(3)}/J^{(2)} = 0.1$. In a similar way as the bulk case, let us first consider the decoupled systems at $\phi = 0$ and $\pi/2$ shown in Figs. 4.6(b)

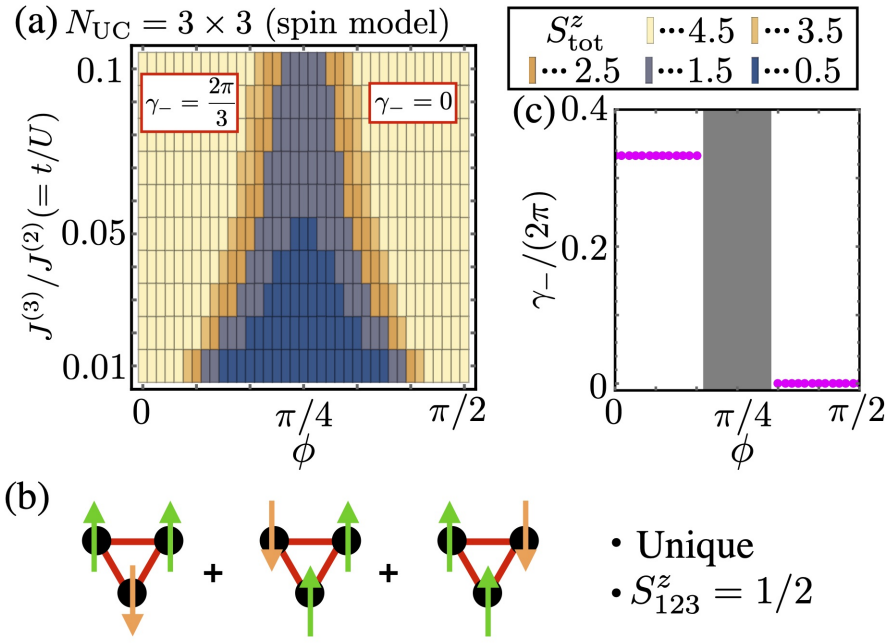

Figure 4.5: (a) Magnetization $S^z_{\rm tot}$ of the ground state. (b) Schematic of the unique ground state at $\phi = 0$. (c) Spin-Berry phase γ_- for $J^{(3)}/J^{(2)} = 0.1$ as a function of ϕ. We calculate γ_- only in the region with $S^z_{\rm tot} = 4.5$. In (a) and (c), the system size is set as $N_{\rm UC} = 9$.

and (c). At $\phi = 0$, there are three-site clusters in the bulk, two-site clusters along the edges, and free spins at the corner. As discussed above, the unique ground state are observed in the three-site problem. Also, as for the two-site problem, $|S_{12} = 1, S^z_{12} = 0\rangle$ become the gapped unique ground state. Consequently, the ground state exhibits the eight-fold degeneracy derived from the three free-spins at the corners. On the other hand, the system at $\phi = \pi/2$ is composed only of the three-site clusters, which implies the emergence of the gapped unique ground state. The result in Fig. 4.6(a) indicates that the above eight-fold degenerated ground state and the unique ground state survive in the finite region of ϕ. To demonstrate that the eight-degeneracy of the ground state around $\phi = 0$ comes from the gapless corner states, let us remove sites at corners and investigate its effects on the degeneracy. In Fig. 4.6(d), we plot the energy spectra for the four types of the geometry shown in Fig. 4.6(d0)-(d3). The ground states of the system in which p sites (corners) are removed exhibit 2^{3-p}-fold degeneracy. This clearly implies the appearance of the gapless states at the $3-p$ corners. Our results on the spin model demonstrate the bulk-edge correspondence of the HOTMI; the gapless corner modes only for the spin excitations appear in the region of ϕ with $\gamma_- = 2\pi/3$ shown in Fig. 4.5(a). In Sec. 4.2.4, we will discuss the relation between this HOTMI and the standard higher-order topological insulator appearing in the noninteracting system.

4.2.3 Derivation of the effective model

Here, we derive the effective Hamiltonian in Eq. (4.9). Readers on the first reading may prefer to skip it and jump to Sec. 4.2.4, where we discuss the emergence of the HOTMI by diagonalizing the Hamiltonian of the Hubbard model.

Let us now rewrite the Hamiltonian as $H = H_{\rm kin} + H_{\rm int}$ with

$$H_{\rm kin} = \sum_{\alpha=\uparrow,\downarrow} \sum_{i,j} t_{\alpha,i,j} c^\dagger_{\alpha,i} c_{\alpha,j}, \tag{4.10}$$

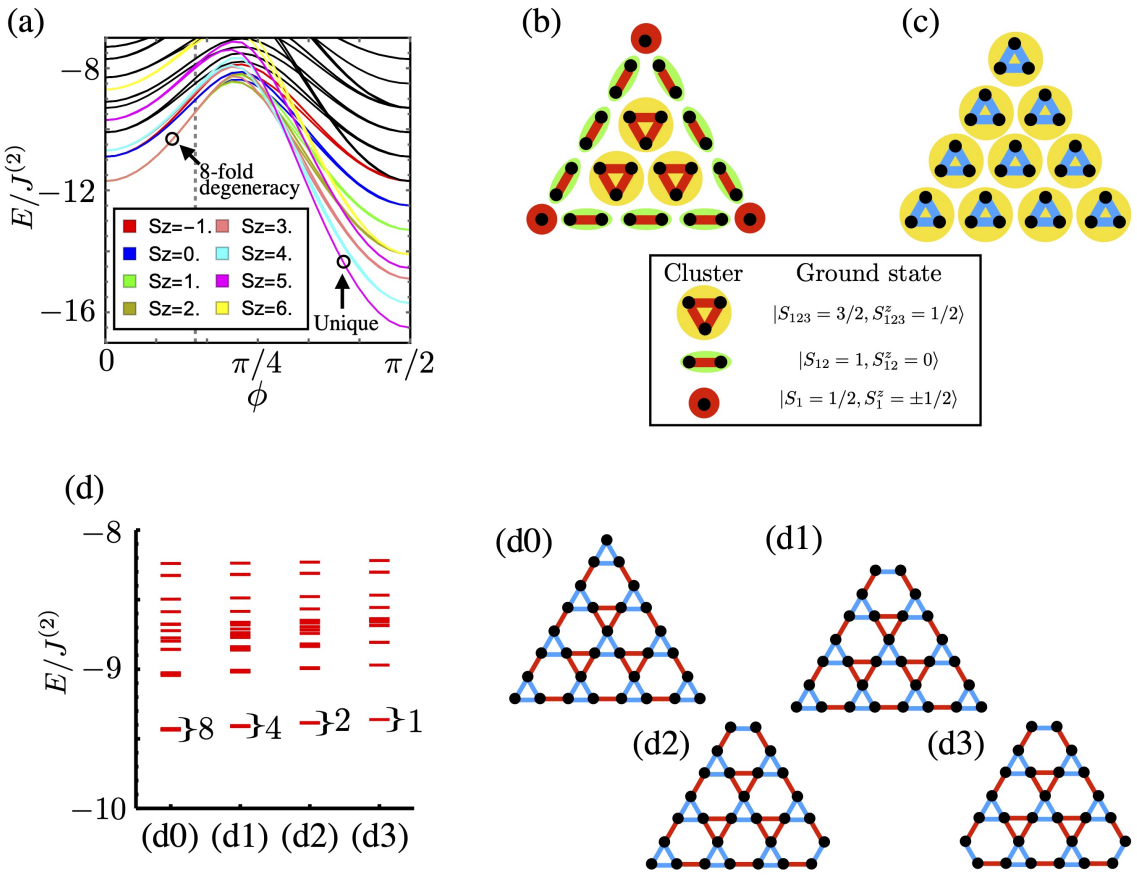

Figure 4.6: (a) Many-body energy as function of ϕ. The magnetization $S^z_{\rm tot}$ is expressed by the color of the plots. The dashed line expresses $\tan\phi = 0.5$. The Black plots indicates the energy for $S^z_{\rm tot} < -1$ or $6 < S^z_{\rm tot} < 1$. (b)(c) Ground states at (b) $\phi = 0$ and (c) $\phi = \pi/2$. (d) Energy spectra at $\tan\phi = 0.5$ for each geometry shown in (d0)-(d4).

$$H_{\rm int} = \sum_i U n_{\uparrow,i} n_{\downarrow,i}. \tag{4.11}$$

Assuming that U is much larger than t_α, we derive the effective Hamiltonian at half-filling. In the unperturbed problem (i.e., $H_{\rm int}$ only), electrons are localized at each site completely and the ground state exhibit the $2^{N_{\rm site}}$-fold degeneracy, where $N_{\rm site}$ is the number of the sites. Based on the degenerated perturbation theory, we consider the first, second, and third-order perturbations with respect to $H_{\rm kin}$ below.

First-order effective Hamiltonian

Defining the ground state multiplet of $H_{\rm int}$ as $\Psi_{\rm G} = (|G_1\rangle, |G_2\rangle, \cdots)$, we have the first-order effective Hamiltonian as

$$H^{(1)}_{\rm eff} = P H_{\rm kin} P = 0, \tag{4.12}$$

where $P = \Psi_{\rm G}\Psi^\dagger_{\rm G}$.

Second-order effective Hamiltonian

The second-order effective Hamiltonian is given by

$$H_{\rm eff}^{(2)} = PH_{\rm kin}\tilde{P}\frac{1}{E^{(0)}-H_{\rm int}}\tilde{P}H_{\rm kin}P, \tag{4.13}$$

where $\tilde{P} = 1 - \Psi_{\rm G}\Psi_{\rm G}^\dagger$ and $H_{\rm int}P = E^{(0)}P$. Since there are two $H_{\rm kin}$'s in the effective Hamiltonian, the explicit expression of Eq. (4.13) is essentially given by solving the two-site problem. The ground state multiplet is given as

$$\Psi_{\rm G}^{12} = (|\uparrow,\uparrow\rangle_{12}, |\downarrow,\downarrow\rangle_{12}, |\uparrow,\downarrow\rangle_{12}, |\downarrow,\uparrow\rangle_{12}), \tag{4.14}$$

where $|\alpha\beta,\gamma\delta,\cdots\rangle_{i,j,\cdots} = c_{\alpha i}^\dagger c_{\beta i}^\dagger c_{\gamma j}^\dagger c_{\delta j}^\dagger \cdots |0\rangle_{i,j,\cdots}$ and $|0\rangle_{i,j,\cdots}$ is the vacuum state. Denoting the Hamiltonians in the two-site problem by $H_{\rm kin}^{12}$, we have

$$\tilde{P}H_{\rm kin}^{12}|\uparrow,\uparrow\rangle_{12} = \tilde{P}H_{\rm kin}^{12}|\downarrow,\downarrow\rangle_{12} = 0 \tag{4.15}$$

$$\begin{aligned}\tilde{P}H_{\rm kin}^{12}|\uparrow,\downarrow\rangle_{12} =& \tilde{P}\sum_\alpha (t_\alpha c_{\alpha,1}^\dagger c_{\alpha,2} + t_\alpha^* c_{\alpha,2}^\dagger c_{\alpha,1}) c_{\uparrow,1}^\dagger c_{\downarrow,2}^\dagger |0\rangle_{12} \\ =& \tilde{P}(-t_\downarrow c_{\downarrow,1}^\dagger c_{\uparrow,1}^\dagger + t_\uparrow^* c_{\uparrow,2}^\dagger c_{\downarrow,2}^\dagger)|0\rangle_{12} \\ =& -t_\downarrow |\downarrow\uparrow,0\rangle_{12} + t_\uparrow^* |0,\uparrow\downarrow\rangle_{12},\end{aligned} \tag{4.16}$$

where $t_\alpha = t_{\alpha,1,2}$, and the double-occupancy in the two-body state is written as $|\uparrow\downarrow,0\rangle_{12} = -|\downarrow\uparrow,0\rangle_{12} = c_{1,\uparrow}^\dagger c_{1,\downarrow}^\dagger |0\rangle_{12}$. We have

$$\begin{aligned}&PH_{\rm kin}^{12}\tilde{P}\frac{1}{E^{(0)}-H_{\rm int}}\tilde{P}H_{\rm kin}^{12}|\uparrow,\downarrow\rangle_{12} \\ =& PH_{\rm kin}^{12}\tilde{P}\frac{1}{E^{(0)}-H_{\rm int}}(-t_\downarrow|\downarrow\uparrow,0\rangle_{12} + t_\uparrow^*|0,\uparrow\downarrow\rangle_{12}) \\ =& PH_{\rm kin}^{12}(\frac{t_\downarrow}{U}|\downarrow\uparrow,0\rangle_{12} - \frac{t_\uparrow^*}{U}|0,\uparrow\downarrow\rangle_{12}) \\ =& \sum_\alpha (t_\alpha c_{\alpha,1}^\dagger c_{\alpha,2} + t_\alpha^* c_{\alpha,2}^\dagger c_{\alpha,1})\frac{t_\downarrow}{U}c_{\downarrow,1}^\dagger c_{\uparrow,1}^\dagger|0\rangle_{12} - \sum_\alpha (t_\alpha c_{\alpha,1}^\dagger c_{\alpha,2} + t_\alpha^* c_{\alpha,2}^\dagger c_{\alpha,1})\frac{t_\uparrow^*}{U}c_{\uparrow,2}^\dagger c_{\downarrow,2}^\dagger|0\rangle_{12} \\ =& \frac{t_\downarrow}{U}(t_\uparrow^* c_{\downarrow,1}^\dagger c_{\uparrow,2}^\dagger - t_\downarrow^* c_{\uparrow,1}^\dagger c_{\downarrow,2}^\dagger)|0\rangle_{12} - \frac{t_\uparrow^*}{U}(t_\uparrow c_{\uparrow,1}^\dagger c_{\downarrow,2}^\dagger - t_\downarrow c_{\downarrow,1}^\dagger c_{\uparrow,2}^\dagger)|0\rangle_{12} \\ =& \left(\frac{2t_\uparrow^* t_\downarrow}{U}|\downarrow,\uparrow\rangle_{12} - \frac{|t_\uparrow|^2+|t_\downarrow|^2}{U}|\uparrow,\downarrow\rangle_{12}\right).\end{aligned} \tag{4.17}$$

One can compute $PH_{\rm kin}^{12}\tilde{P}\frac{1}{E^{(0)}-H_{\rm int}}\tilde{P}H_{\rm kin}^{12}|\downarrow,\uparrow\rangle_{12}$ by replacing the site indices 1 and 2, which corresponds to the transformation $t_\alpha \to t_\alpha^*$, i.e., $t_{\alpha,1,2} \to t_{\alpha,2,1}$. From them, the second-order effective Hamiltonian is given by

$$\begin{aligned}h_{12}^{(2)} =& \Psi_{\rm G}^{12\dagger} H_{\rm eff}^{(2)12}\Psi_{\rm G}^{12} \\ =& \Psi_{\rm G}^{12\dagger} H_{\rm kin}^{12}\tilde{P}\frac{1}{E^{(0)}-H_{\rm int}}\tilde{P}H_{\rm kin}^{12}\Psi_{\rm G}^{12} \\ =& \begin{pmatrix} 0 & & & \\ & -\frac{|t_\uparrow|^2+|t_\downarrow|^2}{U} & \frac{2t_\uparrow t_\downarrow^*}{U} & \\ & \frac{2t_\uparrow^* t_\downarrow}{U} & -\frac{|t_\uparrow|^2+|t_\downarrow|^2}{U} & \\ & & & \end{pmatrix}.\end{aligned} \tag{4.18}$$

Within the subspace Ψ_G^{12}, the $S = 1/2$ spin operators defined as $S_i^z = \frac{1}{2}(n_{\uparrow,i} - n_{\downarrow,i})$, $S_i^+ = c_{\uparrow,i}^\dagger c_{\downarrow,i}$ and $S_i^- = c_{\downarrow,i}^\dagger c_{\uparrow,i}$ are expressed as follows:

$$\Psi_G^{12\dagger} S_1^+ S_2^- \Psi_G^{12} = \begin{pmatrix} 0 & & & \\ & 0 & 1 & \\ & 0 & 0 & \end{pmatrix}, \tag{4.19}$$

$$\Psi_G^{12\dagger} S_1^- S_2^+ \Psi_G^{12} = \begin{pmatrix} 0 & & & \\ & 0 & 0 & \\ & 1 & 0 & \end{pmatrix}, \tag{4.20}$$

$$\Psi_G^{12\dagger} S_1^z S_2^z \Psi_G^{12} = \begin{pmatrix} 1/4 & 0 & 0 & 0 \\ 0 & 1/4 & 0 & 0 \\ 0 & 0 & -1/4 & 0 \\ 0 & 0 & 0 & -1/4 \end{pmatrix}. \tag{4.21}$$

Using these expressions, Eq. (4.18) is written as

$$h_{12}^{(2)} = \Psi_G^\dagger \left(J_{+-} S_1^+ S_2^- + J_{-+} S_1^- S_2^+ + J_z S_1^z S_2^z + C \right) \Psi_G, \tag{4.22}$$

where the parameters in the anisotropic Heisenberg model is given by $J_{+-} = J_{-+}^* = \frac{2t_\uparrow t_\downarrow^*}{U}$, $J_z = 2\frac{|t_\uparrow|^2 + |t_\downarrow|^2}{U}$, and $C = -\frac{1}{2}\frac{|t_\uparrow|^2 + |t_\downarrow|^2}{U}$. For general $N_{\rm site}$, we also have the same results: [1]

$$\begin{aligned} H_{\rm eff}^{(2)} &= \sum_{i,j} \left(J_{+-}^{i,j} S_i^+ S_j^- + J_{-+}^{i,j} S_i^- S_j^+ + J_z^{i,j} S_i^z S_j^z + C \right), \\ J_{+-}^{i,j} &= J_{-+}^{i,j*} = \frac{2t_{\uparrow,i,j} t_{\downarrow,i,j}^*}{U}, \\ J_z &= 2\frac{|t_{\uparrow,i,j}|^2 + |t_{\downarrow,i,j}|^2}{U}, \\ C &= -\frac{1}{2}\frac{|t_{\uparrow,i,j}|^2 + |t_{\downarrow,i,j}|^2}{U}. \end{aligned} \tag{4.24}$$

In our model in which the nearest-neighbor hopping with $t_\uparrow = -t_\downarrow = t$ is only included, the effective Hamiltonian is given by

$$\begin{aligned} H_{\rm eff}^{(2)} &= \sum_{\langle ij \rangle} \left(J_{+-} (S_i^+ S_j^- + S_i^- S_j^+) + J_z S_i^z S_j^z + C \right) \\ &= J \sum_{\langle ij \rangle} \left(-S_i^x S_j^x - S_i^y S_j^y + S_i^z S_j^z - \frac{1}{4} \right), \end{aligned} \tag{4.25}$$

[1] Writing explicitly each term in the Hamiltonian as $H_{\rm kin} = \sum_{ij} H_{\rm kin}^{ij}$, we have

$$\begin{aligned} H_{\rm eff}^{(2)} =& P H_{\rm kin} \tilde{P} \frac{1}{E^{(0)} - H_{\rm int}} \tilde{P} H_{\rm kin} P \\ =& \sum_{ij} P H_{\rm kin} \tilde{P} \frac{1}{E^{(0)} - H_{\rm int}} \tilde{P} H_{\rm kin}^{ij} P \\ =& \sum_{ij} P H_{\rm kin}^{ij} \tilde{P} \frac{1}{E^{(0)} - H_{\rm int}} \tilde{P} H_{\rm kin}^{ij} P \\ =& \sum_{ij} H_{\rm eff}^{(2)ij}. \end{aligned} \tag{4.23}$$

where $J_{+-} = -2t^2/U$, $J_z = 4t^2/U$, $C = -t^2/U$, and $J = 4t^2/U$. Ignoring the constant term, we have

$$\begin{aligned}
&J\sum_{i=1}^{3}\left(-S_i^x S_{i+1}^x - S_i^y S_{i+1}^y + S_i^z S_{i+1}^z\right) \\
=&-J\sum_{i=1}^{3}\boldsymbol{S}_i\cdot\boldsymbol{S}_{i+1} + 2J\sum_{i=1}^{3}S_i^z S_{i+1}^z \\
=&-J\left[\frac{(\boldsymbol{S}_1+\boldsymbol{S}_2+\boldsymbol{S}_3)^2}{2} - \frac{1}{2}\sum_{i=1}^{3}\boldsymbol{S}_i^2\right] + 2J\left[\frac{(S_1^z+S_2^z+S_3^z)^2}{2} - \frac{1}{2}\sum_{i=1}^{3}S_i^{z2}\right] \\
=&J\left[-\frac{1}{2}\boldsymbol{S}_{123}^2 + S_{123}^{z2} + \frac{3}{8}\right].
\end{aligned} \tag{4.26}$$

This is the Hamiltonian of the XXZ model, which we include in the effective Hamiltonian in Eq. (4.9).

Third-order effective Hamiltonian

Let us assume that the degenerated ground state is not lifted by the first and the second-order perturbations. The third-order effective Hamiltonian is given by

$$\begin{aligned}
H_{\text{eff}}^{(3)} = PH_{\text{kin}}\tilde{P}\frac{1}{E^{(0)}-H_{\text{int}}}\tilde{P}H_{\text{kin}}\tilde{P}\frac{1}{E^{(0)}-H_{\text{int}}}\tilde{P}H_{\text{kin}}P \\
+ PH_{\text{kin}}\tilde{P}\frac{1}{(E^{(0)}-H_{\text{int}})^2}\tilde{P}H_{\text{kin}}PH_{\text{kin}}P.
\end{aligned} \tag{4.27}$$

As previously noted, we have $E^{(0)} = 0$ and $PH_{\text{kin}}P = 0$ so that the effective Hamiltonian we consider here is

$$H_{\text{eff}}^{(3)} = PH_{\text{kin}}\tilde{P}\frac{1}{H_{\text{int}}}\tilde{P}H_{\text{kin}}\tilde{P}\frac{1}{H_{\text{int}}}\tilde{P}H_{\text{kin}}P. \tag{4.28}$$

Since there are three H_{kin}'s, the three-site problem is intrinsically important. The ground state multiplet given by the non-perturbative Hamiltonian H_{int} is expressed as

$$\begin{aligned}
\Psi_{\text{G}}^{123} = (&|\uparrow,\uparrow,\uparrow\rangle_{123}, |\uparrow,\uparrow,\downarrow\rangle_{123}, |\uparrow,\downarrow,\uparrow\rangle_{123}, |\downarrow,\uparrow,\uparrow\rangle_{123}, |\downarrow,\downarrow,\uparrow\rangle_{123}, \\
&|\downarrow,\uparrow,\downarrow\rangle_{123}, |\uparrow,\downarrow,\downarrow\rangle_{123}, |\downarrow,\downarrow,\downarrow\rangle_{123}).
\end{aligned} \tag{4.29}$$

Denoting the hopping Hamiltonian in the three-site problem by H_{kin}^{123}, we have

$$\tilde{P}H_{\text{kin}}^{123}|\uparrow,\uparrow,\uparrow\rangle_{123} = \tilde{P}H_{\text{kin}}^{123}|\downarrow,\downarrow,\downarrow\rangle_{123} = 0. \tag{4.30}$$

From Fig. 4.7, we have

$$\begin{aligned}
&H_{\text{eff}}^{(3)123}|\uparrow,\uparrow,\downarrow\rangle_{123} \\
=&\frac{t_{32\downarrow,21\downarrow,13\downarrow} + t_{31\downarrow,12\downarrow,23\downarrow} - t_{23\uparrow,12\uparrow,31\uparrow} - t_{13\uparrow,21\uparrow,32\uparrow}}{U^2}|\uparrow,\uparrow,\downarrow\rangle_{123} \\
+&\frac{-t_{32\uparrow,21\downarrow,13\downarrow} - t_{21\downarrow,32\uparrow,13\downarrow} + t_{12\uparrow,31\uparrow,23\downarrow} + t_{12\uparrow,23\downarrow,31\uparrow} + t_{23\downarrow,12\uparrow,31\uparrow} - t_{21\downarrow,13\downarrow,32\uparrow}}{U^2}|\uparrow,\downarrow,\uparrow\rangle_{123} \\
+&\frac{t_{21\uparrow,32\uparrow,13\downarrow} - t_{31\uparrow,12\downarrow,23\downarrow} - t_{12\downarrow,31\uparrow,23\downarrow} - t_{12\downarrow,23\downarrow,31\uparrow} + t_{21\uparrow,13\downarrow,32\uparrow} + t_{13\downarrow,21\uparrow,32\uparrow}}{U^2}|\downarrow,\uparrow,\uparrow\rangle_{123},
\end{aligned}$$

where $t_{ij\alpha,kl\beta,mn\gamma} = t_{ij\alpha}t_{kl\beta}t_{mn\gamma}$. One can compute $H_{\text{eff}}^{(3)123}|\uparrow,\downarrow,\uparrow\rangle_{123}$ by replacing the site indices as $(1,2,3) \to (2,3,1)$. Also, one calculate $H_{\text{eff}}^{(3)123}|\downarrow,\downarrow,\uparrow\rangle_{123}$ by switching $\uparrow$ and $\downarrow$.

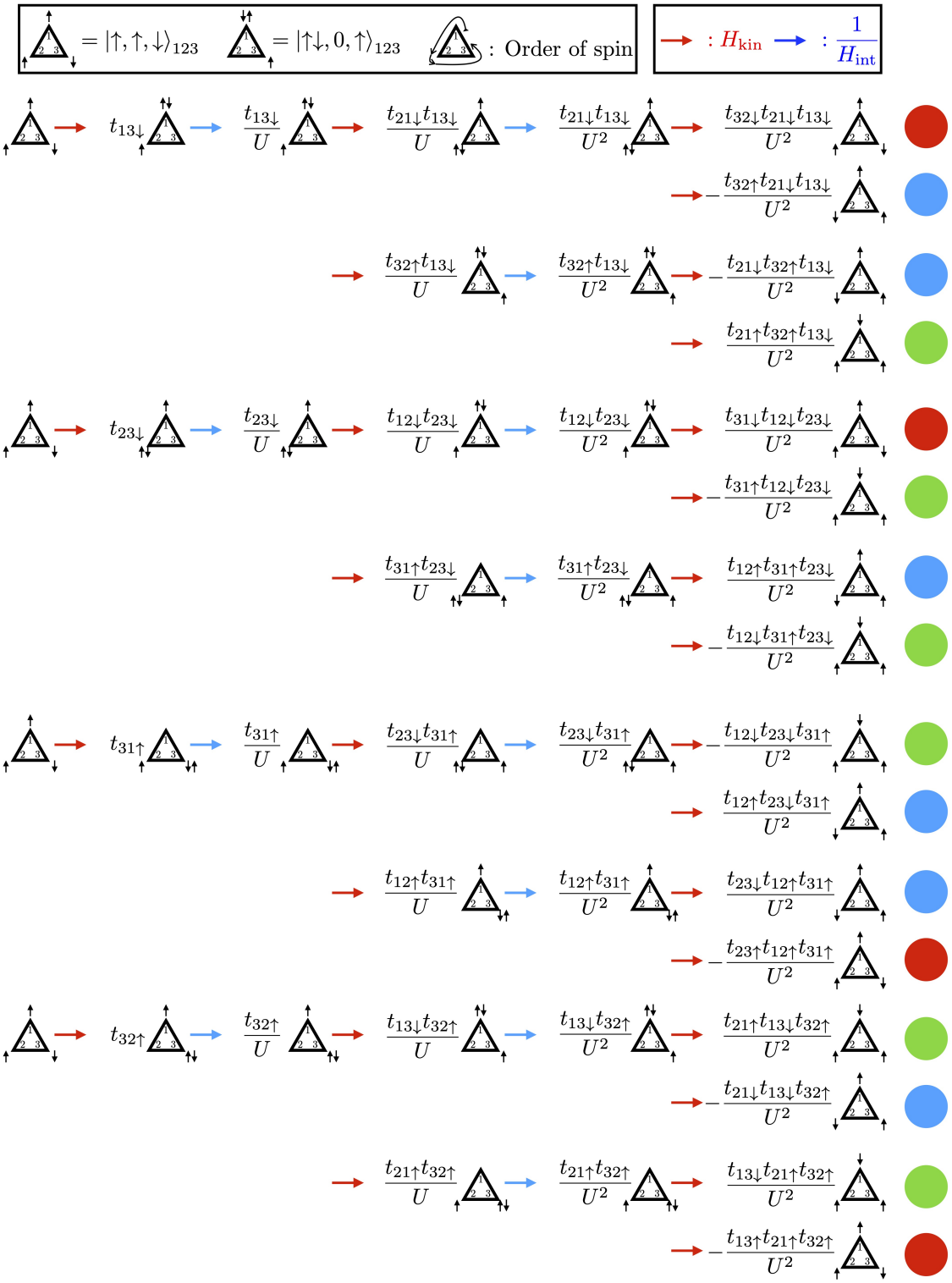

Figure 4.7: 3rd-order perturbation

In our model in which the nearest-neighbor hopping with $t_\uparrow = -t_\downarrow = t$ is only included, we have

$$H_{\rm eff}^{(3)123}\left|\uparrow,\uparrow,\downarrow\right\rangle_{123} = -\frac{t^3}{U^2}\left(4\left|\uparrow,\uparrow,\downarrow\right\rangle_{123} + 6\left|\uparrow,\downarrow,\uparrow\right\rangle_{123} + 6\left|\downarrow,\uparrow,\uparrow\right\rangle_{123}\right). \tag{4.31}$$

This equation gives us the 8×8 matrix $h_{123}^{(3)} = \Psi_G^{123\dagger} H_{\rm eff}^{(3)123} \Psi_G^{123}$ written as

$$h_{123}^{(3)} = \frac{t^3}{U^2}\begin{pmatrix} 0 & & & & & & & \\ & -4 & -6 & -6 & & & & \\ & -6 & -4 & -6 & & & & \\ & -6 & -6 & -4 & & & & \\ & & & & 4 & 6 & 6 & \\ & & & & 6 & 4 & 6 & \\ & & & & 6 & 6 & 4 & \\ & & & & & & & 0 \end{pmatrix}. \tag{4.32}$$

The operators related to $\boldsymbol{S}_{123}$ are given as

$$\Psi_G^{123\dagger}(S_1^z + S_2^z + S_3^z)\Psi_G^{123} = \frac{1}{2}\begin{pmatrix} 3 & & & & & & & \\ & 1 & & & & & & \\ & & 1 & & & & & \\ & & & 1 & & & & \\ & & & & -1 & & & \\ & & & & & -1 & & \\ & & & & & & -1 & \\ & & & & & & & -3 \end{pmatrix}, \tag{4.33}$$

$$\Psi_G^{123\dagger}\left(\boldsymbol{S}_1 + \boldsymbol{S}_2 + \boldsymbol{S}_3\right)^2 \Psi_G^{123} = \frac{1}{4}\begin{pmatrix} 15 & & & & & & & \\ & 7 & 4 & 4 & & & & \\ & 4 & 7 & 4 & & & & \\ & 4 & 4 & 7 & & & & \\ & & & & 7 & 4 & 4 & \\ & & & & 4 & 7 & 4 & \\ & & & & 4 & 4 & 7 & \\ & & & & & & & 15 \end{pmatrix}. \tag{4.34}$$

Using them, we have

$$H_{\rm eff}^{(3)123} = JS_{123}^z(-3\boldsymbol{S}_{123}^2 + 4S_{123}^{z\,2} + \frac{9}{4}), \tag{4.35}$$

where $\boldsymbol{S}_{\rm tot} = \sum_{i=1}^3 \boldsymbol{S}_i$ and $J = 4t^3/U^2$.

4.2.4 From weak to strong correlations

In the previous subsections, we assume that the interactions are sufficiently strong as $t \ll U$ to analyze the spin model. Then, let us now investigate the topological properties of the HOTMI by diagonalizing the Hamiltonian of the Hubbard model in Eq. (4.1) with any values of U/t. We here also clarify the relation between the noninteracting higher-order insulators [86] and the HOTMI.

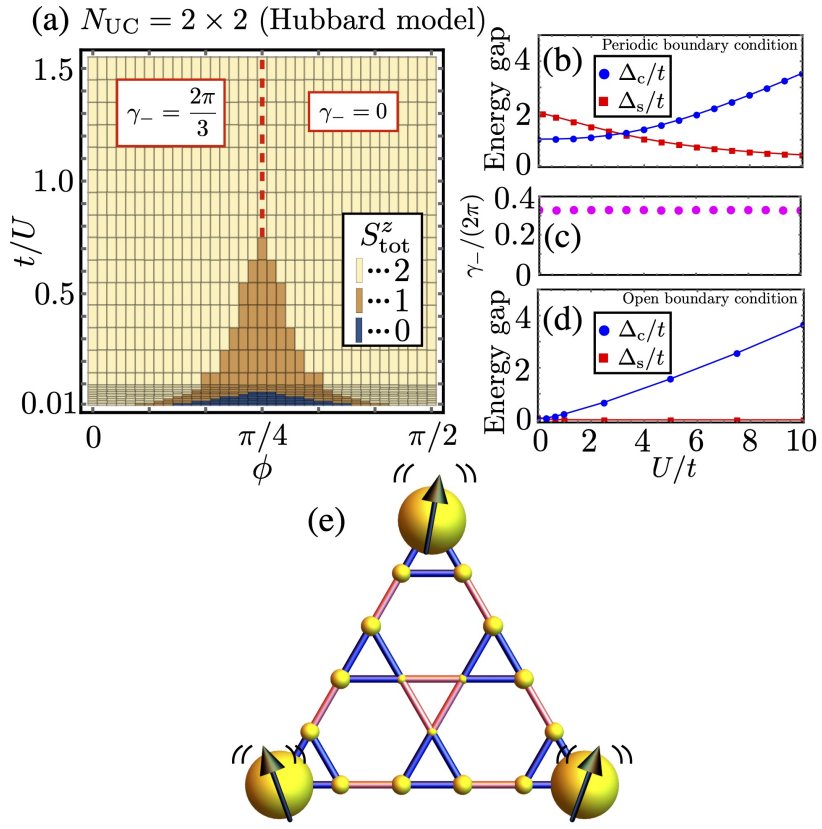

Figure 4.8: (a) Magnetization $S^z_{\rm tot}$ of the ground state. (b) U/t-dependences of the charge gap Δ_c and the spin gap Δ_s under the periodic boundary condition. (c) Quantized Berry phase γ_- as a function of U/t. (d) U/t-dependences of the charge gap Δ_c and the spin gap Δ_s under the open boundary condition. (e) Spin expectation values $\langle \boldsymbol{S}_i^2 \rangle - \langle \boldsymbol{S}_i^2 \rangle_0$. The radii of the spheres express the calculated values. In (a)-(c), the periodic systems with $N_{\rm UC} = 2 \times 2$ is considered. In (d) and (e), the systems with $N_{\rm UC} = 6$ under the open boundary condition is considered. The hopping parameters are set as $t_\triangle/t_\triangledown = 0.4$ in (b)-(e).

Bulk properties

We begin by investigating the bulk properties. Diagonalizing the Hamiltonian in Eq. (4.1) under the periodic boundary condition, we show in Fig. 4.8(a) the $(\phi, U/t)$-dependence of $S^z_{\rm tot}$ of the ground state in the same way as Fig. 4.5(a). In the strongly correlated regions, the magnetization of the ground state around $\phi = 0$ and $\pi/2$ is given by $S^z_{\rm tot} = N_{\rm UC}/2$, which is consistent with the results of the effective spin model. The figure suggests that this strongly correlated states are adiabatically connected to the weakly correlated states. In Fig. 4.8(b), we plot the charge gap $\Delta_{\rm c}$ and the spin gap $\Delta_{\rm s}$ as a function of U/t for $t_\triangle/t_\triangledown = 0.4$. Here, we define both gaps as

$$\Delta_c = \frac{E_{\mathcal{N}_{\rm e}+1,\mathcal{S}^z_{\rm tot}+1/2} + E_{\mathcal{N}_{\rm e}-1,\mathcal{S}^z_{\rm tot}-1/2} - 2E_{\mathcal{N}_{\rm e},\mathcal{S}^z_{\rm tot}}}{2} \tag{4.36}$$

$$\Delta_s = \frac{E_{\mathcal{N}_{\rm e},\mathcal{S}^z_{\rm tot}+1} + E_{\mathcal{N}_{\rm e},\mathcal{S}^z_{\rm tot}-1} - 2E_{\mathcal{N}_{\rm e},\mathcal{S}^z_{\rm tot}}}{2}, \tag{4.37}$$

where $\mathcal{S}^z_{\rm tot}$ ($\mathcal{N}_{\rm e}$) is the value of $S^z_{\rm tot}$ ($N_{\rm e}$) of the ground state. Since we set $N_{\rm UC} = 4$ in Fig. 4.8(b), each value is given by $\mathcal{N}_{\rm e} = 12$ and $\mathcal{S}^z_{\rm tot} = 2$. In the strong correlated region in the figure, the value of the charge gap Δ_c is the order of U, which implies the adiabatic

continuity between the higher-order topological insulator with $U/t = 0$ and the HOTMI. In Fig. 4.8(c), one can confirm that the Berry phase is an adiabatic invariant. In Fig. 4.8(a), we have no signs of the appearance of gapless state at $U/t = 0$ and $\phi \approx \pi/4$, which is came from a finite-size effect. Indeed, one can observe it when introducing the twisted boundary conditions to detect the single-particle momentum in which the band gap closes.

Corner-Mott states

In order to show the bulk-edge correspondence of the HOTMI in the Hubbard model, we move onto the discussions under the open boundary condition as shown in Fig. 4.2. In Fig. 4.8(d), we plot the U/t-dependences of the charge gap Δ_c and the spin gap Δ_s, where we set $N_{\rm UC} = 6$ and $t_\triangle/t_\triangledown = 0.4$. Here, the eight-fold degenerated ground state gives the magnetization as $-1 \leq S^z_{\rm tot} \leq 2$. Therefore, we set $\mathcal{S}^z_{\rm tot} = 1$ and $\mathcal{N}_{\rm e} = 18$ for defining the energy gaps. While the gapless charge excitation seen in the noninteracting system is broken by the correlation effects, the gapless behavior of the spin excitation survives. In Fig. 4.8(e), we show the value of $\langle \boldsymbol{S}_i^2 \rangle - \langle \boldsymbol{S}_i^2 \rangle_0$ of the system with $t_\triangle/t_\triangledown = 0.4$, where $\langle\cdot\rangle$ ($\langle\cdot\rangle_0$) expresses the expectation value defined by the ground state multiplet at $U/t = 1$ ($U/t = 0$) and $\boldsymbol{S}_i^2 = 3(n_{i\uparrow} + n_{i\downarrow} - 2n_{i\uparrow}n_{i\downarrow})/4$. The figure suggests that the gapless spin excitations are derived from the emergence of the free-spins at the corners. Our results demonstrate that the bulk-edge correspondence is modified by the electron-electron interaction even though the bulk topology is not changed. Consequently, the standard higher-order topological insulators are transformed into the HOTMI states by the infinitesimal interaction U.

4.3 Conclusion

In this chapter, we have discussed a new class of the correlated topological phase "higher-order topological Mott insulator". This topological state exhibits a generalized bulk-edge correspondence; a d-dimensional bulk topology relates to the emergence of $d - n$ ($2 \leq n$) boundary modes that are gapped in the charge excitations but gapless in the spin excitations. We have demonstrated that the HOTMI states are observed in the Hubbard model on a kagome lattice. Specifically, the quantized spin-Berry phase $\gamma_- = 2\pi/3$ computed in the bulk system corresponds to the emergence of the corner-Mott states at 0-dimensional boundaries. This topological nature of the HOTMI is simply understood by analyzing adiabatically deformed systems. In the decoupled limit, the corner-Mott states are interpreted as free-spins that are localized at corners, whose information is encoded in the Z_3 quantized Berry phase. The correlation effects of the higher-order physics have become an important research topic recently, which have been studied intensively from various perspectives [156, 159, 160]. We hope that the concept of the HOTMI will be useful for further explorations of topologically nontrivial states in the higher-order topological insulators.

Before closing the conclusion, we would like to mention the realization of the HOTMIs in other models. In this chapter, we consider only the system on a kagome lattice. However, using the approach in Ref. 83, it is expected that one can extend our approach into d-dimensional lattices characterized by the $\mathcal{Z}_{d+1}$ spin-Berry phases. Recently, the idea of the quantized Berry phases associated with the symmetry of the hyper-pyrochlore lattices [83] is generalized into other lattice structures for characterizing the higher-order topological insulators on various materials [143]. Combining this approach with ours, it is expected that one could construct the HOTMI states on various lattices such as a square lattice. Nowadays, experimental realization for some correlated topological phases has been discussed actively [61, 161, 162]. Lastly, let us describe candidates to realize the HOTMI. Although the standard higher-order topological insulators has been observed experimentally in some

materials [138,145,146], the HOTMI states has not been yet. Recently, topological phenomena in organic frameworks and covalent organic frameworks with kagome structures have been investigated [141,163]. For example, the higher-order topological insulating phases are realized in a polymerized triptycene on a decorated star lattice [141]. Its corner modes are characterized by the Z_3 Berry phase, which share the same topological nature as the our model without interactions. Taking into account the fact that the corner-Mott states emerge by the infinitesimal interactions, one expects that the polymerized triptycene on a decorated star lattice is a promising candidate for the HOTMI even if the particles are not strongly correlated.

4.4 Supplemental: Lanczos algorithm and computational costs

4.4.1 Lanczos algorithm

In the above discussions, we have investigated correlation effects by analyzing the effective spin model and the Hubbard model. When diagonalizing their Hamiltonians, we used Lanczos algorithm. In this section, let us describe that algorithm and computational costs required for diagonalizing the Hamiltonians.

We consider the following eigenvalue equation:

$$H\left|\Psi_i\right\rangle = E_i\left|\Psi_i\right\rangle, \tag{4.38}$$

where H is the $N \times N$ hermitian matrix and $|\Psi_i\rangle$ is the N-dimensional vector. Let us first make a N-dimensional vector $|v_1\rangle$ from random numbers satisfying $\langle v_1|v_1\rangle = 1$. Then we compute α_i, β_i and $|v_i\rangle$ as follows:

$$\begin{aligned}
&\alpha_1 = \langle v_1| H |v_1\rangle \\
&|u_1\rangle = H|v_1\rangle - \alpha_1|v_1\rangle \\
&\beta_1 = \sqrt{\langle u_1|u_1\rangle} \\
&|v_2\rangle = |u_1\rangle / \beta_1 \\
&\quad\vdots \\
&\alpha_i = \langle v_i| H |v_i\rangle \\
&|u_i\rangle = H|v_i\rangle - \alpha_i|v_i\rangle \\
&\beta_i = \sqrt{\langle u_i|u_i\rangle} \\
&|v_{i+1}\rangle = |u_i\rangle / \beta_i \\
&\quad\vdots
\end{aligned}$$

Using the values of α's and β's, we define the $M \times M$ tridiagonalized matrix H' as

$$H' = \begin{pmatrix}
\alpha_1 & \beta_1 & & & & \\
\beta_1 & \alpha_2 & \beta_2 & & & \\
 & \beta_2 & \alpha_3 & \beta_3 & & \\
 & & \ddots & \ddots & \ddots & \\
 & & & & \alpha_{M-1} & \beta_{M-1} \\
 & & & & \beta_{M-1} & \alpha_M
\end{pmatrix}, \tag{4.39}$$

where M is an integer. Defining the $N \times M$ matrix as $V = (|v_1\rangle, \cdots, |v_M\rangle)$, we have

$$H' = V^\dagger H V. \tag{4.40}$$

The matrices H and H' for $M = N$ are unitary equivalent; otherwise their eigenvalues are different. However, for sufficiently large M, the lowest eigenvalue of H is estimated from that of H' with high precision. This algorithm is an adaptation of power methods, which is called Lanczos algorithm. The eigenvectors of H is also approximately given by H' as follows. Let us first consider the eigenvalue equation as

$$H' \left|\Psi'_i\right\rangle = E'_i \left|\Psi'_i\right\rangle . \tag{4.41}$$

As mentioned above, we have $E'_1 \approx E_1$ for sufficiently large M. This equation reduces to

$$VV^\dagger H \left|\tilde{\Psi}'_i\right\rangle = E'_i \left|\tilde{\Psi}'_i\right\rangle , \tag{4.42}$$

where $\left|\tilde{\Psi}'_i\right\rangle = V \left|\Psi'_i\right\rangle$ is an N-dimensional vector. One can use $\left|\tilde{\Psi}'_1\right\rangle$ as an approximation of $|\Psi_1\rangle$. In the practical calculations, the numerically obtained V for large M breaks its orthogonality, i.e., $V^\dagger V \neq 1$ due to the rounding errors. This effect also results in the lost of orthogonality of $\left|\tilde{\Psi}'_1\right\rangle$ because of $\left\langle\tilde{\Psi}'_1\middle|\tilde{\Psi}'_1\right\rangle = \langle\Psi'_1| V^\dagger V |\Psi'_1\rangle$. Thus, one should use the normalized vector as $\left|\tilde{\Psi}'_1\right\rangle / \left\langle\tilde{\Psi}'_1\middle|\tilde{\Psi}'_1\right\rangle$.

Since we need to calculate matrix-vector products in the calculation of H', the Lanczos algorithm is a useful tool to find the lowest eigenvalues and eigenvectors of sparse matrices. If the eigenvalues or eigenvectors of the excited state, i.e., $E_{k\neq 1}$ and $|\Psi_{k\neq 1}\rangle$ are required, one should diagonalize the following matrix:

$$H'' = H + E_{\text{shift}} \sum_{i=1}^{k-1} |\Psi_i\rangle \langle\Psi_i| , \tag{4.43}$$

where E_{shift} is a value of the energy shift. For sufficiently large E_{shift}, $E_{k\neq 1}$ and $|\Psi_{k\neq 1}\rangle$ are (approximately) given as the lowest energy state of H''.

4.4.2 Computational costs

In the above discussions on the HOTMI, we apply the Lanczos algorithm to calculate the energy spectra and the topological invariants. The Hamiltonians of the effective spin model and the Hubbard model are given by large sparse matrices. In this section, let us describe the dimensions of their matrices and the number of their nonzero elements. Generally, it is an important step to estimate the required amount of memory space when performing numerical calculations.

Spin model

Let us start by considering the effective spin model. After giving a general discussion, we consider the problem of a kagome lattice we considered above. Let us consider the following Hamiltonian:

$$H = \sum_{i,j} J^x_{ij} S^x_i S^x_j + J^y_{ij} S^y_i S^y_j + J^z_{ij} S^z_i S^z_j, \tag{4.44}$$

where $\boldsymbol{S}_i = (S^x_i, S^y_i, S^z_i)$ is the spin-1/2 operators at the lattice site i. Here, we do not specify the lattice structure. Let us now denote the number of the sites and the interaction pairs (i, j) by N_{site} and N_{pair}. We now assume that the Hamiltonian commutes with the z-component

Data type	Byte (=8bit)
Integer	4
Double precision	8
Complex(kind(0d0))	16

Table 4.1: Data types of FORTRAN.

of the total spin S^z. The dimension of the Hamiltonian H specified by $S^z = \sum_i S_i^z$ is given by

$$N_{\rm D} = {}_{N_{\rm site}}C_{N_\uparrow}, \tag{4.45}$$

where $N_\uparrow$ is the number of the spins with $S_i^z = 1/2$. Let us next calculate the number of non-zero elements of the Hamiltonian, which we denote by $N_{\rm elem} = N_{\rm Diago} + N_{\rm Off\text{-}Diago}$. Since H is a hermitian matrix, we only consider the lower triangular region of the matrix. The number of the off-diagonal elements $N_{\rm Off\text{-}Diago}$ is defined in that sense. We here take the basis which diagonalizes the operators S_i^z's. The diagonal elements of H are given by $\sum_{i,j} S_i^z S_j^z$, and obviously, we have

$$N_{\rm Diago} = N_{\rm D}. \tag{4.46}$$

The off-diagonal elements are given by $\sum_{i,j} S_i^x S_j^x + S_i^y S_j^y = (1/2)\sum_{i,j} S_i^+ S_j^- + S_i^- S_j^+$. To estimate its number, let us focus on the interaction $S_1^+ S_2^-$. States that satisfy $S_1^+ S_2^- |\rangle \neq 0$ are given by $|\downarrow\uparrow\cdots\cdots\cdots\rangle$, where "$\cdots\cdots\cdots$" is any spin configuration. It implies that the number of such states is given by ${}_{N_{\rm site}-2}C_{N_\uparrow-1}$. Because we only consider the lower triangular region of the matrix, the number of nonzero off-diagonal elements specified by $S_1^x S_2^x + S_1^y S_2^y$ are given by ${}_{N_{\rm site}-2}C_{N_\uparrow-1}$. Then we have

$$N_{\rm Off\text{-}Diago} = N_{\rm pair} \times {}_{N_{\rm site}-2}C_{N_\uparrow-1}. \tag{4.47}$$

For reference, the data types are listed in Table 4.1. In the numerical calculations in the above discussions on HOTMIs, double precision is chosen for storing complex numbers of nonzero elements of the Hamiltonian. In Table 4.2, we show $N_{\rm D}$ and $N_{\rm elem} = N_{\rm Diago} + N_{\rm Off\text{-}Diago}$ for the spin model on a kagome lattice under the periodic boundary condition. Here, the interactions between the nearest-neighbor pairs are only considered. We set $N_\uparrow = N_\downarrow$ or $N_\uparrow = N_\downarrow/3$. When the system is put on the $N_x \times N_y$ unit cells, we have $N_{\rm site} = 3N_xN_y$ and $N_{\rm pair} = 6N_xN_y$. In that table, we also give the values of $16 \times N_{\rm D}$ and $16 \times N_{\rm elem}$, which is related to the required memory space for storing vectors and a matrix in the Lanczos algorithm. While the periodic boundary condition is considered in Table 4.2, we show in Table 4.3 the values of $N_{\rm D}$ and $N_{\rm elem} = N_{\rm Diago} + N_{\rm Off\text{-}Diago}$ under the open boundary condition. The sketches of kagome lattices under the open boundary conditions are given in Fig. 4.9.

Hubbard model

Let us move onto the problem of the Hubbard model. In the similar way as the spin model. we will discuss the case of a kagome lattice after general discussions. The Hamiltonian of the Hubbard model is generally written by

$$H = \sum_{i,j,\sigma} t_{ij} c_{i\sigma}^\dagger c_{j\sigma} + U \sum_i n_{i\uparrow} n_{i\downarrow}, \tag{4.48}$$

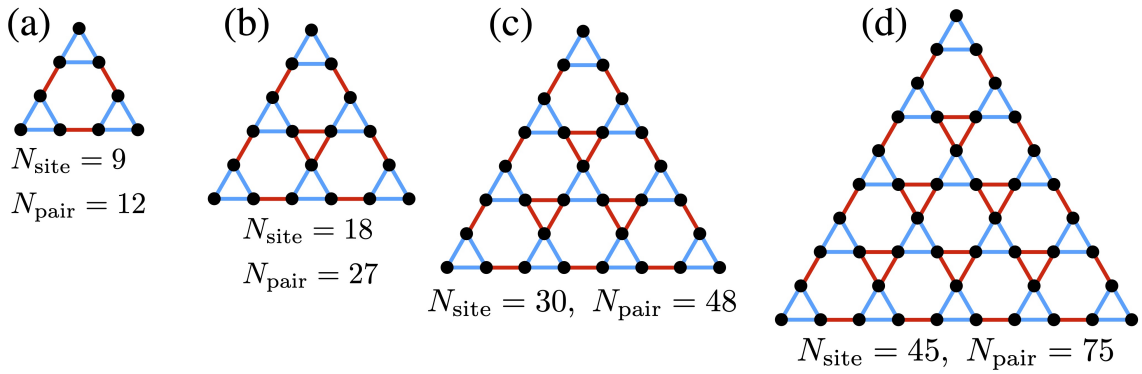

Figure 4.9: Kagome lattices with the open boundary condition.

$N_{\uparrow\downarrow}$	$N_{\rm site}$	$N_{\rm pair}$	$N_{\rm D}$	$16 \times N_{\rm D}$	$16 \times N_{\rm elem}$
$N_\uparrow = N_\downarrow$ ($S^z = 0$ or $1/2$)	3×2^2	24	924	14.8E+3	112E+3
	3×3^2	54	20.1E+6	320E+6	4.81E+9
	3×4^2	96	32.2E+12	516E+12	13.2E+15
$N_\uparrow = N_\downarrow/3$	3×2^2	24	495	7.92E+3	54.0E+3
	3×3^2	54	4.69E+6	75.0E+6	1.01E+9
	3×4^2	96	2.25E+12	36.1E+12	822E+12

Table 4.2: $N_{\rm D}$ and $N_{\rm elem}$ of the spin model on a kagome lattice under the periodic boundary condition.

$N_{\uparrow\downarrow}$	Fig.4.9	$N_{\rm site}$	$N_{\rm pair}$	$N_{\rm D}$	$16 \times N_{\rm D}$	$16 \times N_{\rm elem}$
$N_\uparrow = N_\downarrow$ ($S^z = 0$ or $1/2$)	(a)	9	12	126	2.02E+3	8.73E+3
	(b)	18	27	48.6E+3	778E+3	6.34E+6
	(c)	30	48	115E+6	2.48E+9	33.3E+9
	(d)	45	75	4.12E+12	65.9E+12	1.33E+15
$N_\uparrow = N_\downarrow/3$	(a)	9	12	84	1.34E+3	5.38E+3
	(b)	18	27	18.6E+3	297E+3	2.18E+6
	(c)	30	48	30.0E+6	481E+6	5.79E+9
	(d)	45	75	344E+9	5.52E+12	99.6E+12

Table 4.3: $N_{\rm D}$ and $N_{\rm elem}$ of the spin model on a kagome lattice under the open boundary condition.

where $c^\dagger_{i\sigma}$ is the creation operator on site i in the spin $\alpha =\uparrow,\downarrow$, t_{ij} is a hopping parameter and U is the strength of the Hubbard interaction. We here do not specify the lattice structure, but assume that the numbers of the sites and the hopping pairs (i,j) are given by $N_{\rm site}$ and $N_{\rm pair}$, respectively. The Hamiltonian commutes with the z-component of the total spin $S^z = 1/2\sum_i(n_{i\uparrow}-n_{i\downarrow})$, i.e., $N_{\uparrow(\downarrow)} = \sum_i n_{i\uparrow(\downarrow)}$ is conserved. The dimension of the Hamiltonian H specified by S_z is given by

$$N_{\rm D} = {}_{N_{\rm site}}C_{N_\uparrow} \times_{N_{\rm site}} C_{N_\downarrow}. \tag{4.49}$$

Let us next consider the number of non-zero elements in the Hamiltonian, which we denote by $N_{\rm elem} = N_{\rm Diago} + N_{\text{Off-Diago}}$. Because of the Hermitian matrix, considering the number in the lower triangular region of the Hamiltonian is enough. Then, we define $N_{\text{Off-Diago}}$ in that

$N_{\uparrow\downarrow}$	$N_{\rm site}$	$N_{\rm pair}$	$N_{\rm D}$	$16 \times N_{\rm D}$	$16 \times N_{\rm elem}$
$N_\uparrow = N_\downarrow$ ($S^z = 0$ or $1/2$)	3×2^2	24	854E+3	13.7E+6	192E+6
	$3 \times 2 \times 3$	36	2.36E+9	37.8E+9	759E+9
	3×3^2	54	402E+12	6.44E+15	187E+15
$N_\uparrow = N_\downarrow/3$	3×2^2	24	245E+3	3.92E+6	49.5E+6
	3×3^2	54	22.0E+12	351E+12	9.11E+15

Table 4.4: $N_{\rm D}$ and $N_{\rm elem}$ of the Hubbard model on a kagome lattice under the periodic boundary condition.

$N_{\uparrow\downarrow}$	Fig.4.9	$N_{\rm site}$	$N_{\rm pair}$	$N_{\rm D}$	$16 \times N_{\rm D}$	$16 \times N_{\rm elem}$
$N_\uparrow = N_\downarrow$ ($S^z = 0$ or $1/2$)	(a)	9	12	15.9E+3	254E+3	1.95E+6
	(b)	18	27	2.36E+9	37.8E+9	578E+9
$N_\uparrow = N_\downarrow/3$	(a)	9	12	7.06E+3	113E+3	790E+3
	(b)	18	27	345E+6	5.51E+9	75.6E+9

Table 4.5: $N_{\rm D}$ and $N_{\rm elem}$ of the Hubbard model on a kagome lattice under the open boundary condition.

sense. The diagonal elements are given by $U \sum n_{i\uparrow} n_{i\downarrow}$, which obviously implies that we have

$$N_{\rm Diago} = N_{\rm D}. \tag{4.50}$$

The off-diagonal elements are given by $\sum c^\dagger_{i\sigma} c_{j\sigma}$. To calculate its number, let us first focus on the hopping $c^\dagger_{1\uparrow} c_{2\uparrow}$. The many-body states that satisfy $c^\dagger_{1\uparrow} c_{2\uparrow} |\rangle \neq 0$ are given by $|2_\uparrow \cdots ; \cdots\cdots\rangle$, where the left "$\cdots$" is any configuration with respect to up-spins except for $1_\uparrow$ and $2_\uparrow$, and the right "$\cdots\cdots$" is any configuration with respect to down-spins. Thus, the number of such many-body states is given by ${}_{N_{\rm site}-2}C_{N_\uparrow - 1} \times_{N_{\rm site}} C_{N_\downarrow}$. Since the triangular region of the matrix is considered here, the number of the nonzero elements specified by $c^\dagger_{i\uparrow} c_{j\uparrow} + \text{h.c.}$ is also ${}_{N_{\rm site}-2}C_{N_\uparrow - 1} \times_{N_{\rm site}} C_{N_\downarrow}$. Consequently, we have

$$N_{\text{Off-Diago}} = N_{\rm pair}({}_{N_{\rm site}-2}C_{N_\uparrow - 1} \times_{N_{\rm site}} C_{N_\downarrow} + {}_{N_{\rm site}}C_{N_\uparrow} \times_{N_{\rm site}-2} C_{N_\downarrow - 1}) \tag{4.51}$$

In Table 4.4, we show $N_{\rm D}$ and $N_{\rm elem} = N_{\rm Diago} + N_{\text{Off-Diago}}$ for the Hubbard model on a kagome lattice under the periodic boundary condition. Here, hoppings between the nearest-neighbor pairs are only considered. We set $N_\uparrow = N_\downarrow$ or $N_\uparrow = N_\downarrow/3$. In Table 4.4, we show $N_{\rm D}$ and $N_{\rm elem}$ obtained under the open boundary condition.

Chapter 5

Adiabatic heuristic principle for the quantum Hall states on a torus

The adiabatic deformation is a fundamental concept in the theory of topological phases as shown in the previous chapters. The topological invariants given by bulk systems work as a kind of the order parameters, which is a modern picture for characterizing material phases beyond Landau's symmetry breaking theory. The adiabatic heuristic argument for the QH sates is one of the oldest such trials, which has been successful to describe the origin of the FQH effect in terms of the adiabatic deformation. In this chapter, we start by describing the role of the flux-attachment in the QH effect in relation to the composite fermion theory and the adiabatic heuristic argument. Although the adiabatic heuristic argument for the QH state is physically natural, there are some difficulties if one applies this idea to toroidal systems. This is because it is impossible to continuously change the value of the statistics due to the algebraic constraint in the braid group. By numerical calculations, this puzzle is resolved. By investigating the relation between the topological degeneracy and the Chern number, we also find the generalized Streda formula. This formula implies what is fundamental for topological invariants is the continuity of the energy gap, rather than the continuity of states.

5.1 Flux-attachment for the quantum Hall effect

The FQH effect is a typical example of the topologically ordered phases. Even though the FQH effect is essentially a many-body problem, one can describe it in terms of the IQH effect by applying the flux-attachment. According to the composite fermion theory [164,165], the FQH effect is interpreted as the IQH effect of the composite fermion. Furthermore, the adiabatic heuristic argument [166,167] states that the FQH states are continuously deformed into the IQH effect by adiabatic development of the flux-attachment. In this section, we begin by considering the fractional statistics for the successive arguments on the flux-attachment for the QH states.

5.1.1 Fractional statistics and flux-attachment

According to the quantum mechanics, identical particles are fundamentally indistinguishable. This simple property surprisingly brings tremendous diversity to quantum physics. As is well known, there are two kinds of particles in three-dimensional systems: bosons and fermions. They are defined by the phase of the wave functions associated with interchange of two particles, i.e., $\Psi(\cdots, \boldsymbol{r}_j, \cdots, \boldsymbol{r}_i, \cdots) = \Psi(\cdots, \boldsymbol{r}_i, \cdots, \boldsymbol{r}_j, \cdots)$ for bosons and $\Psi(\cdots, \boldsymbol{r}_j, \cdots, \boldsymbol{r}_i, \cdots) = -\Psi(\cdots, \boldsymbol{r}_i, \cdots, \boldsymbol{r}_j, \cdots)$ for fermions. They are derived from the

fact that the unitary operator of the interchange P_{ij} satisfies $P_{ij}^2 = 1$. Namely, bosons and fermions are identified by the eigenvalues of $P_{ij} = \pm 1$.

Let us now discuss it in more details in terms of Feynman's path-integral formalism [168, 169] for our successive arguments. The time evolution in the quantum mechanics is described by $|\Psi, t'\rangle = U(t', t)\,|\Psi, t\rangle$ with $t \leq t'$. By defining the propagator, it reduces to

$$\Psi(q', t') = \int_C dq K(q', t'; q, t)\Psi(q, t) \tag{5.1}$$

where C denotes the configuration space that is generally multiply connected and q is the coordinate. The propagator K is given by Feynman's path-integral as follows:

$$K(q', t'; q, t) = \sum_{\alpha \in \pi_1(C)} \chi(\alpha) \int_{q(t)\in\alpha} \mathcal{D}[q(t)] \exp\left\{ \frac{i}{\hbar} \int_t^{t'} dt L[q(t)] \right\}, \tag{5.2}$$

where $\int_{q(t)\in\alpha} \mathcal{D}[q(t)]$ indicates the summation over all paths connecting the coordinates q and q' in the configurations space and $\pi_1(C)$ is the fundamental group of the configuration space C. The paths belonging to the different homotopy class can not be continuously deformed with each other. Correspondingly, we here introduce the weight $\chi(\alpha)$. They satisfy $\chi(\alpha)^\dagger = \chi(\alpha)$ and $\chi(\alpha)\chi(\beta) = \chi(\alpha \cdot \beta)$, which implies that χ is itself a representation of $\pi_1(C)$.

Let us now consider the structure of the configuration space C. If distinguishable particles live on d-dimensional space, the configuration space is given by $C_n = R^{dN} \equiv R^d \times \cdots \times R^d$, where N is the particle number. For indistinguishable hard-core particles, on the other hand, we need to modify that obtained configuration space. First, a set of configurations associated with the symmetric group S_N should be identified. Also, due to the hard-core nature, configurations in which coordinates of two or more particles coincide should be removed. Consequently, we have

$$C_N = (R^{dN} - D)/S_N, \tag{5.3}$$

where $D = \{\boldsymbol{x}_1, \boldsymbol{x}_2, \cdots, \boldsymbol{x}_N |^\exists i \neq j, \boldsymbol{x}_i = \boldsymbol{x}_j\}$. When setting $3 \leq d$, we have $\pi_1(R^{dN} - D) = 0$, i.e., $\pi_1(C_N) = S_N$. Assuming the one-dimensional representations, we have only two representations, which corresponds to the statistics of bosons and fermions; a trivial representation $\chi(\alpha) = 1$ for all α is Bose-Einstein statistics and $\chi(\alpha) = 1$ (-1) with α even (odd) permutation is Fermi-Dirac statistics. For $d = 2$, on the other hand, $\pi_1(C)$ is a finite non-Abelian group. This is the so-called braid group, which is defined by

$$B_N(\mathcal{M}) \equiv \pi_1(C_N) = \pi_1((\mathcal{M}^N - D)/S_N), \tag{5.4}$$

where $\mathcal{M} = R^2$ in this case. The generators of this group are given by the operation of exchange between particles at $\boldsymbol{x}_i$ and $\boldsymbol{x}_{i+1}$, which we denote by σ_i $(i = 1, \cdots, N-1)$. The group structure is determined by the following relations:

$$\begin{aligned} &\sigma_i\sigma_j = \sigma_j\sigma_i \ (i \neq j \pm 1) \\ &\sigma_i\sigma_{i+1}\sigma_i = \sigma_{i+1}\sigma_i\sigma_{i+1} \ (1 \leq i \leq N-2). \end{aligned} \tag{5.5}$$

Its one-dimensional representations are given by

$$\chi(\sigma_i) = e^{i\theta}, \tag{5.6}$$

where $0 \leq \theta < 2\pi$. The representations with $\theta = 0$ and $\theta = \pi$ correspond to the Bose-Einstein statistics and Fermi-Dirac statistics obtained in $3 \leq d$, respectively. Other statistics

are called fractional statistics, which is the property peculiar to the two-dimensional systems. The particles with the fractional statistics are called anyons [170, 171].

Even if the representation associated with the fractional statistics is allowed in the analysis of the configuration space, it is a different issue that such particles really exist. Let us now demonstrate that anyons are indeed easily generated by the flux-attachment. As described in Chapter 3, the statistics of particles are diagnosed by computing the Berry phase defined by adiabatic development in which a particle is dragged around another. If the statistics of the particles is written by θ, the Berry phase is given by $e^{i2\theta}$. Thus, the Berry phase of electrons ($\theta = \pi$) is given by $e^{i2\pi} = 1$. Let us then consider the system of electron-flux composites. When the number of the attached fluxes per particle is ϕ, the Berry phase is given by $e^{i(2\pi+\phi)}$. This implies that the electron-flux composites are anyons whose statistics is given by $\theta = \pi + \phi/2$. These fluxes localized at particles are described by the singular gauge field as [171]

$$\boldsymbol{A}_j = -\frac{\phi\phi_0}{2\pi}\sum_{k\neq j}\boldsymbol{\nabla}_j\theta_{jk}, \tag{5.7}$$

where θ_{jk} is defined by $z_j - z_k = |z_j - z_k|e^{i\theta_{jk}}$ and $z_{ij} = x_i + iy_i$ is the coordinate of the ith particle. In the following sections, we describe the flux-attachment in relation to the QH effect.

5.1.2 Composite fermion theory

The composite fermion theory has been quite successful to describe the underlying physics of the FQH effect [164, 165]. This theory gives sophisticated views on not only the ordinary FQH effect but also more complex ones such as the multi-component FQH effects [172, 173] and the non-Abelian FQH effect [25, 27, 28]. In this subsection, we review the composite fermion theory for the single-component FQH effect.

Let us consider the FQH system at the filling factor $\nu = N_{\rm e}/N_\phi$, where $N_{\rm e}$ is the number of electrons and N_ϕ is the number of external fluxes. It means that an average flux per electron is given by $N_\phi/N_{\rm e} = 1/\nu$. We now attach the external magnetic fluxes into each electron. When the number of the fluxes is $2m$ with m integer, the electron-flux composites are fermion. These particles are called composite fermions. For the composite fermions, the number of the external fluxes is given by $N_\phi^* = N_\phi - 2mN_{\rm e}$, while the number of the composite fermions $N_{\rm CF}$ is identical to that of the original electrons. Then, the filling factor of the composite fermions is given by

$$\nu^* = \frac{N_{\rm CF}}{N_\phi^*} = \frac{N_{\rm e}}{N_\phi - 2mN_{\rm e}} = \frac{1}{1/\nu - 2m}. \tag{5.8}$$

Let us here assume that the system of composite fermions exhibits the IQH effect, i.e., $\nu^* = p$ with p integer. Here, the sign of p indicates the z-direction of the magnetic field compared with the original magnetic field associated with N_ϕ. Solving Eq. (5.8), we have

$$\nu = \frac{p}{2mp+1}. \tag{5.9}$$

It implies that the FQH effect of electrons at $\nu = p/(2mp+1)$ is interpreted as the IQH effect of composite fermions at $\nu^* = p$. The denominator of ν is always odd, which is consistent with experimental observations. For example, the Laughlin states is mapped to the $\nu = 1$ IQH state in the composite fermion theory. From this perspective, various properties of the FQH states are diagnosed by studying the IQH states. For example, the excitations

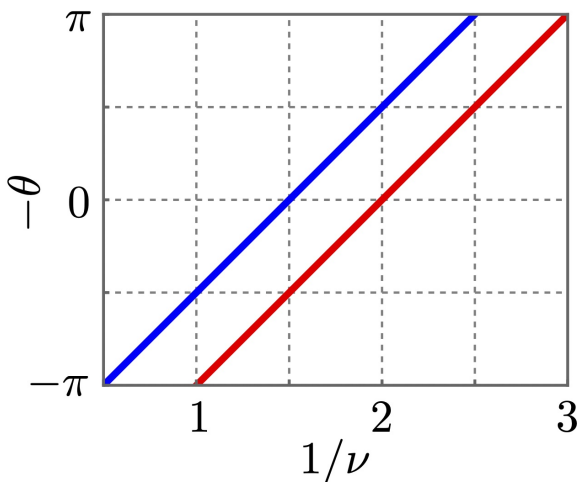

Figure 5.1: Two Series of the $\nu = 1$ IQH states (red) and the $\nu = 2$ IQH state (blue).

of the FQH state is understood from the physics of the IQH effect [174–177]. Also, this theory provides a theoretical framework to construct trial wave functions of the FQH states in a different way from the singular gauge transformation. The excellent overlaps with the exact wave functions with, e.g. the Coulomb interaction, implies the validity of this approach [165]. The composite fermion theory gives simple pictures for understanding other FQH states. For example, the FQH systems of spinful electrons gives fully spin polarized ground states depending on the filling fractions. The composite fermion theory gives clear explanations for this issue [172, 173]. While the FQH states such as the Laughlin state host quasiparticles with the fractional charges and the fractional statistics, the so-called non-Abelian FQH states [178] exhibit non-Abelian anyons obeying the generalized fractional statistics [25–28, 179, 180]. The typical example of the non-Abelian FQH states is the Moore-Read state, which is interpreted as the $p_x + ip_y$ paired state [28] of the composite fermions. The composite fermion theory is also valid for characterizing the gapless state appearing in systems at even denominator filling factors [181]. Recently, these issues have been actively studied in terms of the Dirac fermion theory [182, 183]. The parton construction [184] is a generalization of the composite fermion theory. This theory gives candidates of the FQH states in terms of the IQH states beyond the composite fermion theory. Some of parton states are expected to host non-Abelian excitations [185–189].

5.1.3 Adiabatic heuristic principle

According to the adiabatic heuristic principle [166, 167], the FQH states and the IQH states are adiabatically connected by trading the external magnetic fluxes for the statistical fluxes. Let us discuss it in this subsection.

As mentioned above, the statistics of particles are controlled by attaching flux tubes to particles. Particles with the fractional statistics given by θ are interpreted as bosons with θ/π fluxes. For example, one fermion is composed of one boson and one flux quantum. Then, we consider the system of anyons with θ under the magnetic field. The filling factor is defined as $\nu = N_a/N_\phi$, where N_a is the number of anyons. When considering it as the system of bosons, the number of the total fluxes are given by $N_\phi + N_a\theta/\pi$. Let us consider the flux-attachment in which the total flux remains constant. Noting that $N_\phi + N_a\theta/\pi = N_a(1/\nu + \theta/\pi)$, this

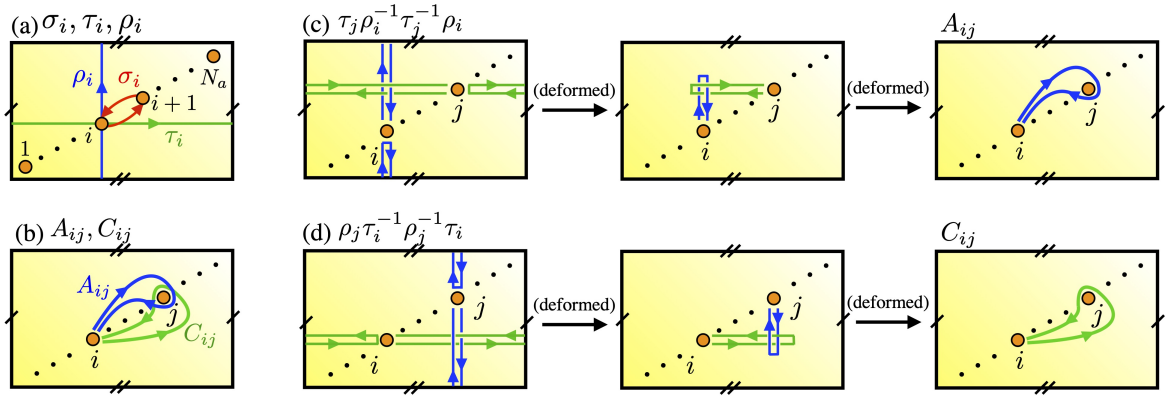

Figure 5.2: (a) Exchange operator σ_i and global operators τ_i and ρ_i. (b) Auxiliary operators A_{ij} and C_{ij}. (c) (d) The pictorial proofs about A_{ij} and C_{ij}.

condition is expressed as

$$\frac{1}{\nu} + \frac{\theta}{\pi} = \text{const.} \tag{5.10}$$

If a series includes the IQH system of fermions ($\theta = \pi$) at $\nu = p$, the filling factor ν and the statistics θ satisfy the relation $1/\nu + \theta/\pi = 1/p + 1$. Solving it, we have

$$\nu = \frac{p}{p(1 - \theta/\pi) + 1}. \tag{5.11}$$

This equation is identical to Eq. (5.9) in the composite fermion picture if θ/π is odd, i.e., particles are fermions. According to the adiabatic heuristic argument, the QH states in a same series are adiabatically connected by that adiabatic process. In Fig. 5.1, we plot Eq. (5.11) as for two series of the $\nu = 1$ IQH state and the $\nu = 2$ IQH state, respectively. A series of the $\nu = 1$ IQH state shown as the red line in the figure includes the Laughlin state. A series of the $\nu = 2$ IQH state shown as the blue line includes the fermion FQH state at $\nu = 2/5$.

While this heuristic argument for adiabatic deformation of the QH state is physically natural, there are some difficulties if one applies this idea to toroidal systems. This is because it is impossible to continuously change the value of the statistics due to the algebraic constraint in the braid group as shown in Sec. 5.2. Also, how does the topological degeneracy [91, 92] change during the process of the flux-attachment? In Sec. 5.3, we discuss the validity of the adiabatic heuristic on a torus numerically.

5.2 Anyons on a torus

As mentioned above, the fractional statistics of anyons are described from the representations of the braid group. For successive discussions on the adiabatic heuristic on a torus, let us now analyze the braid group on a torus [21, 190–192]. Also, we describe how to construct the system of anyons on a lattice on a torus [191, 193] for the numerical demonstration of the adiabatic heuristic principle.

5.2.1 Braid group on a torus

When N indistinguishable hard-core particles live on a manifold $\mathcal{M}$, their configuration space is given by $C_N = (\mathcal{M}^N - D)/S_N$, where D is the subset of configurations in which

two or more coordinate coincide and S_N is the symmetric group. Then the braid group of the manifold $\mathcal{M}$ is given by $B_N(\mathcal{M}) = \pi_1(C_N)$. In this subsection, we investigate the group structure of $B_N(\mathcal{M})$ with $\mathcal{M} = T^2$, which governs the fractional statistics of anyons on a torus.

The generators of the braid group $B_N(\mathcal{M})$ consist of σ_i $(i = 1, \cdots, N-1)$, τ_j, and ρ_j $(j = 1, \cdots, N)$, where σ_i is the counterclockwise interchange of the ith and $i+1$th particles, and τ_i and ρ_i take ith particle along a noncontractible loop in x and y directions, respectively. For convenience, let us introduce the auxiliary operators A_{ij} and C_{ij} defined as

$$A_{ij} = \tau_j \rho_i^{-1} \tau_j^{-1} \rho_i, \ C_{ij} = \rho_j \tau_i^{-1} \rho_j^{-1} \tau_i, \tag{5.12}$$

where $1 \le i < j \le N$. Their paths are shown in Figs. 5.2(a) and (b). The pictorial explanations about A_{ij} and C_{ij} are given in Figs. 5.2(c) and (d). The complete set of the relations of the braid group on a torus are divided into three categories [21, 190, 192]. The first category involves only the global operators τ_i's and ρ_i's:

$$A_{lm}\tau_k = \tau_k A_{lm}, \ A_{lm}\rho_k = \rho_k A_{lm}, \tag{5.13a}$$
$$\tau_i \tau_j = \tau_j \tau_i, \ \rho_i \rho_j = \rho_j \rho_i, \tag{5.13b}$$
$$C_{ij} = \left(\tau_i^{-1}\tau_j^{-1}\right) A_{ij}^{-1} \left(\tau_j \tau_i\right), \tag{5.13c}$$
$$A_{ij} = \left(\rho_i^{-1}\rho_j^{-1}\right) C_{ij}^{-1} \left(\rho_j \rho_i\right), \tag{5.13d}$$
$$C_{ij} = \left(A_{j-1,j}^{-1} A_{j-2,j}^{-1} \cdots A_{i+1,j}^{-1}\right) A_{ij}^{-1} \left(A_{i+1,j} \cdots A_{j-2,j} A_{j-1,j}\right), \tag{5.13e}$$
$$\tau_1^{-1}\rho_1^{-1}\tau_1\rho_1 = A_{1,2}A_{1,3}\cdots A_{1,n-1}A_{1,n}, \tag{5.13f}$$

where $1 \le k < l < m \le N$, $1 \le i < j \le N$. The pictorial proofs of Eqs. (5.13c) and (5.13d) are given in Figs. 5.3(a) and (b). The proofs of Eqs. (5.13e) and (5.13f) for $N = 3$ are also given in Figs. 5.3(c) and (d). The second category involves only σ_i's:

$$\sigma_i \sigma_j = \sigma_j \sigma_i \ (i \ne j \pm 1) \tag{5.14a}$$
$$\sigma_i \sigma_{i+1} \sigma_i = \sigma_{i+1} \sigma_i \sigma_{i+1} \ (1 \le i \le N-2). \tag{5.14b}$$

The third category mixes the global and the exchange operators:

$$\tau_{i+1} = \sigma_i^{-1} \tau_i \sigma_i^{-1}, \ \rho_{i+1} = \sigma_i \rho_i \sigma_i, \tag{5.15a}$$
$$\tau_1 \sigma_j = \sigma_j \tau_1, \ \rho_1 \sigma_j = \sigma_j \rho_1, \tag{5.15b}$$
$$\left(\sigma_i^{-1}\right)^2 = A_{i,i+1}, \tag{5.15c}$$

where $1 \le i \le N-1$ and $2 \le j \le N-1$. The pictorial proof of Eq. (5.15a) is given in Figs. 5.3(e) and (f).

From the relations of the braid group described above, let us discuss the universal features of anyons on a torus. Taking the basis $|\boldsymbol{r}_1, \boldsymbol{r}_2, \cdots, \boldsymbol{r}_N; w\rangle$, let us here assume that the representation of σ_i is given by

$$\sigma_i = e^{i\theta} \mathbf{1}_M, \tag{5.16}$$

where $w = 1, \cdots, M$ is the additional index, $\boldsymbol{r}_i$ is the position of the ith anyon, and M is the dimension of the representation. Hereafter, the symbol indicating the representations as $\chi(\sigma_i)$ is omitted. From Eqs. (5.15a) and (5.15b), we have

$$\tau_i = e^{-i2(i-1)\theta} \tau_1 \tag{5.17a}$$
$$\rho_i = e^{i2(i-1)\theta} \rho_1. \tag{5.17b}$$

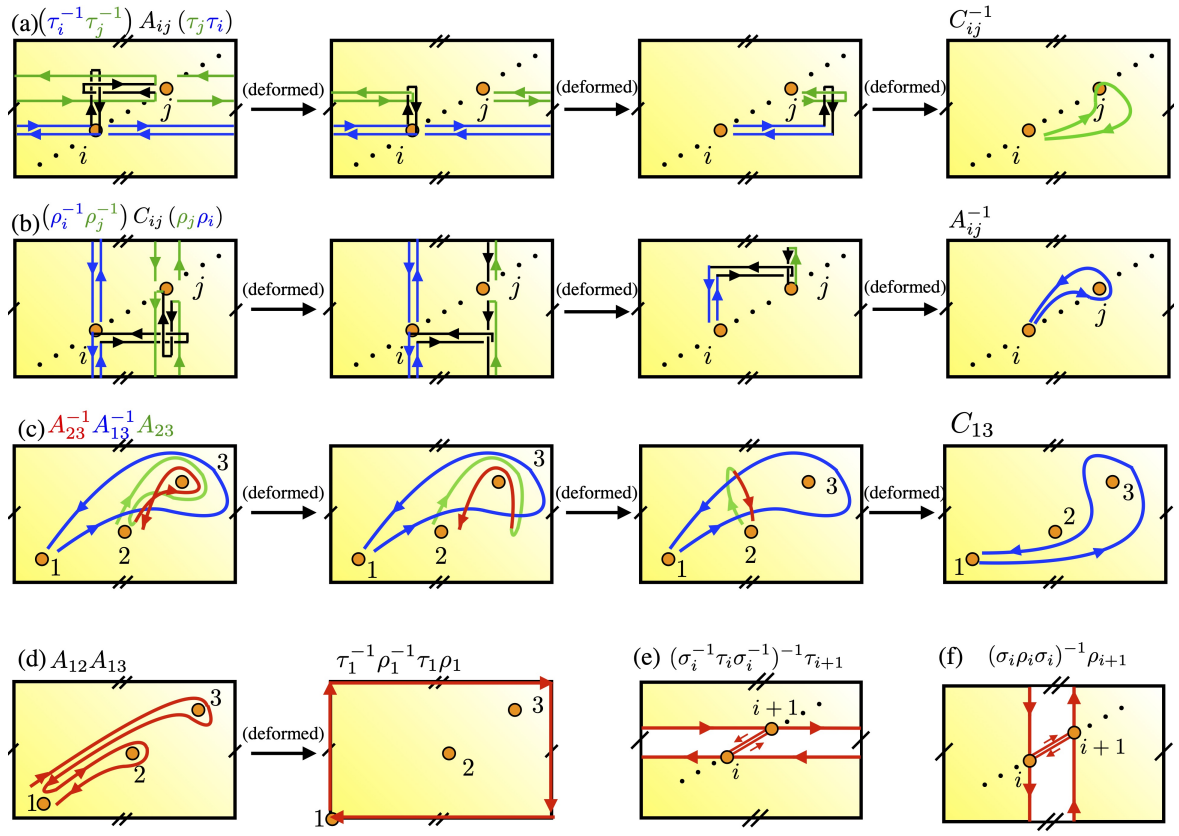

Figure 5.3: Pictorial proofs of (a) Eq. (5.13c), (b) Eq. (5.13d), (c) Eq. (5.13e) for $N = 3$, (d) Eq. (5.13f) for $N = 3$, and (e)(f) Eq. (5.15a).

It is consistent with Eq. (5.13b). Using it with Eqs. (5.12), (5.15c) and (5.13e), we have

$$A_{ij} = C_{ij}^{-1} = A_{12} = e^{-i2\theta}. \tag{5.18}$$

It is consistent with Eqs. (5.13a), (5.13c), (5.13d). Then, the remaining problems is to find the representations of τ_i's and ρ_i's satisfying Eqs. (5.12) and (5.13f). Equation (5.12) is rewritten as $A_{ij} = \tau_1\rho_1^{-1}\tau_1^{-1}\rho_1 = e^{-i2\theta}$ and $C_{ij} = \rho_1\tau_1^{-1}\rho_1^{-1}\tau_1 = e^{i2\theta}$, i.e., $\tau_1\rho_1 = e^{i2\theta}\rho_1\tau_1$. Therefore, we have

$$\begin{aligned} \tau_1\rho_1 &= e^{i2\theta}\rho_1\tau_1, \\ \tau_1\rho_1 &= e^{-i2(N-1)\theta}\rho_1\tau_1. \end{aligned} \tag{5.19}$$

Clearly these two relations require the restriction for the statistical phase as $e^{i2N\theta} = 1$, i.e.,

$$\theta = \frac{s\pi}{N}, \quad s = 0, \cdots, N-1. \tag{5.20}$$

Furthermore, calculating the determinant of Eqs. (5.19), we have the constraints on the dimension of the representation M and the statistical phase θ as $1 = e^{i2M\theta}$, i.e.,

$$\theta = \frac{s\pi}{M}, \quad s = 1, \cdots, M-1. \tag{5.21}$$

It means that when the statistics is given by $\theta = n\pi/m$ with n and m coprime integers, the dimension of the representation M should be a multiple of m. Matrices that meet Eqs. (5.19)

are given by $\tau_1 = W_x$ and $\rho_1 = W_y$ with, for example,

$$W_x = \begin{bmatrix} 0 & 1 & \dots & 0 \\ \vdots & \vdots & \ddots & \vdots \\ 0 & 0 & \dots & 1 \\ e^{i\eta_x} & 0 & \dots & 0 \end{bmatrix}, \tag{5.22}$$

$$W_y = e^{i\eta_y}\mathrm{diag}[e^{i2\theta}, e^{i4\theta}, \cdots, e^{i2M\theta}], \tag{5.23}$$

where the phase factor $e^{i\eta_x}$ and $e^{i\eta_y}$ correspond to the twisted angles of the boundary conditions. Indeed, they satisfy

$$W_x W_y = e^{-i2\theta} W_y W_x \tag{5.24}$$

for any $\vec{\eta} = (\eta_x, \eta_y)$. Consequently, the representations of τ_i and ρ_i are given by

$$\tau_j = e^{-i2\theta(j-1)} W_x \tag{5.25}$$

$$\rho_j = e^{i2\theta(j-1)} W_y. \tag{5.26}$$

Let us now move onto the discussions on anyons on a torus under the magnetic field [194]. Naively, some of the relations described above are modified. Assuming that the system size is $L_x \times L_y$ and the external magnetic field B is described by the vector potential $\boldsymbol{A}$, Eqs. (5.13f) and (5.15a) are replaced with

$$\tau_1^{-1}\rho_1^{-1}\tau_1\rho_1 = e^{-i\frac{e}{\hbar}BL_xL_y} A_{1,2}A_{1,3}\cdots A_{1,n-1}A_{1,n}, \tag{5.27}$$

$$\tau_{i+1} = e^{i\frac{e}{\hbar}(\alpha_{i+1}-\alpha_i)}\sigma_i^{-1}\tau_i\sigma_i^{-1}, \ \rho_{i+1} = e^{i\frac{e}{\hbar}(\beta_{i+1}-\beta_i)}\sigma_i\rho_i\sigma_i, \tag{5.28}$$

where the charge is $-e$, α_i and β_i are defined by

$$\alpha_i = \oint_{L_{\tau_i}} d\boldsymbol{r}\cdot\boldsymbol{A}(\boldsymbol{r}), \tag{5.29}$$

$$\beta_i = \oint_{L_{\rho_i}} d\boldsymbol{r}\cdot\boldsymbol{A}(\boldsymbol{r}). \tag{5.30}$$

Here L_{τ_i} and L_{ρ_i} are the path defined by the global operators τ_i and ρ_i, respectively. As seen in Figs. 5.3(e) and (f), the path given by $(\sigma_i^{-1}\tau_i\sigma_i^{-1})^{-1}\tau_{i+1}$ and $(\sigma_i\rho_i\sigma_i)^{-1}\rho_{i+1}$ define closed regions, respectively. Correspondingly, the AB phases are added in the relations. These modifications make a little change in the characteristics of anyons mentioned above. Instead of Eqs. (5.26), the representations of τ_j and ρ_j are given by

$$\tau_j = e^{i\frac{e}{\hbar}\alpha_j} e^{-i2\theta(j-1)} W_x \tag{5.31}$$

$$\rho_j = e^{i\frac{e}{\hbar}\beta_j} e^{i2\theta(j-1)} W_y. \tag{5.32}$$

In addition, Eq. (5.19) is replaced with the following relations as

$$\begin{aligned} \tau_1\rho_1 &= e^{i2\theta}\rho_1\tau_1, \\ \tau_1\rho_1 &= e^{-i2\pi N_\phi - i2(N-1)\theta}\rho_1\tau_1, \end{aligned} \tag{5.33}$$

where $N_\phi = BL_xL_y/\phi_0$ is the total number of external fluxes. Due to it, the constraint in Eq. (5.20) is changed as $e^{i2\pi N_\phi + i2N\theta} = 1$, i.e.,

$$\frac{N_\phi}{N} + \frac{\theta}{\pi} = \frac{s}{N}, \tag{5.34}$$

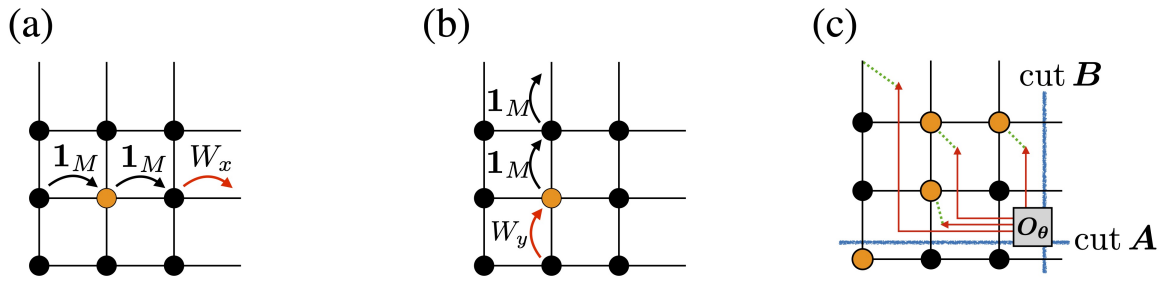

Figure 5.4: Anyons on lattices.

where s is the total number of fluxes including to the external magnetic fluxes and statistical fluxes. Assuming that s/N is constant, this equation is identical to Eq. (5.10) in the adiabatic heuristic argument. On the other hand, the constraint in Eq. (5.21) on the dimension of the representation is given again.

In this subsection, we analyze the braid group on a torus and derive the fundamental relations of the adiabatic heuristic argument consistently. However, some constraints of the braid group implies that continuous deformation of the statistics θ is prohibited on a torus even though the magnetic field is present. In the following, we resolve this issue of the adiabatic heuristic principle on a torus by numerical calculations.

5.2.2 Anyon model on a torus

In this subsection, let us describe our model of anyons on a torus [191, 193] under the magnetic field for numerical calculations. This system is put on the $N_x \times N_y$ square lattices. The number of anyons is N_a. We here denote the number of external fluxes per plaquette and the statistics of anyons by ϕ and θ, respectively. We consider the Hamiltonian including hoppings and interactions as

$$H = t \sum_{\langle ij \rangle} e^{i\phi_{ij}} e^{i\theta_{ij}} c_i^\dagger c_j \otimes W^{(ij)} + V \sum_{\langle ij \rangle} n_i n_j \otimes \mathbf{1}_M, \tag{5.35}$$

where $c_i^\dagger$ is the creation operator of a hard-core boson at site i, $n_i = c_i^\dagger c_i$, the phase factors $e^{i\phi_{ij}}$ is the Peierls phase describing the external magnetic field, $e^{i\theta_{ij}}$ describes the statistical fluxes localized into particles, and $W^{(ij)}$ is the $M \times M$ matrix that describes the global behavior of anyons on a torus. For ϕ_{ij}, the string gauge [113] is chosen, which we have mentioned in Chapter 2. How to construct θ_{ij} and the matrix $W^{(ij)}$ is described below [191, 193].

Let us now first describe the matrix $W^{(ij)}$. When the statistics is given by $\theta = n\pi/m$ with n, m coprime integers, we set the irreducible representation, i.e., $M = m$. As shown in Figs. 5.4(a) and (b), it is defined as $W^{(ij)} = W_{x(y)}$ for hoppings across the boundary in the $x(y)$ direction, and $W^{(ij)} = \mathbf{1}_M$ for other hoppings. The matrices W_x and W_y are given in Eqs. (5.22) and (5.23), where $|\boldsymbol{r}_1, \boldsymbol{r}_2, \cdots, \boldsymbol{r}_N; w\rangle$ is used for the basis. It means that when an anyon hops across the boundary in the x-direction [cut B in Fig. 5.4(c)], the index is modified from w to $w-1$. In addition, the twisted angle $e^{i\eta_x}$ is applied if $w = 1$. When an anyon hops across the boundary in the y-direction [cut A in Fig. 5.4(c)], the phase factor $e^{i2w\theta} e^{i\eta_y}$ is given. While the global behavior of anyons are given by the matrix $W^{(ij)}$, their local features are described by $e^{i\theta_{ij}}$. In a similar way with the string gauge, θ_{ij} is also described by the strings as shown in Fig. 5.4(c). While the initial point of the string is fixed at one plaquette with the origin O_θ, the terminal point is located at a plaquette adjacent to an anyon and it carries the phase $e^{i\theta}$. In addition, we need to require other rules as follows.

(i) When a string of a hopping anyon wipes other anyons, the phase factor is given as if the wiped anyons hop across the string.

(ii) When an anyon hops across the boundary in x direction [cut B in Fig. 5.4(c)], the additional phase factor $e^{i(N_a-1)\theta}$ is given. This rule removes the artificial twisted angle of the boundary condition in x-direction that is made by statistical strings.

(iii) Horizontal strings carry the phase factor $e^{i2\theta}$ instead of $e^{i\theta}$. This rule also correct the boundary condition in y-direction. For otherwise, the artificial angle in y-direction appears.

(iv) When an anyon hops across the boundary in y-direction [cut A in Fig. 5.4(c)], the additional phase factor $e^{iX\theta}$ is given, where X is the number of anyons that locate at sites in the same x-axis. This rule describes the fractional statistics with respect to the interchange of anyons in the same x-axis.

This formulation of anyons in this framework are consistent with the representation of τ_i and ρ_i shown in Eqs. (5.31) and (5.32). We would like to note that the artificial fluxes are given at the plaquette with the origin O_θ [193]. Therefore, the condition of the uniform magnetic field shown in Eq. (2.5) is rewritten as

$$e^{i2\pi\phi(1-N_xN_y)-i2\theta N_a} = e^{i2\pi\phi}. \tag{5.36}$$

This condition consistently rederive the fundamental relation of the adiabatic heuristic.

5.3 Numerical demonstration of the adiabatic heuristic principle

In this section, by using the above framework, we demonstrate the validity of the adiabatic heuristic principle on a torus. Unless otherwise stated, the parameters are set as $N_x = N_y = 10$, $t = -1$, $V = 5$, and $\vec{\eta} = \vec{0}$. Also, we mention topological invariants of this adiabatic development. In the following discussions, we assume that states are degenerated when their energy difference ΔE is given by $\Delta E < 0.001$.

5.3.1 Energy gap and adiabatic deformation

Let us first consider a series of the $\nu = 1$ IQH state. This series includes the Laughlin state. In Fig. 5.5(a), we plot the many-body energy as function of $1/\nu$, where the statistics is given by

$$\nu = \frac{p}{p(1-\theta/\pi)+1} \tag{5.37}$$

with $p = 1$. Since the system at ν is identical to that at $-\nu$, we only consider systems at $0 \leq \nu$. In the calculation, we set $\theta = n\pi/m$ with various n and $m \leq 7$. The denominator of θ/π is expressed by colors of the plots. It means that the plots with different colors in the figure are given by the Hamiltonian with different dimensions. Nevertheless, the gaps defined by a dense set of the Hamiltonians seen in Fig. 5.5(a) are smooth. At $\nu = 1/3$, the gapped ground state with the three-fold degeneracy is obtained, which is consistent with the lattice analogue of the Laughlin state [103]. Furthermore, the gap at $0 < \nu$ are always finite, which demonstrates the adiabatic continuity between the $\nu = 1$ IQH state and the Laughlin state. This finite gap closes at $1/\nu = 0$ in which the particles are bosons. This gapless behavior implies the emergence of the Nambu-Goldston modes of the superconductor of hard-core bosons [195]. In contrast to the smoothness of the gaps, the topological degeneracy is surprisingly changed wildly as shown in Fig. 5.5(b). We will give its explanation in terms of the many-body Chern number. In Fig. 5.5(a), we also plot the energy gap of the noninteracting systems, i.e., $V = 0$. While the FQH states of anyons have the finite gaps, they collapse at $\nu = 1/3$

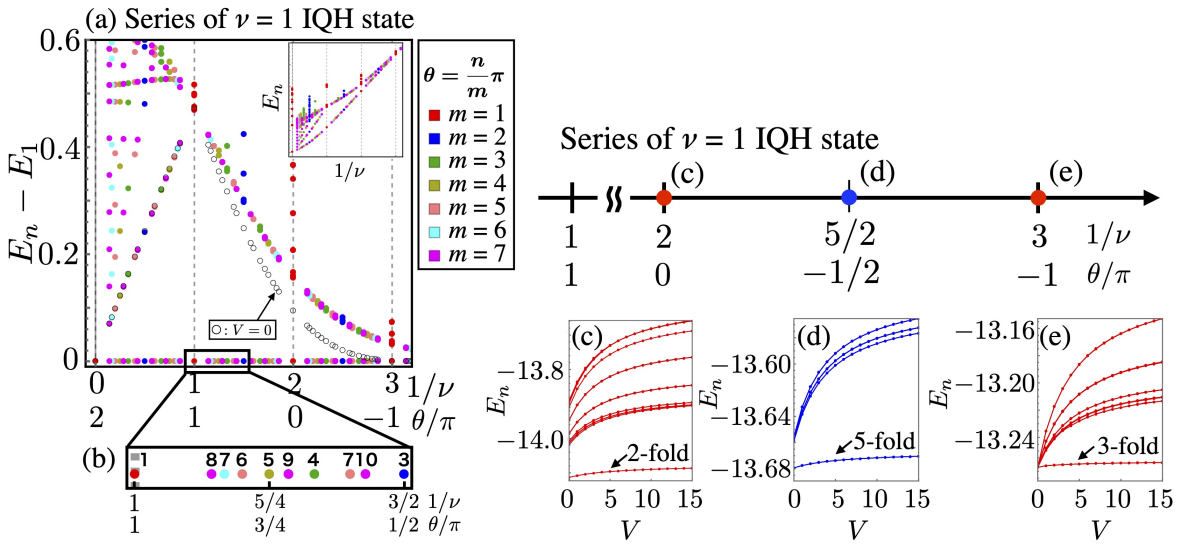

Figure 5.5: Many-body energy in a series of the $\nu = 1$ IQH state. We set $N_x = N_y = 10$, $t = -1$, $V = 5$, and $N_a = 4$. The lowest 40 states are shown in the figures. (a) Energy gap as function of the inverse of the filling factor ν. The dashed lines indicate systems of bosons or fermions. The gaps for $V = 0$ are plotted as the empty circles. The inset in (a) is the energy spectrum E_n. (b) Ground state degeneracy N_D. (c)(d)(e) Energy spectra as functions of the strength of the interaction V. The filling factor and the statistics are given as (c) $(\nu, \theta) = (1/2, 0)$, (d) $(\nu, \theta) = (2/5, -\pi/2)$, and (e) $(\nu, \theta) = (1/3, -\pi)$.

in which the FQH state of fermions is realized. This is because this ground state of fermions is described by the partially filled lowest Landau bands. This suggests that the electron-electron interactions are fundamental only for systems of fermions to show the FQH effects. In Figs. 5.5(c)-(e), the energy spectra are shown as functions of the strength of the interaction V. As long as V is finite, the global features of the spectra are independent of the value of V. It implies that the adiabatic behavior shown in Fig. 5.5(a) for $V = 5$ is also nearly independent of the value of V as long as $V \neq 0$.

Let us next discuss other series of the FQH effects. Figures 5.6(a) and (b) show the energy gaps as functions of $1/\nu$ in the same way as Fig. 5.5(a) but we fix $p = 2$ or $p = 3$ in Eq. (5.37). For example, a series of the $\nu = 2$ and $\nu = 3$ IQH state include the FQH state of fermions at $\nu = 2/5$ and $\nu = 3/7$, respectively. The results imply that the gaps of these FQH states are connected to the IQH states without gap closing, while their topological degeneracy changes wildly as seen in Figs. 5.6(c) and (d). In both figures, the energy gaps close at $1/\nu = 0$. These are the systems of anyons with $\theta = 3\pi/2$ and $\theta = 4\pi/3$ under no magnetic field, respectively. This gapless behaviors are consistent with the emergence of the Nambu-Goldston modes of the anyon-superconductor [196–198]. Our results imply that the adiabatic heuristic principle for other series with larger p is also valid and the anyon-superconductor with $\theta = (1 + 1/p)\pi$ appears when all external fluxes are attached into particles.

Before moving to the next subsection, let us mention the relation of the Hofstadter butterfly of the single-particle problem [199, 200]. In Fig. 5.5(a) and Fig. 5.6(a) and (b), the horizontal-axis and the vertical-axis indicate the inverse of the filling factor ν and the energy E_n. Because of $1/\nu = N_\phi/N_a = N_x N_y \phi/N_a$ and we fix N_x, N_y and N_a in the figures, the horizontal-axis also represents the number of external fluxes per plaquette ϕ. In this sense, unusual adiabatic deformation, where the gap is smooth but the ground state degeneracy is changed wildly, is associated with a many-body generalization of the Hofstadter butterfly.

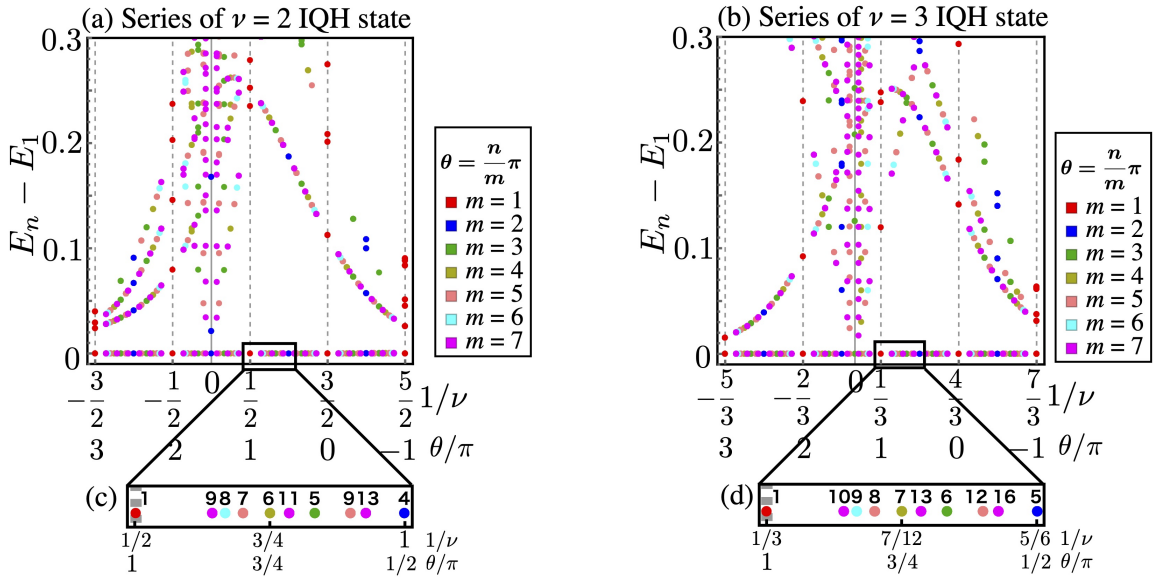

Figure 5.6: Energy gaps in a series of (a) the $\nu = 2$ and (b) the $\nu = 3$ IQH state. The number of anyons is set as (a) $N_a = 4$ and (b) $N_a = 3$. The dashed lines indicate systems of bosons or fermions. The lowest (a) 40 and (b) 70 states are shown in the figures. (c)(d) Ground state degeneracy N_D.

This similarity implies that the many-body Chern number would work as the topological and adiabatic invariant for characterizing the finite many-body gap in the manner similar to the single-particle Chern number for the Hofstadter bands. As demonstrated below, this expectation of the Chern number is correct.

5.3.2 Topological invariants

In this subsection, let us discuss the topological invariance of the adiabatic heuristic argument. Based on the above discussions on the relation to the Hofstadter butterfly, we calculate the many-body Chern number defined by

$$C = \frac{1}{2\pi i}\int_{T^2} \mathrm{Tr}\, \boldsymbol{F}, \tag{5.38}$$

where $\boldsymbol{F} = d\boldsymbol{A} + \boldsymbol{A}^2$, $\boldsymbol{A} = \Psi^\dagger d\Psi$, $d = \sum_\alpha \partial_{\eta_\alpha}$, $T^2 = [0, 2\pi]\times[0, 2\pi]$, and $\Psi = (|G_1\rangle, |G_2\rangle, \cdots)$ is the ground state multiplet. Figures 5.7(a), (b), and (c) show the Chern number of a series of the $\nu = p$ IQH state with $p = 1, 2, 3$. These results imply that the many-body Chern number works well as the topological (adiabatic) invariant. The Chern number jumps at $1/\nu = 0$, which is consistent with the gap closing behavior seen in Figs. 5.5 and 5.6. It is suggested that the Chern number defined by a series of the $\nu = p$ IQH state is given by

$$C = \mathrm{sgn}(\nu) \times p, \tag{5.39}$$

where $\mathrm{sgn}(x) = 1$ for $0 < x$ and -1 for $x < 0$. Namely, it means that the topology of the $\nu = p$ IQH state remains valid as long as the energy gap remains open even though the topological degeneracy is changed wildly.

It is confirmed that the many-body energy of the QH systems nearly independent of the value of the twisted angles $\vec{\eta}$. On the other hand, the spectral flows at the transition point, i.e., $1/\nu = 0$, show completely different features. In Fig. 5.7(d), (e), and (f), we

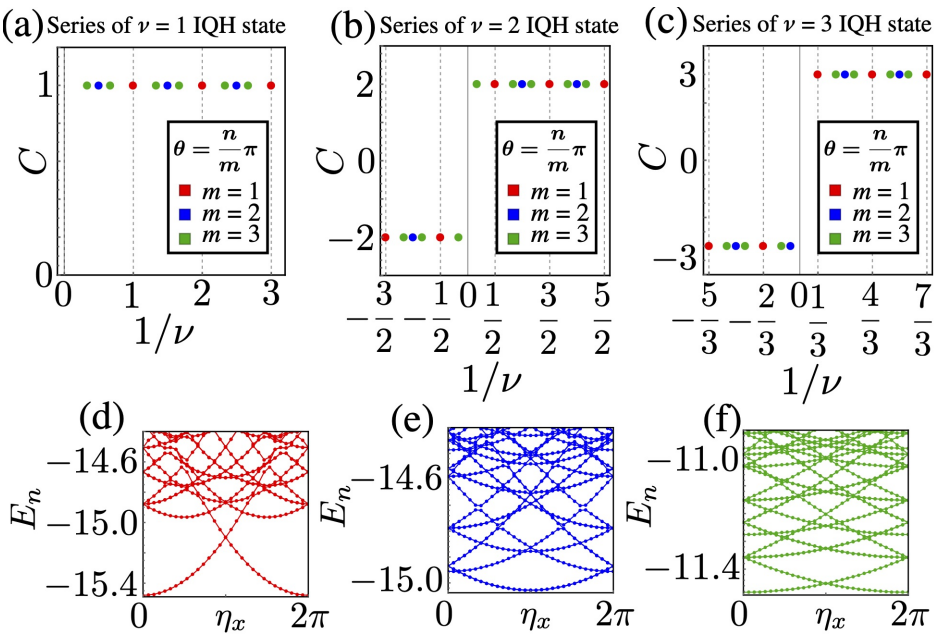

Figure 5.7: (a)-(c) Many-body Chern number for a series of $\nu = p$ IQH state with (a) $p = 1$, (a) $p = 2$, and (c) $p = 3$. (d)-(f) Spectral flows of the systems of anyons with $\theta = (1 + 1/p)\pi$ with (d) $p = 1$, (e) $p = 2$, and (f) $p = 3$. The twisted angles in the y-direction are fixed at $\eta_y = 0$.

show the energy as functions of η_y for the systems of anyons with $\theta = (1 + 1/p)\pi$ with $p = 1, 2, 3$. These are systems in which the gap closing occurs for a series of the $\nu = p$ IQH state. Their energies depend greatly on the boundary conditions. This strong dependence is indeed consistent with the absence of the energy gap. This gapless behavior implies the emergence of the Nambu-Goldston modes of the anyon-superconductor.

5.4 Generalized Streda formula

In this section, we clarify the problem of the topological degeneracy that changes wildly during the unusual adiabatic deformation. Specifically, we show that the topological degeneracy is described by the many-body Chern number. Our finding corresponds to a generalization of the Streda formula [201], which we call the generalized Streda formula. When the magnetic field ϕ is sufficiently weak, the magnetic length becomes larger compared to the lattice constant. This implies that physics of this lattice model is diagnosed by studying a continuous system. For ease of analysis, we consider the continuous system below.

5.4.1 Topological degeneracy

Fermions

For the successive discussions on anyons, let us begin by considering the fermionic FQH states [91–93, 202]. We first consider a one-body system in a uniform magnetic field. Here, the system with the size $L_x \times L_y$ under the twisted boundary conditions is considered. The Hamiltonian is given by

$$H = \frac{1}{2m}\boldsymbol{\pi}^2, \tag{5.40}$$

where $\boldsymbol{\pi} = \boldsymbol{p} - e\boldsymbol{A}(\boldsymbol{r})$ with $e < 0$. Due to the magnetic field, the operator $e^{\frac{i}{\hbar}\boldsymbol{p}\cdot\boldsymbol{a}}$ no longer work well as a translation operation. Defining another momentum as $\boldsymbol{K} = \boldsymbol{\pi} + e\boldsymbol{B}\times\boldsymbol{r}$ [203], let us define the magnetic translation operator as

$$t(\boldsymbol{a}) = e^{\frac{i}{\hbar}\boldsymbol{K}\cdot\boldsymbol{a}}. \tag{5.41}$$

It gives the following commutation relations as

$$\begin{aligned} t(\boldsymbol{a})\,\boldsymbol{r}\,t(\boldsymbol{a})^{-1} &= \boldsymbol{r} + \boldsymbol{a} \\ t(\boldsymbol{a})\boldsymbol{\pi}t^{-1}(\boldsymbol{a}) &= \boldsymbol{\pi}. \end{aligned}$$

However, this translations do not commute with each other:

$$t(\boldsymbol{b})t(\boldsymbol{a}) = t(\boldsymbol{b}+\boldsymbol{a})e^{-\frac{1}{2}\frac{i}{\hbar}eB(\boldsymbol{a}\times\boldsymbol{b})} = t(\boldsymbol{a})t(\boldsymbol{b})e^{-\frac{i}{\hbar}eB(\boldsymbol{a}\times\boldsymbol{b})}. \tag{5.42}$$

One can interpret the phase factor $e^{-\frac{i}{\hbar}eB(\boldsymbol{a}\times\boldsymbol{b})}$ as the AB phase.

Let us move on to the many-body problem. We assume that the Hamiltonian is given by

$$H = \sum_{k=1}^{N_\mathrm{e}} \frac{1}{2m}\boldsymbol{\pi}_k^2 + \sum_{k,l} V(\boldsymbol{r}_k - \boldsymbol{r}_l). \tag{5.43}$$

The above results of the one-body problem lead the following relations:

$$\begin{aligned} &t_i(\boldsymbol{a})\,\boldsymbol{r}_j\,t_i(\boldsymbol{a})^{-1} = \boldsymbol{r}_j + \delta_{ij}\boldsymbol{a} \\ &[\boldsymbol{\pi}_i, t_j(\boldsymbol{a})] = 0 \\ &[t_i(\boldsymbol{a}), t_j(\boldsymbol{b})] = 0 \ (i \neq j) \\ &t_i(\boldsymbol{b})t_i(\boldsymbol{a}) = t_i(\boldsymbol{a})t_i(\boldsymbol{b})e^{i2\pi N_\phi \frac{\boldsymbol{a}\times\boldsymbol{b}}{L_x L_y}}, \end{aligned} \tag{5.44}$$

where we have used $N_\phi = BL_xL_y/\phi_0$, $\phi_0 = \hbar/|e|$. Those relations imply

$$\begin{aligned} &[H, t_i(L_x\boldsymbol{e}_x)] = [H, t_i(L_y\boldsymbol{e}_y)] = [t_j(L_x\boldsymbol{e}_x), t_i(L_y\boldsymbol{e}_y)] = 0, \\ &t_i(L_y\boldsymbol{e}_y)t_i(L_x\boldsymbol{e}_x) = t_i(L_x\boldsymbol{e}_x)t_i(L_y\boldsymbol{e}_y)e^{i2\pi N_\phi}, \end{aligned} \tag{5.45}$$

for any i and j. This implies that if N_ϕ is an integer, the operators H, $t_i(L_x\boldsymbol{e}_x)$'s, and $t_i(L_y\boldsymbol{e}_y)$'s commute with each other. The twisted boundary conditions are specified by $t_i(L_x\boldsymbol{e}_x)$'s and $t_i(L_y\boldsymbol{e}_y)$'s. Let us now define the center-of-mass translation operator as

$$T(\boldsymbol{a}) = \prod_{k=1}^{N_e} t_k(\boldsymbol{a}), \tag{5.46}$$

where we denote the particle number by N_e We try to find the condition of $\boldsymbol{a}$ such that $T(\boldsymbol{a})$ commutes with H, $t_i(L_x\boldsymbol{e}_x)$'s, and $t_i(L_y\boldsymbol{e}_y)$'s. Because of

$$\left[\sum_{k=1}^{N_e}\frac{1}{2m}\boldsymbol{\pi}_k^2, T(\boldsymbol{a})\right] = \left[\sum_{k,l} V(\boldsymbol{r}_k - \boldsymbol{r}_l), T(\boldsymbol{a})\right] = 0 \tag{5.47}$$

with any $\boldsymbol{a}$, we have $[H, T(\boldsymbol{a})] = 0$. Also we have the following commutation relations

$$\begin{aligned} t_i(L_y\boldsymbol{e}_y)T(a_x\boldsymbol{e}_x) &= T(a_x\boldsymbol{e}_x)t_i(L_y\boldsymbol{e}_y)e^{i2\pi N_\phi\frac{a_x}{L_x}}, \\ t_i(L_x\boldsymbol{e}_x)T(a_y\boldsymbol{e}_y) &= T(a_y\boldsymbol{e}_y)t_i(L_x\boldsymbol{e}_x)e^{-i2\pi N_\phi\frac{a_y}{L_y}}, \end{aligned}$$

which implies that their simultaneous diagonalization requires the relations $a_x = (L_x/N_\phi) \times$ (int.) and $a_y = (L_y/N_\phi) \times$ (int.). It means that the center-of-mass translation operators that commute with H, $t_i(L_x \boldsymbol{e}_x)$'s, and $t_i(L_y \boldsymbol{e}_y)$'s are given by the linear combination of $T(\frac{L_x}{N_\phi}\boldsymbol{e}_x)$ and $T(\frac{L_y}{N_\phi}\boldsymbol{e}_y)$. Noting that

$$T(a_y \boldsymbol{e}_y)T(a_x \boldsymbol{e}_x) = T(a_x \boldsymbol{e}_x)T(a_y \boldsymbol{e}_y) e^{i2\pi N_e N_\phi \frac{a_x a_y}{L_x L_y}},$$

we have the important commutation relations

$$T(\frac{L_y}{N_\phi}\boldsymbol{e}_y)T(\frac{L_x}{N_\phi}\boldsymbol{e}_x) = T(\frac{L_x}{N_\phi}\boldsymbol{e}_x)T(\frac{L_y}{N_\phi}\boldsymbol{e}_y) e^{i2\pi \frac{N_e}{N_\phi}}. \tag{5.48}$$

Specifying the ground state by the eigenvalues of $T(\frac{L_y}{N_\phi}\boldsymbol{e}_y)$, i.e. $T(\frac{L_y}{N_\phi}\boldsymbol{e}_y)\,|\lambda\rangle = e^{i\lambda}\,|\lambda\rangle$, we have

$$T^s(\frac{L_x}{N_\phi}\boldsymbol{e}_x)\,|\lambda\rangle = |\lambda + 2s\pi\nu\rangle\,. \tag{5.49}$$

It implies that the ground state is at least q-fold degenerated, where $\nu = p/q$ with p and q being co-primes.

Anyons

Let us extend the above discussions to the systems of anyons. We now assume that the center-of-mass translation operator $T(\boldsymbol{a})$, where all anyons are translated by $\boldsymbol{a}$, commutes with the Hamiltonian and satisfies the following relations:

$$T^{-1}(\boldsymbol{b})T^{-1}(\boldsymbol{a})T(\boldsymbol{b})T(\boldsymbol{a}) = \exp\Big\{-i\frac{e}{\hbar}B(\boldsymbol{a}\times\boldsymbol{b})N_a\Big\}, \tag{5.50}$$

$$\rho_i^{-1}T^{-1}(\boldsymbol{a})\rho_i T(\boldsymbol{a}) = \exp\Big\{-i\frac{e}{\hbar}B(\boldsymbol{a}\times L_y\boldsymbol{e}_y)\Big\}, \tag{5.51}$$

$$T^{-1}(\boldsymbol{b})\tau_i^{-1}T(\boldsymbol{b})\tau_i = \exp\Big\{-i\frac{e}{\hbar}B(L_x\boldsymbol{e}_x\times\boldsymbol{b})\Big\}. \tag{5.52}$$

This is the natural assumption since the loops defined by above operators enclose no anyons. According to the arguments of the braid group, the global operators of anyons τ_i and ρ_j, which specify the twisted boundary condition, do not commute with each other. Instead, we have

$$[\tau_i^m, \rho_j] = 0, \tag{5.53}$$

where the statistics is given by $\theta = n\pi/m$. Then let us try to find $\boldsymbol{a}$ such that $T(\boldsymbol{a})$ commutes with τ_i^m and ρ_j. By using Eqs. (5.51) and (5.52) and generalizing the above discussions on fermions, we naively have such operator as

$$\mathcal{T}_x \equiv T(\frac{L_x}{N_\phi}\boldsymbol{e}_x), \tag{5.54}$$

$$\mathcal{T}_y \equiv T(\frac{1}{m}\frac{L_y}{N_\phi}\boldsymbol{e}_y). \tag{5.55}$$

From Eq. (5.50) with $N_\phi = BL_xL_y/\phi_0$, and $\phi_0 = \hbar/|e|$, we have

$$\mathcal{T}_y^{-1}\mathcal{T}_x^{-1}\mathcal{T}_y\mathcal{T}_x = e^{i2\pi\frac{N_a}{mN_\phi}}. \tag{5.56}$$

Specifying the ground state by the eigenvalues of $\mathcal{T}_y$, i.e., $\mathcal{T}_y |\lambda\rangle = e^{i\lambda} |\lambda\rangle$, we have

$$\mathcal{T}_x^s |\lambda\rangle = |\lambda + 2s\pi\nu/m\rangle . \tag{5.57}$$

This implies that when $\nu/m = \mathcal{P}/\mathcal{Q}$ with $\mathcal{P}$, $\mathcal{Q}$ coprime integers, the ground state is $\mathcal{Q}$-fold degenerated. However, the numerically obtained degeneracy is indeed larger than the number given by the above formulation. It means that there is another operator that characterizes the internal structure of the degenerated ground state. Then let us now define a new translation operator as

$$\mathcal{T}'_x \equiv \tau_1 T(\frac{n}{m}\frac{L_x}{N_\phi}\boldsymbol{e}_x). \tag{5.58}$$

From Eq. (5.51) and $\tau_i^{-1}\rho_j^{-1}\tau_i\rho_j = e^{i2\theta}$, we have $[\mathcal{T}'_x, \tau_i^m] = [\mathcal{T}'_x, \rho_j] = 0$. We also have

$$\mathcal{T}_y^{-1}\mathcal{T}_x'^{-1}\mathcal{T}_y\mathcal{T}'_x = e^{i2\pi\left(\frac{1}{m}+\frac{nN_a}{m^2N_\phi}\right)}. \tag{5.59}$$

Then, we have

$$\begin{aligned} &\mathcal{T}_x^s\mathcal{T}_x'^t |\lambda\rangle = |\lambda + 2\pi f_{s,t}\rangle , \\ &f_{s,t} = \frac{\nu}{m}s + \left(\frac{1}{m} + \frac{n\nu}{m^2}\right)t. \end{aligned} \tag{5.60}$$

This implies that the number of the degeneracy is identical to the number of pairs s, t that gives different value of $e^{i2\pi f_{s,t}}$. In a series of the $\nu = p$ IQH state, the filling factor ν and the statistical phase θ satisfy the relation in Eq. (5.37), i.e.,

$$\frac{\theta}{\pi} = -\frac{1}{\nu} + \frac{1}{p} + 1. \tag{5.61}$$

Substituting it into Eq. (5.60), we have

$$f_{s,t} = \frac{\nu}{m}s + \left(\frac{1}{m} + \frac{n\nu}{m^2}\right)t \tag{5.62}$$

$$= \frac{\nu}{m}s + \left(\frac{1}{m} + \left(-\frac{1}{\nu} + \frac{1}{p} + 1\right)\frac{\nu}{m}\right)t \tag{5.63}$$

$$= (t + pt + ps)\frac{\nu}{mp} \tag{5.64}$$

We here would like to note that mp/ν is always integer as

$$\frac{mp}{\nu} = mp \times \frac{p(1 - n/m) + 1}{p} = p(m - n) + m \tag{5.65}$$

where Eq. (5.37) has been used. This implies that the possible values of $e^{i2\pi f_{s,t}}$ is given by $e^{i2\pi f_{-a,a}}$ with $a = 1, \cdots, mp/|\nu|$. Namely, the topological degeneracy is given by

$$N_{\mathrm{TD}} = \frac{mp}{|\nu|}. \tag{5.66}$$

This expression is completely consistent with the numerically obtained results. In the above calculation, we set the dimension of the representation as $M = m$. If one sets reducible representation, i.e., $M = \alpha m$ with α integer, the degeneracy increases by α times. This implies that Eq. (5.66) is extended for the any dimensions of the representation as follows:

$$N_{\mathrm{TD}} = \frac{Mp}{|\nu|}. \tag{5.67}$$

5.4.2 Generalization of the Streda formula

Let us now demonstrate that the relation in Eq. (5.67) reduces to the generalized Streda formula. As mentioned above, our numerical calculations suggests that the Chern number works as an adiabatic invariant. Substituting Eq. (5.39) into Eq.(5.67), we have

$$N_{\mathrm{TD}} = \frac{MC}{\nu}. \tag{5.68}$$

Taking difference between two states belonging to a same series, it reduces to

$$\Delta N_{\mathrm{TD}} = \Delta\left(\frac{M}{\nu}\right) C. \tag{5.69}$$

Let us now define the number of "partons" and the extended number of sites as $N_p = N_{\mathrm{TD}} N_a$ and $N'_{\mathrm{site}} = M N_x N_y$, respectively. Because of $\Delta N_{\mathrm{TD}} = (\Delta N_p)/N_a$ and $\Delta(M/\nu) = \Delta(M N_x N_y \phi)/N_a = \Delta(N'_{\mathrm{site}}\phi)/N_a$, we finally have

$$\frac{\Delta N_p / N'_{\mathrm{site}}}{\Delta\phi} = C. \tag{5.70}$$

We call this equation the "generalized Streda formula". Indeed, this formula for fermions reduces to the standard Streda formula; the FQH system of fermions gives the parameters as $M = 1$, $\nu = p/q$, $N_{\mathrm{TD}} = q$ and $C = p$. In this case, $N_p/N'_{\mathrm{site}} = qN_a/N_{\mathrm{site}}$ is identical to the density of particles for the system in which the p Landau bands are completely filled.

Before closing this section, we would like to mention the generalized Streda formula. Equation (5.70) indicates that the difference of the topological degeneracy induced by the flux-attachment is described by the topological (adiabatic) invariant. This implies that what is deformed continuously in adiabatic developments is not states but energy gaps.

5.5 Conclusion

In this chapter, we have showed that the adiabatic heuristic argument on a torus is valid even though the continuous deformation of the statistics θ is not allowed due to the constraints of the braid group on a torus. Namely, it has been numerically confirmed that the FQH states on a torus are adiabatically connected to the IQH states without gap closing although their topological degeneracy wildly changes during the deformation. The Chern number defined by the degenerated ground state multiplet works well as an adiabatic invariant of this unusual development. By the analysis based on the translational invariance of anyons, we have clarified the problem of the wild change in the topological degeneracy. From this result, we have discovered the generalized Streda formula, which makes the connection between the wild change of the topological degeneracy and the topological invariant (i.e., the many-body Chern number). This implies that what is fundamental for topological invariants is the continuity of the energy gap, rather than the continuity of states.

Summary and Conclusions

In this thesis, we have presented theoretical studies of topological invariants and the adiabatic principle in correlated systems. The first part was dedicated to theoretical investigations of the topological invariants. In Chapter 1, we have given general arguments for topological invariants associated with the Berry connection and their gauge structures. By reviewing the TKNN formula and the Niu-Thouless-Wu formula, we have also showed that how the quantization of the Hall conductance is described by the Chern number. Nowadays, a wide variety of correlated topological materials have been characterized by numerical calculations of the many-body Chern number in the Niu-Thouless-Wu formula. In Chapter 2, we have numerically demonstrated that the integration in evaluating it can be indeed skipped if the system size is sufficiently large. Introducing the one-plaquette Chern number as a topological index without the integration, we have showed its exponential accuracy in the integer and fractional quantum Hall (IQH and FQH) systems. Our findings provide a concise way to numerically identify correlated topological phases since the lack of the integration essentially reduces the computational costs inherent to the many-body problems.

The second part was dedicated to theoretical investigations regarding to the adiabatic principle. The adiabatic deformation is a fundamental concept for theory of topological phases. In Chapter 3, we have revisited a simple problem to show that the (non-Abelian) Berry phases characterize the geometrical structures of wave functions involved in the adiabatic development. These topological characters are invariant under certain adiabatic deformations of systems (quantized Berry phase in Chapter 1). From this perspective, in Chapter 4, we have proposed a new topological state called "higher-order topological Mott insulator" (HOTMI). This state exhibits a generalized bulk-edge correspondence derived from correlation effects; the bulk topology in d-dimensions predicts the appearance of boundary modes only with gapless spin excitations around $d-n$-dimensional boundaries ($2 \leq n$). We have numerically confirmed that the HOTMIs appear in the Hubbard model on a kagome lattice, where the emergence of the corner-Mott sates are associated with the quantized spin-Berry phase. This gapless nature can be described by free-spins that emerge from the adiabatically deformed systems. While its emergence is confirmed only in the kagome lattice in this thesis, the HOTMI is expected to be ubiquitous. In Chapter 5, moving on to the problem of the adiabatic deformations of the QH states, we have investigated the validity of the adiabatic heuristic principle on a torus. According to the braid group on a torus, the continuous change of the statistical phase is not algebraically allowed. By the numerical analysis of the periodic systems of anyons, we have demonstrated that the energy gaps of the QH states are indeed smooth and finite even though the topological degeneracy is changed wildly. Our numerical results imply that the many-body Chern number of the ground state multiplet works as an adiabatic invariant in this unusual adiabatic continuity. From the arguments on the translational invariance of anyons, we also have shown that the wild change of the topological degeneracy is described by the Chern number. We call this relation the generalized Streda formula. This formula implies what is fundamental for topological invariants is the continuity of the energy gap, rather than the continuity of states.

This thesis gives not only an efficient way to evaluate the topological invariant but also propose a new correlated topological states. Furthermore, a new formula is discovered that provides a new perspective on topological invariants. We hope that our finding opens up a new way for understanding correlated topological phases.

Acknowledgments

I would like to express my deepest appreciation to Prof. Y. Hatsugai not only for his fruitful discussions, but also continuous encouragements and strong supports during my undergraduate, master, and doctor courses. Without his thoughtful guidance, I could not have done this work. I would like to express special thanks to all my collaborators Dr. T. Kariyado, Dr. H. Watanabe, and Dr. T. Yoshida, for their stimulating and helpful discussions. I also would like to express my gratitude to the examiners of this thesis, Prof. Y. Tokura, Prof. X. Hu, and Prof. S. Nomura for valuable advice and comments. I would like to thank all my colleagues, Dr Y. Kuno, Dr. T. Mizoguchi, Dr. S. Oono, Dr. H. Araki, K. Hoda, K. Kohda, Y. Takahashi, S. Fubasami, S. Nishizawa, S. Suzuki, T. Isobe, R. Kamoda, H. Kurihara, S. Ito, S. Oka, H. Wakao, G. Najima for enlightening discussions and the warm atmosphere. I would like to thank University of Tsukuba, JSPS and JASSO for financial supports. Lastly, I am deeply grateful to my parents for unconditional support and encouragement which made it possible to complete the study.

Publications

Journal publications

1. Koji Kudo, Haruki Watanabe, Toshikaze Kariyado, and Yasuhiro Hatsugai. "Many-body chern number without integration", Phys. Rev. Lett., **122**, 146601 (2019)

2. Koji Kudo, Tsuneya Yoshida, and Yasuhiro Hatsugai. "Higher-order topological mott insulators", Phys. Rev. Lett., **123**, 196402, (2019)

3. Koji Kudo and Yasuhiro Hatsugai. "Adiabatic heuristic principle on a torus and generalized streda formula", Phys. Rev. B, **102**, 125108, (2020)

4. Tsuneya Yoshida, Koji Kudo, and Yasuhiro Hatsugai. "Non-hermitian fractional quantum hall states", Scientific Reports, **9**, 16895, (2019)

5. Tsuneya Yoshida, Koji Kudo, Hosho Katsura, and Yasuhiro Hatsugai. "Fate of fractional quantum hall states in open quantum systems: Characterization of correlated topological states for the full liouvillian", Phys. Rev. Research, **2**, 033428 (2020)

International conference contributions

1. Koji Kudo and Yasuhiro Hatsugai, "Many-body Chern number matrix in fractional quantum Hall effect of graphene", International Workshop on SYMMETRY and TOPOLOGY in Condensed-Matter physics, Tokyo, Japan, June 2018 (poster)

2. Koji Kudo and Yasuhiro Hatsugai, "Halperin 331 state of the FQH system of the $n = 0$ Landau band of graphene", The 23rd International Conference on High Magnetic Fields in Semiconductor Physics (HMF-23), Toulouse, France, July 2018 (poster)

3. Koji Kudo, Haruki Watanabe, Toshikaze Kariyado, and Yasuhiro Hatsugai, "Exponential accuracy of many-body Chern number without integration", Bulk-Edge Correspondence 2018X, Japan, Tokyo, Dec. 2018 (poster)

4. Koji Kudo, Haruki Watanabe, Toshikaze Kariyado, and Yasuhiro Hatsugai, "One-plaquette Chern number: Many-body Chern number without integration ", APS March Meeting 2019, USA, Boston, Mar. 2019 (oral)

5. Koji Kudo, Haruki Watanabe, Toshikaze Kariyado, and Yasuhiro Hatsugai, "Exponential precision of Chern number without integration by twisted angles", Synthetic Topological Matter, Germany, Dresden, May 2019 (poster)

6. Koji Kudo, Tsuneya Yoshida, and Yasuhiro Hatsugai, "Correlated higher-order topological insulator on kagome lattice", International Conference on Frontiers of Correlated Electron Sciences (FCES19), Japan, Tokyo, May 2019 (poster)

7. Koji Kudo, Tsuneya Yoshida, and Yasuhiro Hatsugai, "Hubbard model on the kagome lattice and higher-order topological Mott insulators", New Trends in Topological Insulators 2019 and Variety and Universality of Bulk-edge Correspondence in Topological Phases 2019, Japan, Hiroshima, July 2019 (poster)

8. Koji Kudo, Tsuneya Yoshida, and Yasuhiro Hatsugai, "Higher-Order Topological Mott Insulator on the Kagome Lattice", International Conference on Strongly Correlated Electron Systems (SCES) 2019, Japan, Okayama, Sep. 2019 (poster)

9. Koji Kudo, Tsuneya Yoshida, and Yasuhiro Hatsugai, "Mott physics of the higher-order topological insulator on the kagome lattice", Trends in Theory of Correlated Materials (TTCM2019), Japan, Kyoto, Oct. 2019 (poster)

10. Koji Kudo, Tsuneya Yoshida, and Yasuhiro Hatsugai, "Higher-order bulk-boundary correspondence of a topological Mott insulator", International Conference on Topological Materials Science 2019 (TopoMat2019), Japan, Kyoto, Dec. 2019 (poster)

11. Koji Kudo, and Yasuhiro Hatsugai, "Numerical Study of Adiabatic Heuristic for the Quantum Hall States", BE/BC2020F, Japan, Tokyo, Feb. 2020 (poster, online)

Bibliography

[1] K. v. Klitzing, G. Dorda, and M. Pepper. New method for high-accuracy determination of the fine-structure constant based on quantized hall resistance. *Phys. Rev. Lett.*, 45:494–497, Aug 1980.

[2] R. B. Laughlin. Quantized hall conductivity in two dimensions. *Phys. Rev. B*, 23:5632–5633, May 1981.

[3] D. J. Thouless, M. Kohmoto, M. P. Nightingale, and M. den Nijs. Quantized hall conductance in a two-dimensional periodic potential. *Phys. Rev. Lett.*, 49:405–408, Aug 1982.

[4] M. V. Berry. Quantal phase factors accompanying adiabatic changes. *Proceedings of the Royal Society of London. A. Mathematical and Physical Sciences*, 392(1802):45, 03 1984.

[5] Barry Simon. Holonomy, the quantum adiabatic theorem, and berry's phase. *Phys. Rev. Lett.*, 51:2167–2170, Dec 1983.

[6] M. Kohmoto. Topological invariant and the quantization of the Hall conductance. *Annals of Physics*, 160:343–354, 1985.

[7] Yasuhiro Hatsugai. Edge states in the integer quantum hall effect and the riemann surface of the bloch function. *Phys. Rev. B*, 48:11851–11862, Oct 1993.

[8] Yasuhiro Hatsugai. Chern number and edge states in the integer quantum hall effect. *Phys. Rev. Lett.*, 71:3697–3700, Nov 1993.

[9] F.D.M. Haldane. Continuum dynamics of the 1-d heisenberg antiferromagnet: Identification with the o(3) nonlinear sigma model. *Physics Letters A*, 93(9):464 – 468, 1983.

[10] Ian Affleck, Tom Kennedy, Elliott H. Lieb, and Hal Tasaki. Rigorous results on valence-bond ground states in antiferromagnets. *Phys. Rev. Lett.*, 59:799–802, Aug 1987.

[11] D. C. Tsui, H. L. Stormer, and A. C. Gossard. Two-dimensional magnetotransport in the extreme quantum limit. *Phys. Rev. Lett.*, 48:1559–1562, May 1982.

[12] R. B. Laughlin. Anomalous quantum hall effect: An incompressible quantum fluid with fractionally charged excitations. *Phys. Rev. Lett.*, 50:1395–1398, May 1983.

[13] Xiao-Gang Wen. Topological orders and edge excitations in fractional quantum hall states. *Advances in Physics*, 44(5):405–473, 1995.

[14] Xiao-Gang Wen. Colloquium: Zoo of quantum-topological phases of matter. *Rev. Mod. Phys.*, 89:041004, Dec 2017.

[15] Daniel Arovas, J. R. Schrieffer, and Frank Wilczek. Fractional statistics and the quantum hall effect. *Phys. Rev. Lett.*, 53:722–723, Aug 1984.

[16] F. D. M. Haldane. Fractional quantization of the hall effect: A hierarchy of incompressible quantum fluid states. *Phys. Rev. Lett.*, 51:605–608, Aug 1983.

[17] B. I. Halperin. Statistics of quasiparticles and the hierarchy of fractional quantized hall states. *Phys. Rev. Lett.*, 52:1583–1586, Apr 1984.

[18] M. Stone. *Quantum Hall Effect*. World Scientific, 1992.

[19] David Tong. Lectures on the quantum hall effect. 2016.

[20] X. G. Wen. Vacuum degeneracy of chiral spin states in compactified space. *Phys. Rev. B*, 40:7387–7390, Oct 1989.

[21] Torbjörn Einarsson. Fractional statistics on a torus. *Phys. Rev. Lett.*, 64:1995–1998, Apr 1990.

[22] Masaki Oshikawa and T. Senthil. Fractionalization, topological order, and quasiparticle statistics. *Phys. Rev. Lett.*, 96:060601, Feb 2006.

[23] Masatoshi Sato, Mahito Kohmoto, and Yong-Shi Wu. Braid group, gauge invariance, and topological order. *Phys. Rev. Lett.*, 97:010601, Jul 2006.

[24] Masaki Oshikawa, Yong Baek Kim, Kirill Shtengel, Chetan Nayak, and Sumanta Tewari. Topological degeneracy of non-abelian states for dummies. *Annals of Physics*, 322(6):1477 – 1498, 2007.

[25] Gregory Moore and Nicholas Read. Nonabelions in the fractional quantum hall effect. *Nuclear Physics B*, 360(2):362 – 396, 1991.

[26] Martin Greiter, Xiao-Gang Wen, and Frank Wilczek. Paired hall state at half filling. *Phys. Rev. Lett.*, 66:3205–3208, Jun 1991.

[27] N. Read and E. Rezayi. Beyond paired quantum hall states: Parafermions and incompressible states in the first excited landau level. *Phys. Rev. B*, 59:8084–8092, Mar 1999.

[28] N. Read and Dmitry Green. Paired states of fermions in two dimensions with breaking of parity and time-reversal symmetries and the fractional quantum hall effect. *Phys. Rev. B*, 61:10267–10297, Apr 2000.

[29] V. Kalmeyer and R. B. Laughlin. Equivalence of the resonating-valence-bond and fractional quantum hall states. *Phys. Rev. Lett.*, 59:2095–2098, Nov 1987.

[30] X. G. WEN. Topological orders in rigid states. *International Journal of Modern Physics B*, 04(02):239–271, 1990.

[31] N. Read and Subir Sachdev. Large-n expansion for frustrated quantum antiferromagnets. *Phys. Rev. Lett.*, 66:1773–1776, Apr 1991.

[32] X. G. Wen. Mean-field theory of spin-liquid states with finite energy gap and topological orders. *Phys. Rev. B*, 44:2664–2672, Aug 1991.

[33] A.Yu. Kitaev. Fault-tolerant quantum computation by anyons. *Annals of Physics*, 303(1):2 – 30, 2003.

[34] Michael A. Levin and Xiao-Gang Wen. String-net condensation: A physical mechanism for topological phases. *Phys. Rev. B*, 71:045110, Jan 2005.

[35] Alexei Kitaev and John Preskill. Topological entanglement entropy. *Phys. Rev. Lett.*, 96:110404, Mar 2006.

[36] Michael Levin and Xiao-Gang Wen. Detecting topological order in a ground state wave function. *Phys. Rev. Lett.*, 96:110405, Mar 2006.

[37] Xie Chen, Zheng-Cheng Gu, and Xiao-Gang Wen. Local unitary transformation, long-range quantum entanglement, wave function renormalization, and topological order. *Phys. Rev. B*, 82:155138, Oct 2010.

[38] Alexei Kitaev. Anyons in an exactly solved model and beyond. *Annals of Physics*, 321(1):2 – 111, 2006. January Special Issue.

[39] Chetan Nayak, Steven H. Simon, Ady Stern, Michael Freedman, and Sankar Das Sarma. Non-abelian anyons and topological quantum computation. *Rev. Mod. Phys.*, 80:1083–1159, Sep 2008.

[40] C. L. Kane and E. J. Mele. Quantum spin hall effect in graphene. *Phys. Rev. Lett.*, 95:226801, Nov 2005.

[41] M. Z. Hasan and C. L. Kane. Colloquium: Topological insulators. *Rev. Mod. Phys.*, 82:3045–3067, Nov 2010.

[42] Xiao-Liang Qi and Shou-Cheng Zhang. Topological insulators and superconductors. *Rev. Mod. Phys.*, 83:1057–1110, Oct 2011.

[43] Markus König, Steffen Wiedmann, Christoph Brüne, Andreas Roth, Hartmut Buhmann, Laurens W. Molenkamp, Xiao-Liang Qi, and Shou-Cheng Zhang. Quantum spin hall insulator state in hgte quantum wells. *Science*, 318(5851):766–770, 2007.

[44] Andreas P. Schnyder, Shinsei Ryu, Akira Furusaki, and Andreas W. W. Ludwig. Classification of topological insulators and superconductors in three spatial dimensions. *Phys. Rev. B*, 78:195125, Nov 2008.

[45] Xiao-Liang Qi, Taylor L. Hughes, and Shou-Cheng Zhang. Topological field theory of time-reversal invariant insulators. *Phys. Rev. B*, 78:195424, Nov 2008.

[46] Alexei Kitaev. Periodic table for topological insulators and superconductors. *AIP Conference Proceedings*, 1134(1):22–30, 2009.

[47] Shinsei Ryu, Andreas P Schnyder, Akira Furusaki, and Andreas W W Ludwig. Topological insulators and superconductors: tenfold way and dimensional hierarchy. *New Journal of Physics*, 12(6):065010, jun 2010.

[48] Titus Neupert, Luiz Santos, Claudio Chamon, and Christopher Mudry. Fractional quantum hall states at zero magnetic field. *Phys. Rev. Lett.*, 106:236804, Jun 2011.

[49] D. N. Sheng, Zheng-Cheng Gu, Kai Sun, and L. Sheng. Fractional quantum hall effect in the absence of landau levels. *Nature Communications*, 2:389 EP –, 07 2011.

[50] N. Regnault and B. Andrei Bernevig. Fractional chern insulator. *Phys. Rev. X*, 1:021014, Dec 2011.

[51] Michael Levin and Ady Stern. Fractional topological insulators. *Phys. Rev. Lett.*, 103:196803, Nov 2009.

[52] Titus Neupert, Luiz Santos, Shinsei Ryu, Claudio Chamon, and Christopher Mudry. Fractional topological liquids with time-reversal symmetry and their lattice realization. *Phys. Rev. B*, 84:165107, Oct 2011.

[53] Dmytro Pesin and Leon Balents. Mott physics and band topology in materials with strong spin–orbit interaction. *Nature Physics*, 6:376 EP –, 03 2010.

[54] Stephan Rachel and Karyn Le Hur. Topological insulators and mott physics from the hubbard interaction. *Phys. Rev. B*, 82:075106, Aug 2010.

[55] Tsuneya Yoshida, Robert Peters, Satoshi Fujimoto, and Norio Kawakami. Characterization of a topological mott insulator in one dimension. *Phys. Rev. Lett.*, 112:196404, May 2014.

[56] Tsuneya Yoshida and Norio Kawakami. Topological edge mott insulating state in two dimensions at finite temperatures: Bulk and edge analysis. *Phys. Rev. B*, 94:085149, Aug 2016.

[57] Mehdi Kargarian and Gregory A. Fiete. Topological crystalline insulators in transition metal oxides. *Phys. Rev. Lett.*, 110:156403, Apr 2013.

[58] Maxim Dzero, Kai Sun, Victor Galitski, and Piers Coleman. Topological kondo insulators. *Phys. Rev. Lett.*, 104:106408, Mar 2010.

[59] Maxim Dzero, Kai Sun, Piers Coleman, and Victor Galitski. Theory of topological kondo insulators. *Phys. Rev. B*, 85:045130, Jan 2012.

[60] Feng Lu, JianZhou Zhao, Hongming Weng, Zhong Fang, and Xi Dai. Correlated topological insulators with mixed valence. *Phys. Rev. Lett.*, 110:096401, Feb 2013.

[61] Hongming Weng, Jianzhou Zhao, Zhijun Wang, Zhong Fang, and Xi Dai. Topological crystalline kondo insulator in mixed valence ytterbium borides. *Phys. Rev. Lett.*, 112:016403, Jan 2014.

[62] Lukasz Fidkowski and Alexei Kitaev. Effects of interactions on the topological classification of free fermion systems. *Phys. Rev. B*, 81:134509, Apr 2010.

[63] Lukasz Fidkowski and Alexei Kitaev. Topological phases of fermions in one dimension. *Phys. Rev. B*, 83:075103, Feb 2011.

[64] Ari M. Turner, Frank Pollmann, and Erez Berg. Topological phases of one-dimensional fermions: An entanglement point of view. *Phys. Rev. B*, 83:075102, Feb 2011.

[65] Yuan-Ming Lu and Ashvin Vishwanath. Theory and classification of interacting integer topological phases in two dimensions: A chern-simons approach. *Phys. Rev. B*, 86:125119, Sep 2012.

[66] Michael Levin and Ady Stern. Classification and analysis of two-dimensional abelian fractional topological insulators. *Phys. Rev. B*, 86:115131, Sep 2012.

[67] Hong Yao and Shinsei Ryu. Interaction effect on topological classification of superconductors in two dimensions. *Phys. Rev. B*, 88:064507, Aug 2013.

[68] Shinsei Ryu and Shou-Cheng Zhang. Interacting topological phases and modular invariance. *Phys. Rev. B*, 85:245132, Jun 2012.

[69] Yi-Zhuang You and Cenke Xu. Symmetry-protected topological states of interacting fermions and bosons. *Phys. Rev. B*, 90:245120, Dec 2014.

[70] Hiroki Isobe and Liang Fu. Theory of interacting topological crystalline insulators. *Phys. Rev. B*, 92:081304, Aug 2015.

[71] Tsuneya Yoshida and Akira Furusaki. Correlation effects on topological crystalline insulators. *Phys. Rev. B*, 92:085114, Aug 2015.

[72] Takahiro Morimoto, Akira Furusaki, and Christopher Mudry. Breakdown of the topological classification $\mathbb{Z}$ for gapped phases of noninteracting fermions by quartic interactions. *Phys. Rev. B*, 92:125104, Sep 2015.

[73] Tsuneya Yoshida and Norio Kawakami. Reduction of $\mathbb{Z}$ classification of a two-dimensional weak topological insulator: Real-space dynamical mean-field theory study. *Phys. Rev. B*, 95:045127, Jan 2017.

[74] Tsuneya Yoshida, Akito Daido, Youichi Yanase, and Norio Kawakami. Fate of majorana modes in $\mathrm{cecoin}_5/\mathrm{ybcoin}_5$ superlattices: A test bed for the reduction of topological classification. *Phys. Rev. Lett.*, 118:147001, Apr 2017.

[75] Tsuneya Yoshida, Ippei Danshita, Robert Peters, and Norio Kawakami. Reduction of topological $\mathbb{Z}$ classification in cold-atom systems. *Phys. Rev. Lett.*, 121:025301, Jul 2018.

[76] Frank Wilczek and A. Zee. Appearance of gauge structure in simple dynamical systems. *Phys. Rev. Lett.*, 52:2111–2114, Jun 1984.

[77] Yasuhiro Hatsugai. Explicit gauge fixing for degenerate multiplets: A generic setup for topological orders. *Journal of the Physical Society of Japan*, 73(10):2604–2607, 2004.

[78] Yasuhiro Hatsugai. Characterization of topological insulators: Chern numbers for ground state multiplet. *Journal of the Physical Society of Japan*, 74(5):1374–1377, 2005.

[79] Yasuhiro Hatsugai. Quantized berry phases as a local order parameter of a quantum liquid. *Journal of the Physical Society of Japan*, 75(12):123601, 2006.

[80] K. Nomura. *Toporogikaru zetuentai, tyoudenndoutai [Topological insulator and superconductivety]*. Maruzen syuppan, 2016.

[81] Tohru Eguchi, Peter B. Gilkey, and Andrew J. Hanson. Gravitation, gauge theories and differential geometry. *Physics Reports*, 66(6):213 – 393, 1980.

[82] Yasuhiro Hatsugai. Symmetry-protected $\mathbb{Z}_2$-quantization and quaternionic berry connection with kramers degeneracy. *New Journal of Physics*, 12(6):065004, jun 2010.

[83] Y. Hatsugai and I. Maruyama. $\mathbb{Z}_{\mathrm{Q}}$ topological invariants for polyacetylene, kagome and pyrochlore lattices. *EPL (Europhysics Letters)*, 95(2):20003, jun 2011.

[84] Toshikaze Kariyado, Takahiro Morimoto, and Yasuhiro Hatsugai. Z_N berry phases in symmetry protected topological phases. *Phys. Rev. Lett.*, 120:247202, Jun 2018.

[85] Wladimir A. Benalcazar, B. Andrei Bernevig, and Taylor L. Hughes. Quantized electric multipole insulators. *Science*, 357(6346):61–66, 2017.

[86] Motohiko Ezawa. Higher-order topological insulators and semimetals on the breathing kagome and pyrochlore lattices. *Phys. Rev. Lett.*, 120:026801, Jan 2018.

[87] E. H. Hall. On a new action of the magnet on electric currents. *American Journal of Mathematics*, 2(3):287–292, 1879.

[88] Neil W. Ashcroft and N. David Mermin. *Solid State Physics 1e.* Thomson Learning, 1976.

[89] Daijiro Yoshioka. *The Quantum Hall Effect.* Springer, 2002.

[90] N. Byers and C. N. Yang. Theoretical considerations concerning quantized magnetic flux in superconducting cylinders. *Phys. Rev. Lett.*, 7:46–49, Jul 1961.

[91] X. G. Wen and Q. Niu. Ground-state degeneracy of the fractional quantum hall states in the presence of a random potential and on high-genus riemann surfaces. *Phys. Rev. B*, 41:9377–9396, May 1990.

[92] F. D. M. Haldane. Many-particle translational symmetries of two-dimensional electrons at rational landau-level filling. *Phys. Rev. Lett.*, 55:2095–2098, Nov 1985.

[93] R. Tao and F. D. M. Haldane. Impurity effect, degeneracy, and topological invariant in the quantum hall effect. *Phys. Rev. B*, 33:3844–3850, Mar 1986.

[94] Qian Niu, D. J. Thouless, and Yong-Shi Wu. Quantized hall conductance as a topological invariant. *Phys. Rev. B*, 31:3372–3377, Mar 1985.

[95] D. N. Sheng, Xin Wan, E. H. Rezayi, Kun Yang, R. N. Bhatt, and F. D. M. Haldane. Disorder-driven collapse of the mobility gap and transition to an insulator in the fractional quantum hall effect. *Phys. Rev. Lett.*, 90:256802, Jun 2003.

[96] M. Hafezi, A. S. Sørensen, E. Demler, and M. D. Lukin. Fractional quantum hall effect in optical lattices. *Phys. Rev. A*, 76:023613, Aug 2007.

[97] G. Möller and N. R. Cooper. Composite fermion theory for bosonic quantum hall states on lattices. *Phys. Rev. Lett.*, 103:105303, Sep 2009.

[98] Yi-Fei Wang, Hong Yao, Chang-De Gong, and D. N. Sheng. Fractional quantum hall effect in topological flat bands with chern number two. *Phys. Rev. B*, 86:201101, Nov 2012.

[99] Yin-Chen He, Subhro Bhattacharjee, R. Moessner, and Frank Pollmann. Bosonic integer quantum hall effect in an interacting lattice model. *Phys. Rev. Lett.*, 115:116803, Sep 2015.

[100] Gunnar Möller and Nigel R. Cooper. Fractional chern insulators in harper-hofstadter bands with higher chern number. *Phys. Rev. Lett.*, 115:126401, Sep 2015.

[101] Tian-Sheng Zeng, W. Zhu, and D. N. Sheng. Two-component quantum hall effects in topological flat bands. *Phys. Rev. B*, 95:125134, Mar 2017.

[102] Zheng Zhu, Liang Fu, and D. N. Sheng. Numerical study of quantum hall bilayers at total filling $\nu_T = 1$: A new phase at intermediate layer distances. *Phys. Rev. Lett.*, 119:177601, Oct 2017.

[103] Koji Kudo, Toshikaze Kariyado, and Yasuhiro Hatsugai. Many-body chern numbers of $\nu = 1/3$ and $1/2$ states on various lattices. *Journal of the Physical Society of Japan*, 86(10):103701, 2017.

[104] Akishi Matsugatani, Yuri Ishiguro, Ken Shiozaki, and Haruki Watanabe. Universal relation among the many-body chern number, rotation symmetry, and filling. *Phys. Rev. Lett.*, 120:096601, Feb 2018.

[105] Eric M. Spanton, Alexander A. Zibrov, Haoxin Zhou, Takashi Taniguchi, Kenji Watanabe, Michael P. Zaletel, and Andrea F. Young. Observation of fractional chern insulators in a van der waals heterostructure. *Science*, 360(6384):62–66, 2018.

[106] Koji Kudo and Yasuhiro Hatsugai. Fractional quantum hall effect in n = 0 landau band of graphene with chern number matrix. *Journal of the Physical Society of Japan*, 87(6):063701, 2018.

[107] Matthew B. Hastings and Spyridon Michalakis. Quantization of hall conductance for interacting electrons on a torus. *Comm. Math. Phys.*, 334(1):433–471, Feb 2015.

[108] T. Koma. Topological Current in Fractional Chern Insulators. *ArXiv e-prints*, April 2015.

[109] S. Bachmann, A. Bols, W. De Roeck, and M. Fraas. Quantization of conductance in gapped interacting systems. *Ann. Henri Poincare*, 19:695–708, mar 2018.

[110] Haruki Watanabe. Insensitivity of bulk properties to the twisted boundary condition. *Phys. Rev. B*, 98:155137, Oct 2018.

[111] Koji Kudo, Haruki Watanabe, Toshikaze Kariyado, and Yasuhiro Hatsugai. Many-body chern number without integration. *Phys. Rev. Lett.*, 122:146601, Apr 2019.

[112] Takahiro Fukui, Yasuhiro Hatsugai, and Hiroshi Suzuki. Chern numbers in discretized brillouin zone: Efficient method of computing (spin) hall conductances. *J. Phys. Soc. Jpn.*, 74(6):1674–1677, 2005.

[113] Y. Hatsugai, K. Ishibashi, and Y. Morita. Sum rule of hall conductance in a random quantum phase transition. *Phys. Rev. Lett.*, 83:2246–2249, Sep 1999.

[114] S. M. Girvin and A. H. MacDonald. Off-diagonal long-range order, oblique confinement, and the fractional quantum hall effect. *Phys. Rev. Lett.*, 58:1252–1255, Mar 1987.

[115] Euler-Maclaurin formula gives a relation between integrals and finite sums. See, for example, M. Abramowitz and I. A. Stegun, *Handbook of Mathematical Functions* (Dover Publications, Inc., 1974).

[116] Rui Li and Michael Fleischhauer. Finite-size corrections to quantized particle transport in topological charge pumps. *Phys. Rev. B*, 96:085444, Aug 2017.

[117] Yuji Hamamoto, Hideo Aoki, and Yasuhiro Hatsugai. Chiral condensate with topological degeneracy in graphene and its manifestation in edge states. *Phys. Rev. B*, 86:205424, Nov 2012.

[118] Yuji Hamamoto, Tohru Kawarabayashi, Hideo Aoki, and Yasuhiro Hatsugai. Spin-resolved chiral condensate as a spin-unpolarized $\nu = 0$ quantum hall state in graphene. *Phys. Rev. B*, 88:195141, Nov 2013.

[119] Y Hatsugai, T Morimoto, T Kawarabayashi, Y Hamamoto, and H Aoki. Chiral symmetry and its manifestation in optical responses in graphene: interaction and multilayers. *New Journal of Physics*, 15(3):035023, mar 2013.

[120] Tsuneya Yoshida, Koji Kudo, and Yasuhiro Hatsugai. Non-hermitian fractional quantum hall states. *Scientific Reports*, 9(1):16895, 2019.

[121] Y. Hatsugai, T. Fukui, and H. Suzuki. Topological description of (spin) hall conductances on brillouin zone lattices: quantum phase transitions and topological changes. *Physica E: Low-dimensional Systems and Nanostructures*, 34(1):336 – 339, 2006.

[122] R. B. Laughlin. Levitation of extended-state bands in a strong magnetic field. *Phys. Rev. Lett.*, 52:2304–2304, Jun 1984.

[123] D.E. Khmelnitskii. Quantum hall effect and additional oscillations of conductivity in weak magnetic fields. *Physics Letters A*, 106(4):182 – 183, 1984.

[124] Steven Kivelson, Dung-Hai Lee, and Shou-Cheng Zhang. Global phase diagram in the quantum hall effect. *Phys. Rev. B*, 46:2223–2238, Jul 1992.

[125] Hui Song, Isao Maruyama, and Yasuhiro Hatsugai. Levitation and percolation in quantum hall systems with correlated disorder. *Phys. Rev. B*, 76:132202, Oct 2007.

[126] Yu Xue and Emil Prodan. Quantum criticality at the chern-to-normal insulator transition. *Phys. Rev. B*, 87:115141, Mar 2013.

[127] C. Repellin and N. Goldman. Detecting fractional chern insulators through circular dichroism. *Phys. Rev. Lett.*, 122:166801, Apr 2019.

[128] Tomoki Ozawa and Nathan Goldman. Probing localization and quantum geometry by spectroscopy. *Phys. Rev. Research*, 1:032019, Nov 2019.

[129] Bruno Mera. Localization anisotropy and complex geometry in two-dimensional insulators. *Phys. Rev. B*, 101:115128, Mar 2020.

[130] Y Hatsugai. Quantized berry phases for a local characterization of spin liquids in frustrated spin systems. *Journal of Physics: Condensed Matter*, 19(14):145209, mar 2007.

[131] T. Hirano, H. Katsura, and Y. Hatsugai. Degeneracy and consistency condition for berry phases: Gap closing under a local gauge twist. *Phys. Rev. B*, 78:054431, Aug 2008.

[132] Toshikaze Kariyado and Yasuhiro Hatsugai. Fractionally quantized berry phase, adiabatic continuation, and edge states. *Phys. Rev. B*, 90:085132, Aug 2014.

[133] Shota Fubasami, Tomonari Mizoguchi, and Yasuhiro Hatsugai. Sequential quantum phase transitions in J_1-J_2 heisenberg chains with integer spins ($s > 1$): Quantized berry phase and valence-bond solids. *Phys. Rev. B*, 100:014438, Jul 2019.

[134] Koji Hashimoto, Xi Wu, and Taro Kimura. Edge states at an intersection of edges of a topological material. *Phys. Rev. B*, 95:165443, Apr 2017.

[135] Frank Schindler, Ashley M. Cook, Maia G. Vergniory, Zhijun Wang, Stuart S. P. Parkin, B. Andrei Bernevig, and Titus Neupert. Higher-order topological insulators. *Science Advances*, 4(6), 2018.

[136] Wladimir A. Benalcazar, B. Andrei Bernevig, and Taylor L. Hughes. Electric multipole moments, topological multipole moment pumping, and chiral hinge states in crystalline insulators. *Phys. Rev. B*, 96:245115, Dec 2017.

[137] Shin Hayashi. Topological invariants and corner states for hamiltonians on a three-dimensional lattice. *Communications in Mathematical Physics*, 364(1):343–356, Nov 2018.

[138] Stefan Imhof, Christian Berger, Florian Bayer, Johannes Brehm, Laurens W. Molenkamp, Tobias Kiessling, Frank Schindler, Ching Hua Lee, Martin Greiter, Titus Neupert, and Ronny Thomale. Topolectrical-circuit realization of topological corner modes. *Nature Physics*, 14(9):925–929, 2018.

[139] Hiromu Araki, Tomonari Mizoguchi, and Yasuhiro Hatsugai. Phase diagram of a disordered higher-order topological insulator: A machine learning study. *Phys. Rev. B*, 99:085406, Feb 2019.

[140] Sayed Ali Akbar Ghorashi, Xiang Hu, Taylor L. Hughes, and Enrico Rossi. Second-order dirac superconductors and magnetic field induced majorana hinge modes. *Phys. Rev. B*, 100:020509, Jul 2019.

[141] Tomonari Mizoguchi, Mina Maruyama, Susumu Okada, and Yasuhiro Hatsugai. Flat bands and higher-order topology in polymerized triptycene: Tight-binding analysis on decorated star lattices. *Phys. Rev. Materials*, 3:114201, Nov 2019.

[142] Hiromasa Wakao, Tsuneya Yoshida, Hiromu Araki, Tomonari Mizoguchi, and Yasuhiro Hatsugai. Higher-order topological phases in a spring-mass model on a breathing kagome lattice. *Phys. Rev. B*, 101:094107, Mar 2020.

[143] Hiromu Araki, Tomonari Mizoguchi, and Yasuhiro Hatsugai. $\mathbb{Z}_q$ berry phase for higher-order symmetry-protected topological phases. *Phys. Rev. Research*, 2:012009, Jan 2020.

[144] Tomonari Mizoguchi, Yoshihito Kuno, and Yasuhiro Hatsugai. Square-root higher-order topological insulator on a decorated honeycomb lattice. *Phys. Rev. A*, 102:033527, Sep 2020.

[145] Frank Schindler, Zhijun Wang, Maia G. Vergniory, Ashley M. Cook, Anil Murani, Shamashis Sengupta, Alik Yu. Kasumov, Richard Deblock, Sangjun Jeon, Ilya Drozdov, Hélène Bouchiat, Sophie Guéron, Ali Yazdani, B. Andrei Bernevig, and Titus Neupert. Higher-order topology in bismuth. *Nature Physics*, 14(9):918–924, 2018.

[146] Marc Serra-Garcia, Valerio Peri, Roman Süsstrunk, Osama R. Bilal, Tom Larsen, Luis Guillermo Villanueva, and Sebastian D. Huber. Observation of a phononic quadrupole topological insulator. *Nature*, 555:342 EP –, 01 2018.

[147] Zhongbo Yan, Fei Song, and Zhong Wang. Majorana corner modes in a high-temperature platform. *Phys. Rev. Lett.*, 121:096803, Aug 2018.

[148] Changming Yue, Yuanfeng Xu, Zhida Song, Hongming Weng, Yuan-Ming Lu, Chen Fang, and Xi Dai. Symmetry-enforced chiral hinge states and surface quantum anomalous hall effect in the magnetic axion insulator bi2–xsmxse3. *Nature Physics*, 2019.

[149] M. Hohenadler, T. C. Lang, and F. F. Assaad. Correlation effects in quantum spin-hall insulators: A quantum monte carlo study. *Phys. Rev. Lett.*, 106:100403, Mar 2011.

[150] Shun-Li Yu, X. C. Xie, and Jian-Xin Li. Mott physics and topological phase transition in correlated dirac fermions. *Phys. Rev. Lett.*, 107:010401, Jun 2011.

[151] Tsuneya Yoshida, Satoshi Fujimoto, and Norio Kawakami. Correlation effects on a topological insulator at finite temperatures. *Phys. Rev. B*, 85:125113, Mar 2012.

[152] Y. Tada, R. Peters, M. Oshikawa, A. Koga, N. Kawakami, and S. Fujimoto. Correlation effects in two-dimensional topological insulators. *Phys. Rev. B*, 85:165138, Apr 2012.

[153] Tsuneya Yoshida, Robert Peters, Satoshi Fujimoto, and Norio Kawakami. Topological antiferromagnetic phase in a correlated bernevig-hughes-zhang model. *Phys. Rev. B*, 87:085134, Feb 2013.

[154] M Hohenadler and F F Assaad. Correlation effects in two-dimensional topological insulators. *Journal of Physics: Condensed Matter*, 25(14):143201, mar 2013.

[155] Stephan Rachel. Interacting topological insulators: a review. *Reports on Progress in Physics*, 81(11):116501, oct 2018.

[156] Yizhi You, Trithep Devakul, F. J. Burnell, and Titus Neupert. Higher-order symmetry-protected topological states for interacting bosons and fermions. *Phys. Rev. B*, 98:235102, Dec 2018.

[157] Koji Kudo, Tsuneya Yoshida, and Yasuhiro Hatsugai. Higher-order topological mott insulators. *Phys. Rev. Lett.*, 123:196402, Nov 2019.

[158] Tohru Kawarabayashi, Kota Ishii, and Yasuhiro Hatsugai. Fractionally quantized berry's phase in an anisotropic magnet on the kagome lattice. *Journal of the Physical Society of Japan*, 88(4):045001, 2019.

[159] Alex Rasmussen and Yuan-Ming Lu. Classification and construction of higher-order symmetry-protected topological phases of interacting bosons. *Phys. Rev. B*, 101:085137, Feb 2020.

[160] Julian Bibo, Izabella Lovas, Yizhi You, Fabian Grusdt, and Frank Pollmann. Fractional corner charges in a two-dimensional superlattice bose-hubbard model. *Phys. Rev. B*, 102:041126, Jul 2020.

[161] Rui-Xing Zhang, Cenke Xu, and Chao-Xing Liu. Interacting topological phases in thin films of topological mirror kondo insulators. *Phys. Rev. B*, 94:235128, Dec 2016.

[162] Zhen Bi, Ruixing Zhang, Yi-Zhuang You, Andrea Young, Leon Balents, Chao-Xing Liu, and Cenke Xu. Bilayer graphene as a platform for bosonic symmetry-protected topological states. *Phys. Rev. Lett.*, 118:126801, Mar 2017.

[163] Masahiko G. Yamada, Tomohiro Soejima, Naoto Tsuji, Daisuke Hirai, Mircea Dincă, and Hideo Aoki. First-principles design of a half-filled flat band of the kagome lattice in two-dimensional metal-organic frameworks. *Phys. Rev. B*, 94:081102, Aug 2016.

[164] J. K. Jain. Composite-fermion approach for the fractional quantum hall effect. *Phys. Rev. Lett.*, 63:199–202, Jul 1989.

[165] Jainendra K. Jain. *Composite Fermions*. Cambridge University Press, 2007.

[166] MARTIN GREITER and FRANK WILCZEK. Heuristic principle for quantized hall states. *Modern Physics Letters B*, 04(16):1063–1069, 1990.

[167] Martin Greiter and Frank Wilczek. Exact solutions and the adiabatic heuristic for quantum hall states. *Nuclear Physics B*, 370(3):577 – 600, 1992.

[168] Michael G. G. Laidlaw and Cécile Morette DeWitt. Feynman functional integrals for systems of indistinguishable particles. *Phys. Rev. D*, 3:1375–1378, Mar 1971.

[169] Yong-Shi Wu. General theory for quantum statistics in two dimensions. *Phys. Rev. Lett.*, 52:2103–2106, Jun 1984.

[170] Frank Wilczek. Magnetic flux, angular momentum, and statistics. *Phys. Rev. Lett.*, 48:1144–1146, Apr 1982.

[171] Frank Wilczek. Quantum mechanics of fractional-spin particles. *Phys. Rev. Lett.*, 49:957–959, Oct 1982.

[172] X. G. Wu, G. Dev, and J. K. Jain. Mixed-spin incompressible states in the fractional quantum hall effect. *Phys. Rev. Lett.*, 71:153–156, Jul 1993.

[173] V. W. Scarola and J. K. Jain. Phase diagram of bilayer composite fermion states. *Phys. Rev. B*, 64:085313, Aug 2001.

[174] R. K. Kamilla, X. G. Wu, and J. K. Jain. Composite fermion theory of collective excitations in fractional quantum hall effect. *Phys. Rev. Lett.*, 76:1332–1335, Feb 1996.

[175] R. K. Kamilla, X. G. Wu, and J. K. Jain. Excitons of composite fermions. *Phys. Rev. B*, 54:4873–4884, Aug 1996.

[176] Gun Sang Jeon, Kenneth L. Graham, and Jainendra K. Jain. Fractional statistics in the fractional quantum hall effect. *Phys. Rev. Lett.*, 91:036801, Jul 2003.

[177] Ajit C. Balram, Arkadiusz Wójs, and Jainendra K. Jain. State counting for excited bands of the fractional quantum hall effect: Exclusion rules for bound excitons. *Phys. Rev. B*, 88:205312, Nov 2013.

[178] R. Willett, J. P. Eisenstein, H. L. Störmer, D. C. Tsui, A. C. Gossard, and J. H. English. Observation of an even-denominator quantum number in the fractional quantum hall effect. *Phys. Rev. Lett.*, 59:1776–1779, Oct 1987.

[179] Martin Greiter, X.G. Wen, and Frank Wilczek. Paired hall states. *Nuclear Physics B*, 374(3):567 – 614, 1992.

[180] K. Park, V. Melik-Alaverdian, N. E. Bonesteel, and J. K. Jain. Possibility of p-wave pairing of composite fermions at $\nu = \frac{1}{2}$. *Phys. Rev. B*, 58:R10167–R10170, Oct 1998.

[181] B. I. Halperin, Patrick A. Lee, and Nicholas Read. Theory of the half-filled landau level. *Phys. Rev. B*, 47:7312–7343, Mar 1993.

[182] Dam Thanh Son. Is the composite fermion a dirac particle? *Phys. Rev. X*, 5:031027, Sep 2015.

[183] Dam Thanh Son. The dirac composite fermion of the fractional quantum hall effect. *Annual Review of Condensed Matter Physics*, 9(1):397–411, 2018.

[184] J. K. Jain. Incompressible quantum hall states. *Phys. Rev. B*, 40:8079–8082, Oct 1989.

[185] X. G. Wen. Non-abelian statistics in the fractional quantum hall states. *Phys. Rev. Lett.*, 66:802–805, Feb 1991.

[186] Ying-Hai Wu, Tao Shi, and Jainendra K. Jain. Non-abelian parton fractional quantum hall effect in multilayer graphene. *Nano Letters*, 17(8):4643–4647, 2017. PMID: 28649831.

[187] Ajit C. Balram, Maissam Barkeshli, and Mark S. Rudner. Parton construction of a wave function in the anti-pfaffian phase. *Phys. Rev. B*, 98:035127, Jul 2018.

[188] W. N. Faugno, Ajit C. Balram, Maissam Barkeshli, and J. K. Jain. Prediction of a non-abelian fractional quantum hall state with f-wave pairing of composite fermions in wide quantum wells. *Phys. Rev. Lett.*, 123:016802, Jul 2019.

[189] Bertrand I Halperin and Jainendra K Jain. *Fractional Quantum Hall Effects*. WORLD SCIENTIFIC, 2020.

[190] Joan S. Birman. On braid groups. *Communications on Pure and Applied Mathematics*, 22(1):41–72, 1969.

[191] X. G. Wen, E. Dagotto, and E. Fradkin. Anyons on a torus. *Phys. Rev. B*, 42:6110–6123, Oct 1990.

[192] TORBJORN EINARSSON. Fractional statistics on compact surfaces. *Modern Physics Letters B*, 05(10):675–686, 1991.

[193] Yasuhiro Hatsugai, Mahito Kohmoto, and Yong-Shi Wu. Anyons on a torus: Braid group, aharonov-bohm period, and numerical study. *Phys. Rev. B*, 43:10761–10768, May 1991.

[194] DINGPING LI. Hierarchical wave functions and fractional statistics in fractional quantum hall effect on the torus. *International Journal of Modern Physics B*, 07(15):2779–2794, 1993.

[195] SHOU CHENG ZHANG. The chern–simons–landau–ginzburg theory of the fractional quantum hall effect. *International Journal of Modern Physics B*, 06(01):25–58, 1992.

[196] R. B. Laughlin. Superconducting ground state of noninteracting particles obeying fractional statistics. *Phys. Rev. Lett.*, 60:2677–2680, Jun 1988.

[197] A. L. Fetter, C. B. Hanna, and R. B. Laughlin. Random-phase approximation in the fractional-statistics gas. *Phys. Rev. B*, 39:9679–9681, May 1989.

[198] YI-HONG CHEN, FRANK WILCZEK, EDWARD WITTEN, and BERTRAND I. HALPERIN. On anyon superconductivity. *International Journal of Modern Physics B*, 03(07):1001–1067, 1989.

[199] M. Y. Azbel, ZhETF 46, 929 (1964) [J. Exp. Theor. Phys. 19, 634 (1964)].

[200] Douglas R. Hofstadter. Energy levels and wave functions of bloch electrons in rational and irrational magnetic fields. *Phys. Rev. B*, 14:2239–2249, Sep 1976.

[201] P Streda. Theory of quantised hall conductivity in two dimensions. *Journal of Physics C: Solid State Physics*, 15(22):L717–L721, aug 1982.

[202] Kenichi Asano. *Quantum Theory of Electrons in Solids*. University of Tokyo Press, 2019.

[203] J. Zak. Magnetic translation group. *Phys. Rev.*, 134:A1602–A1606, Jun 1964.